Doctoral Dissertation

Studies on Synthesis of Novel Organic Cations and Exploration of Their Functions by an Effective Incorporation of Main-Group Elements

（効果的な典型元素導入による新規有機カチオン種の合成および機能開拓に関する研究）

Su-Gi CHONG

Laboratory of Organic Chemistry I
Graduate School of Chemical Sciences and Engineering
Hokkaido University

2024

Table of Contents

Chapter 1

General Introduction

1-1. π-Conjugated Organic Cations

Organic cations are roughly classified into two categories: heteroatom-centered cations and carbon-centered cations, which have attracting properties based on their specific electronic character. The former heteroatom-centered cations, especially those containing positive-charged main-group elements such as pyridinium, ammonium, sulfonium, phosphonium, and so on, are widely used due to their stability. They are well-known as not only synthetic reagents but also organic functional materials, e.g., ionic liquids[1] and anion exchange membranes.[2] Particularly in highly π-conjugated cations containing positively charged heteroatom, cationic nitrogen-doped π-conjugated systems are well-examined as a part of nitrogen-doped graphenes.[3] In such cationic π-conjugated molecules, since the positive charge is localized at doped quaternary cationic nitrogen, their electronic structures can be controlled by the number and/or the position of cationic heteroatoms. In fact, cationic nitrogen-doped π-conjugated systems are applied to bioactive compounds,[4] fluorescent dyes,[5] DNA intercalators,[6] ionic liquids,[7] and organic materials,[8] thanks to a drastic change in electronic structures of π-conjugated systems by doping cationic nitrogen atom.

On the other hand, carbon-centered cations are widely known as intermediates in many chemical reactions and are generally unstable due to their high reactivity,[9] unlike the case of heteroatom-centered cations. To overcome this intrinsic instability, resonance stabilization is of great importance for making carbocations stable, as seen in conjugated compounds, such as allyl and benzyl cations. In fact, the isolation of carbocations has been achieved by gaining chemical stability based on a resonance effect with a substitution of π-conjugated systems. Especially, di-/tri-arylmethyliums are one of the most well-known stable carbon-centered cations. They have potential applications in organic dyes because they have strong absorptions in the visible region due to the narrow HOMO-LUMO gap based on an effective delocalization of π-electrons.[10] Furthermore, the HOMO-LUMO gap can be controlled by the length of π-conjugation, therefore, the absorption can be reached to the NIR region by extending π-conjugation as increasing numbers of conjugating carbons such as cyanine dye.[11]

1-2. Electrochromic Materials Based on Redox Interconversion of Di-/Tri-Arylmethyliums

As mentioned in Section 1-1, di-/tri-arylmethyliums show strong absorptions in the visible to the NIR region due to the narrow HOMO-LUMO gap. Recently, for further development of the functions of organic dyes, several types of response systems using di-/tri-arylmethylium have

been studied on their chromic behaviors, such as electrochromism[12,18,19] and mechanofluorochromism.[13] Especially, electrochromic molecules, accompanying a drastic change in color based on their redox interconversion with the corresponding neutral species, has much attention due to the potential application for smart windows,[14] and bio-imaging in living cells.[15]

Regarding the construction of the electrochromic materials using di-/tri-arylmethylium unit, violene/cyanine hybrid is known as the versatile molecular design concept[16] (Figure 1-1a). For example, when two Michler's hydrol blue units as a cyanine part are linked with conjugating carbons, the drastic color change is induced by redox interconversion between the dicationic species and the corresponding neutral butadiene derivative (Figure 1-1b).[17] This redox process accompanying π-type C-C bond making/breaking proceeds reversibly in the voltammogram, probably due to the structural flexibility in both neutral and dicationic states, where a rapid change in structures occurs between s-*cis*/s-*trans* forms and *E*/*Z* forms for neutral butadiene and dicationic species, respectively (Figure 1-1b).

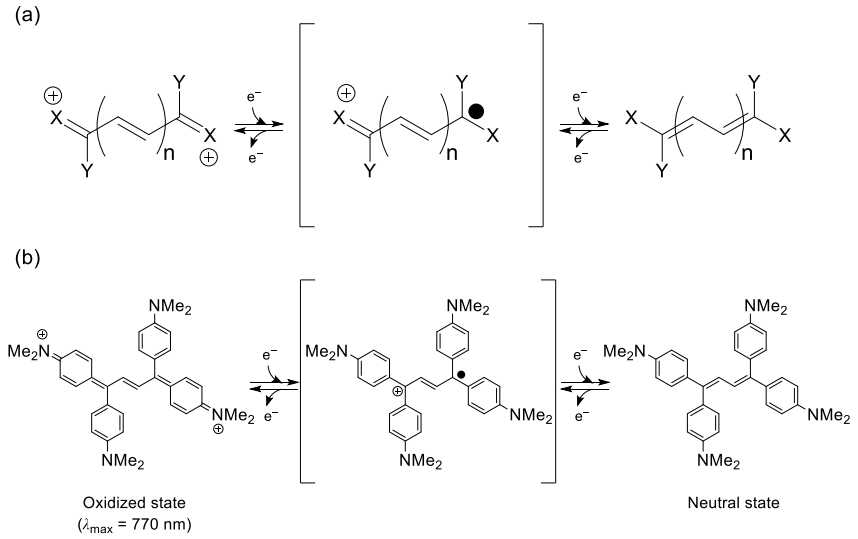

Figure 1-1. Violene/cyanine hybrid: versatile molecular design concept for electrochromic molecules.

On the other hand, the author's group has developed phenanthraquinodimethane-based electrochromic molecules, classified as violene/cyanine hybrid, which shows a drastic change in geometry thanks to the incorporation into the rigid framework (Figure 1-2).[18] For the compound exhibiting such a structural change, a characteristic irreversible voltammogram can be observed with electrochemical bistability ("*dyrex*" behavior), based on the difference between the oxidation potential of the neutral species and the reduction potential of the dicationic species.

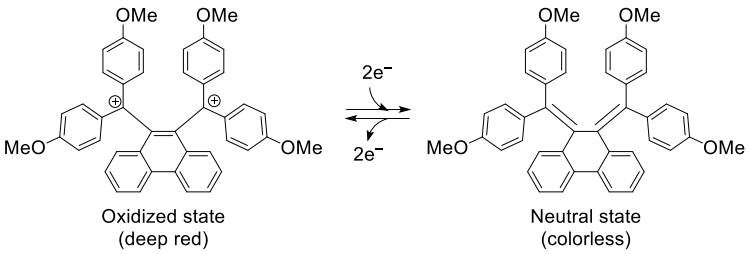

Figure 1-2. A representative π-type system with a dynamic change in structure upon two-electron redox processes.

In addition, the author's group has also developed *dyrex* molecules with intramolecular σ-type C-C bond making/breaking (Figure 1-3).[19]

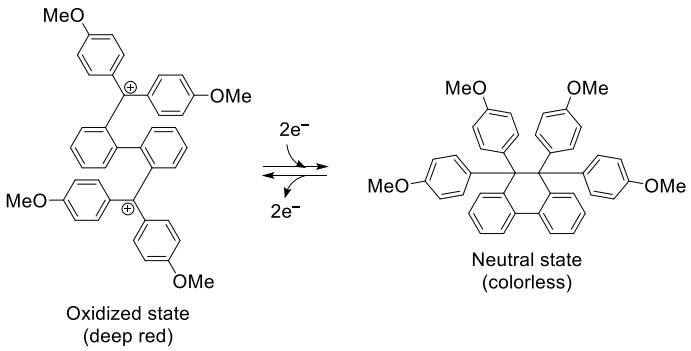

Figure 1-3. A representative σ-type system with a dynamic change in the structure upon two-electron redox processes.

As shown in Figures 1-1, 1-2, and 1-3, previously synthesized electrochromic molecules all consist of two cyanine units within the conjugated molecular scaffold. This is because molecules composed of only one cyanine unit with odd numbers of conjugating carbons[20] generate neutral and highly reactive radicals upon one-electron reduction, therefore their redox interconversion is less reversible.

In this context, if the reactivity of reduced species generated by one-electron reduction of cyanines with odd numbers of conjugating carbons could be controlled, a new type of electrochromic materials utilizing not only the cationic species but also neutral radical species would be developed, however, there is no strategy for molecular design at present.

1-3. Cationic Nitrogen-Doped π-Conjugated Systems

As mentioned in Section 1-1, the incorporation of cationic nitrogen into π-conjugated systems is an effective way to tailor the electronic structure of sp^2-carbon frameworks, thus making cationic nitrogen-doped π-conjugated molecules would be a promising approach for developing functional materials such as optical and electronic applications.

The most direct method is the doping of cationic quaternary nitrogen into graphene, accomplished by various top-down methods,[3] such as chemical vapor deposition, segregation growth, solvothermal, and arc-discharge approaches. However, as shown in Figure 1-4, the incorporation of not only cationic quaternary nitrogen but also other three types of nitrogen such as pyridinic, pyridinic N^+-O^-, and pyrrolic nitrogen, into graphene is unavoidable using the above-mentioned methods.[3] Therefore, controlling the nitrogen doping at specific positions on graphene architecture at the molecular level is a long-standing synthetic challenge.[3]

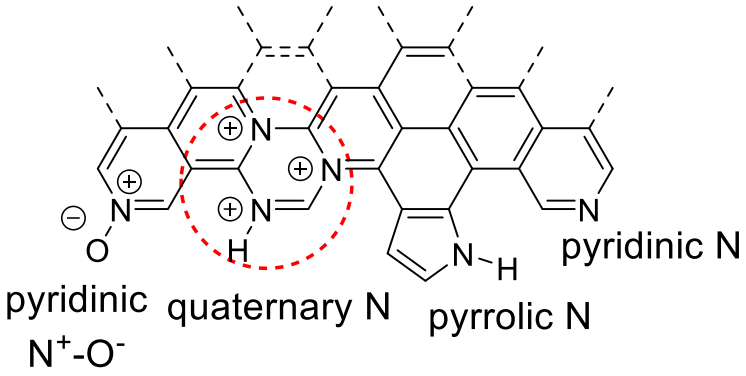

Figure 1-4. Bonding configurations for nitrogen atoms in N-doped graphene.

On the other hand, bottom-up organic synthesis enables the replacement of a quaternary sp^2-carbon atom with a quaternary cationic nitrogen atom at the desired position in parent polyaromatic π-conjugated scaffolds to provide perfectly designated cationic aza-doped nanocarbons, which are classified as azonia aromatic heterocycles (AZAHs). In fact, so many π-conjugated molecules containing a cationic nitrogen atom with not only a planar skeleton (e.g., phenanthrenes) but also a distorted structure (e.g., helicenes) have been synthesized via transition-metal-catalyzed reactions (Figure 1-5a, b)[21,22] and ~~nucleophilic aromatic substitution~~ photocyclization of *N*-vinyl pyridinium salts (Figure 1-5c).[23]

However, most of previously synthesized AZAHs are composed of only hexagonal rings. A few studies on the synthesis of pentagonal ring containing AZAHs have been reported, but they are almost limited to [2.3.3]cyclizine[24] reported by Leaver's group and pyrazole or imidazole containing AZAHs.[25,26] Furthermore, the examples of the incorporation of cationic nitrogen into strained π-conjugated systems are only limited to carbohelicenes.[22,27] Therefore, the novel

synthetic methods enabling the cationic nitrogen-doping into various π-conjugated scaffolds, which are composed not only of six-membered rings such as graphene, are desired for further development of AZAH-based organic materials.

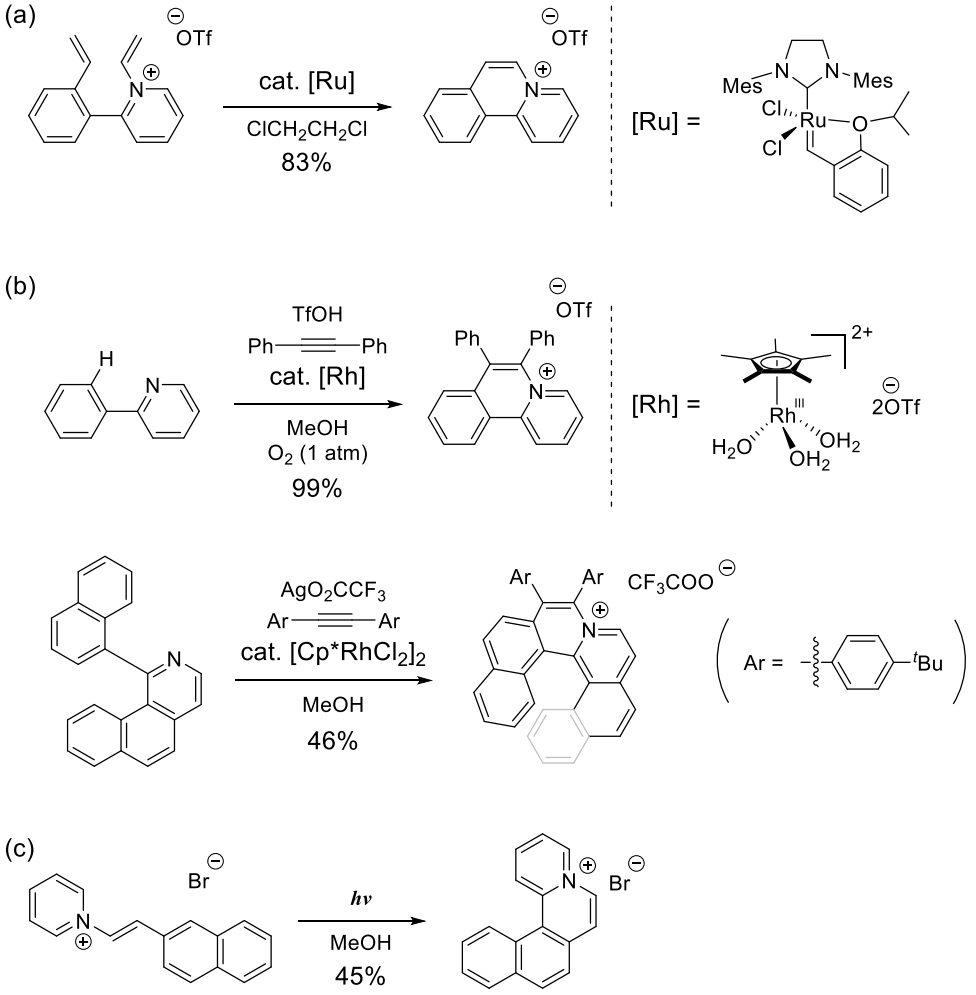

Figure 1-5 Representative synthetic methods of cationic nitrogen-doped π-conjugated systems

1-4. Contents of This Dissertation

Based on such background, the author reports here the study on the novel organic cations and the exploration of their functions by an effective incorporation of main-group elements in this dissertation.

In Chapter 2, the author constructed the novel electrochromic system based on 4-methoxyphenyl substituted di(2-thienyl)methyliums (Figure 1-6). The incorporation of the thiophene ring into a cyanine unit gave stability to not only a cation but also a neutral radical thanks to an effective π-electron delocalization. As a result, the generated neutral radicals upon reduction of the corresponding cations were able to be isolated as stable entities when an anthryl-type substituent is attached to the central methine carbon while the secondary radical without any substituent quantitatively converted to a sigma-bonded dimer. Since both the stable radical and the dimer regenerated the starting cyanine dyes upon oxidation, the present redox pairs can serve as electrochromic materials that exhibit a change in absorption in the Vis-NIR region. This is the first demonstration of the electrochromism for a carbocation-based material consisting of one cyanine dye, with a change in the Vis-NIR absorption.

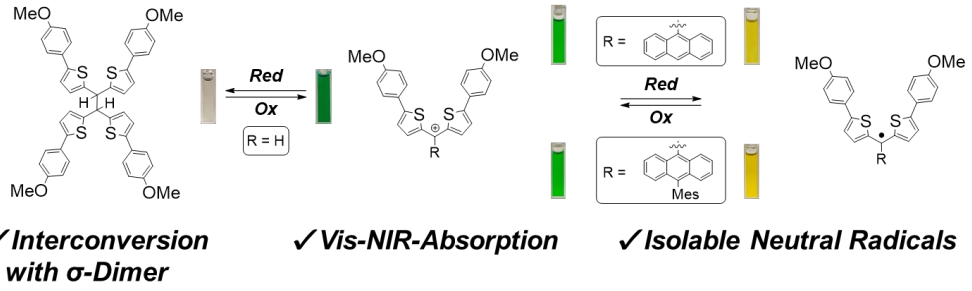

Figure 1-6. Two types of electrochromic systems based on 4-methoxyphenyl substituted di(2-thienyl)methyliums.

In Chapter 3, cationic azaacenaphthylenes (CAAs), which can be applied to an acceptor unit for constructing donor (D)-acceptor (A) type organic dyes, were designed and synthesized as a new family of AZAHs (Figure 1-7). The method that the author newly developed enabled a rapid access to the CAA skeleton from 8-quinoline substituted triarylethenes in a one-pot reaction, unlike the conventional method.[24] In comparison with the conventional dyes utilizing AZAHs as an acceptor unit, the absorption bands of the newly prepared donor-acceptor dyes are drastically red-shifted and reach around 1000 nm thanks to the high π-electron acceptability of the CAA skeleton. Furthermore, CAA-based D-A-type dyes showed unique red-shifted absorptions only in chlorinated solvents, regardless of solvent polarity. Based on the unsymmetric structure of newly

prepared dyes due to the position of doped cationic nitrogen, the author disclosed tri-color halochromic behavior upon protonation/deprotonation of bis(4-dimethylaminophenyl)stilbene moiety in a stepwise manner.

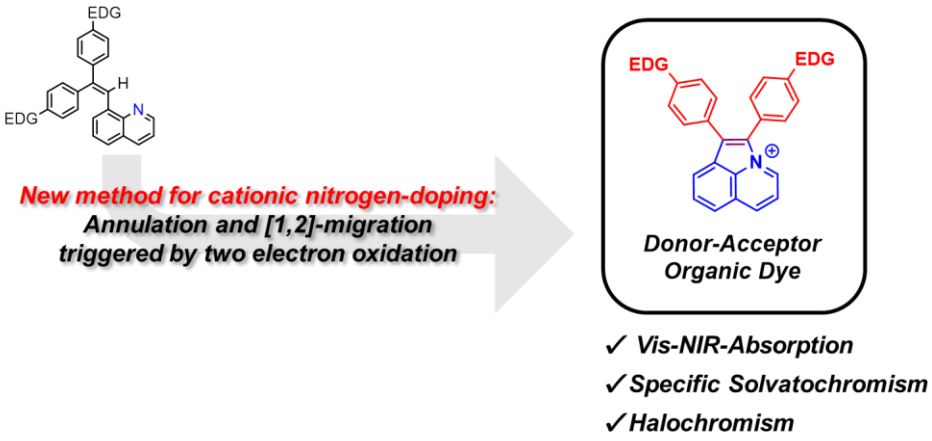

Figure 1-7. The newly synthesized D-A type cationic dye via two-electron oxidation of the corresponding triarylethene.

In Chapter 4, the author developed the new synthetic method of cationic nitrogen-embedded bis(tricyclic) aromatic enes (BAEs) as a new family of strained-AZAHs (Figure 1-8). Desired cationic dyes were successfully synthesized in one step from phenylpyridine-substituted triarylethene derivatives in good yield. Single-crystal X-ray analyses revealed that the prepared cations exist as a twisted or a folded conformer depending on the electronic and structural characters of the tricyclic aromatic core, which is the opposite side from the cationic aza-fluorenylidene unit. In the UV-Vis-NIR spectra, acridinium-type compound showed strong absorption in the NIR region, but dibenzosuberene-type compound exhibited absorptions only in the UV-Vis region. In the case of thioxanthene-type compound, a weak yet obvious NIR absorption was observed. These results suggested that the conformation of thioxanthene-type derivative can change in solution due to a thermal equilibrium whereas acridinium-type and dibenzosuberene-type compounds only adopt the twisted and folded conformations, respectively, even in solution. Focusing on the solid-state properties, on the other hand, thioxanthene-type and dibenzosuberene-type derivatives showed fluorescence while acridinium-type derivative showed no emission, indicating that the folded conformation in the solid state is important for emissive properties. Notably, only one replacement of quaternary carbon into cationic nitrogen of hydrocarbon-based BAE, which was reported by Nguyen in 2019, caused a large red-shifted emission from 458 nm to 602 nm in the solid-state emission spectra. Based on the newly developed cationic nitroge-doped strategy, both red-shifted absorption/emission could be realized.

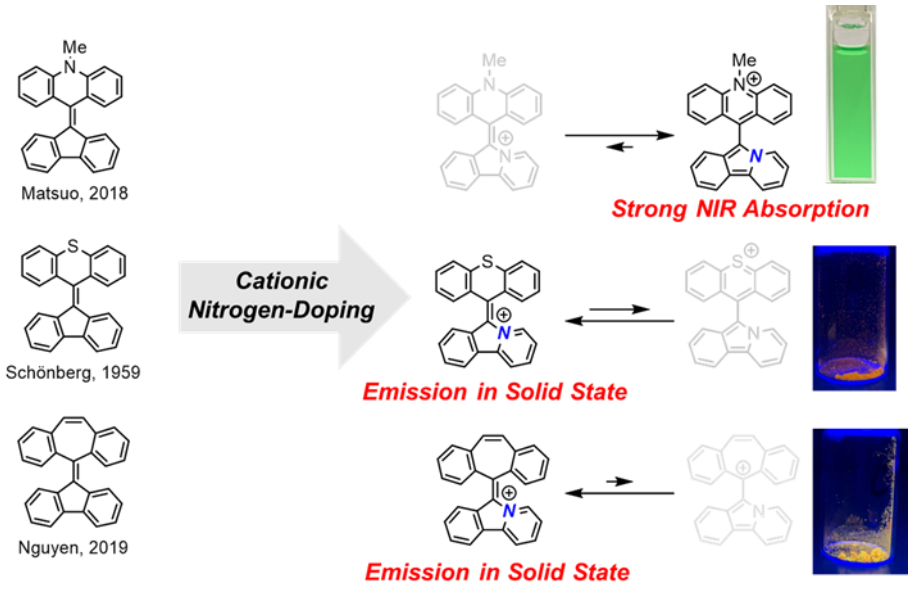

Figure 1-8 The newly synthesized cationic nitrogen-embedded BAEs.

1-5. References

[1] K. Goossens, K. Lava, C. W., K. Binnemans, *Chem. Rev.* **2016**, *116*, 4643.

[2] L. Gao, C.-Y. V. Li, K.-Y. Chan, Z.-N. Chen, *J. Am. Chem. Soc.* **2014**, *136*, 7209.

[3] H. Wang, T. Maiyalagan, X. Wang, *ACS Catal.* **2012**, *2*, 781.

[4] Bortolozzi. R, Ihmels. H,Thomas. L, Tian. M, Viola. G, *Chem. – A Eur. J.* **2013**, *19*, 8736.

[5] Cañeque. T, Cuadro. A. M, Alvarez-Builla. J, Perez-Moreno. J, Clays. K, Castaño. O, Andres. J. L, Vaquero. J. J, *Dyes Pigm.* **2014**, *101*, 116.

[6] Pedro. B, Gema. M, A. Matamoros-Recio, D. Sucunza, F. Mendicuti, A. Domingo, Vaquero. J. J, *Dyes Pigm.* **2021**, *192*, 109443.

[7] Z. Chen, S. Zhang, X. Qi, S. Liu, Q. Zhanga, Y. Deng, *J. Mater. Chem.* 2011, *21*, 8979.

[8] Yue. X, Armijo. Z, King. K, Bondar. M. V, Morales. A. R, Frazer. A, Mikhailov. I. A, Przhonska. O. V, Belfield. K. D. *ACS Appl. Mater. Interfaces* **2015**, *7*, 2833.

[9] R. R. Naredla, D. A. Klumpp, *Chem. Rev.* **2013**, *113*, 6905.

[10] D. F. Duxbury, *Chem. Rev.* **1993**, *93*, 381.

[11] Y. Y. Davidson, B. M. Gunn, S. A. Soper, *Appl. Spectrosc.* **1996**, *50*, 211.

[12] (a) T. Suzuki, H. Higuchi, M. Ohkita, T. Tsuji, *Chem. Commun.* **2001**, 1574. (b) T. Suzuki, Y. Sakano, T. Iwai, S. Iwashita, Y. Miura, R. Katoono, H. Kawai, K. Fujiwara, Y. Tsuji, T. Fukushima, *Pure Appl. Chem.* **2014**, *86*, 507.

[13] Y. Ishigaki, T. Tachibana, K. Sugawara, M. Kikuchi, T. Suzuki. *ChemPlusChem* **2023**, *88*, e202300110.

[14] R. J. Mortimer, *Annu. Rev. Marer. Res.* **2011**, *41*, 241.

[15] (a) L. Wu, Y. Sun, K. Sugimoto, Z. Luo, Y. Ishigaki, K. Pu, T. Suzuki, H.-Y. Chen, D. Ye. *J. Am. Chem. Soc.* **2018**, *140*, 16340. (b) L. Wu, Y. Ishigaki, Y. Hu, K. Sugimoto, W. Zeng, T. Harimoto, Y. Sun, J. He, T. Suzuki, X. Jiang, H.-Y. Chen, D. Ye. *Nat. Commun.* **2020**, *11*, 446.

[16] S. Hünig, M. Kemmer, H. Wenner, I. F. Perepichka, P. Bäuerle, A. Emge, G. Gescheid, *Chem. – A Eur. J.* **1999**, *5*, 1969.

[17] S. Hünig, M. Kemmer, H. Wenner, F. Barbosa, G. Gescheidt, I. F. Perepichka, P. Bäuerle, A. Emge, K. Peters, *Chem. – A Eur. J.* **2000**, *6*, 2618.

[18] S. Iwashita, E. Ohta, H. Higuchi, H. Kawai, K. Fujiwara, K. Ono, M. Takenaka, T. Suzuki, *Chem. Commun*. **2004**, 2076.

[19] T. Suzuki, J. Nishida, T. Tsuji, *Angew. Chem. Int. Ed. Engl.* **1997**, *36*, 1329.

[20] J. R. Lenhard, A. D. Cameron, *J. Phys. Chem.* **1993**, *97*, 4916.

[21] D. Sucunza, A. A. Cuadro, J. Alvarez-Builla, J. J. Vaquero, *J. Org. Chem.* **2016**, *81*, 10126.

[22] Xu. K, Fu. Y, Zhou. Y, Hennersdorf. F, Machata. P, Vincon. I, Weigand. J. J, Popov. A. A, Berger. R, Feng. X, *Angew. Chem. Int. Ed.* **2017**, *56*, 15876.

[23] Arai. S, Hida. M, *Adv. Heterocycl. Chem.* **1992**, *55*, 261.

[24] D. Farquhar, T. T. Gough, D. Leaver, J. F. Miller, J. W. Dick, M. A. Jessep, *J. Chem. Soc., Perkin Trans. 1,* **1984**, 2553.

[25] Davies. D. L, Ellul. C. E, Macgregor. S. A, McMullin. C. L, Singh. K, *J. Am. Chem. Soc.* **2015**, *137*, 9659.

[26] P. Bosch, G. Marcelo, A. Matamoros-Recio, D. Sucunza, F. Mendicuti, A. Domingo, J. J. Vaquero, *Dye. Pigment.* **2021**, *192*, 109443.

[27] S. Arai, M. Ishikura, T. Yamagishi, *J. Chem. Soc., Perkin Trans.* 1, **1998**, 1561.

Chapter 2

π-Extension of Cyanine Dyes by Incorporation of Thiophene Ring and Their Vis-NIR-Electrochromic Interconversion with a σ-Bonded Dimer or Isolable Neutral Radical

2-1. Introduction

Cyanines[1–6] are an important class of organic cationic dyes that have a narrow energy gap thanks to a long-range π-conjugation based on effective π-electron delocalization. When a π-extended cyanine moiety is incorporated as a subunit in the molecular skeleton of electrochromic material (EM),[7–9] a change in the absorption spectrum in response to an electric potential could be induced not only in the visible (Vis) region but also in the near-infrared (NIR) region (700 - 2500 nm). Despite an increasing interest in organic EM that enables ON/OFF switching of NIR absorption,[10–21] the construction of redox systems that are suitable for such EM while exhibiting high reversibility and durability during interconversion is still a challenge.

Cyanines with odd numbers of conjugating carbon atoms are converted to the corresponding neutral radicals upon one-electron (1e) reduction,[22] and the latter are usually very reactive so that redox interconversion is less reversible. To avoid this drawback, a series of EMs were designed to include two cyanine units within the conjugated molecular framework,[23] as represented by the violene/cyanine-hybrid approach[24–27] or cyanine/cyanine-hybrid approach.[28–30] In this way, the two-electron (2e) reduced forms can remain as closed-shell species by spin annihilation. On the other hand, in a non-conjugating approach,[31–34] the biradicals generated upon reduction of two cyanine units undergo intramolecular single-bond formation to convert into the closed-shell cyclic compounds [dynamic redox (*dyrex*) behavior],[35–37] which is the key process to attain reversibility of the redox cycle.

Under the new molecular design concept using a di(2-thienyl)methylium (DTM) chromophore[38,39] (Scheme 1a), the author envisaged that only one cyanine unit would be enough to serve as EM, which makes the largest difference from the above-mentioned examples containing two cyanine units. Based on the effective π-extension of DTM, the author, in this Chapter, succeeded in the design and synthesis of novel EM molecules exhibiting an electrochromic response with a spectral change in the Vis-NIR region.

2-2. Results and Discussion

2-2-1. Molecular Design

Thiophene is an electron-donating aromatic heterocycle that can stabilize a carbocation when attached at its C2 position.[40–42] For DTM chromophores, a cyanine-type conjugation with alternating positive charges was demonstrated.[38,39] Thus, the author designed a new NIR-absorbing cyanine dye $\mathbf{1}^+$, in which 4-methoxyphenyl groups are attached at the C5 position of each thiophene ring of DTM. A coplanar arrangement of four aromatic rings is expected for $\mathbf{1}^+$, with delocalization of the positive charge over the whole molecular skeleton of π-extended DTM (Scheme 2-1b), with a strong absorption band in the NIR region.

Scheme 2-1. The concept of molecular design of thiophene incorporated cyanine dye.

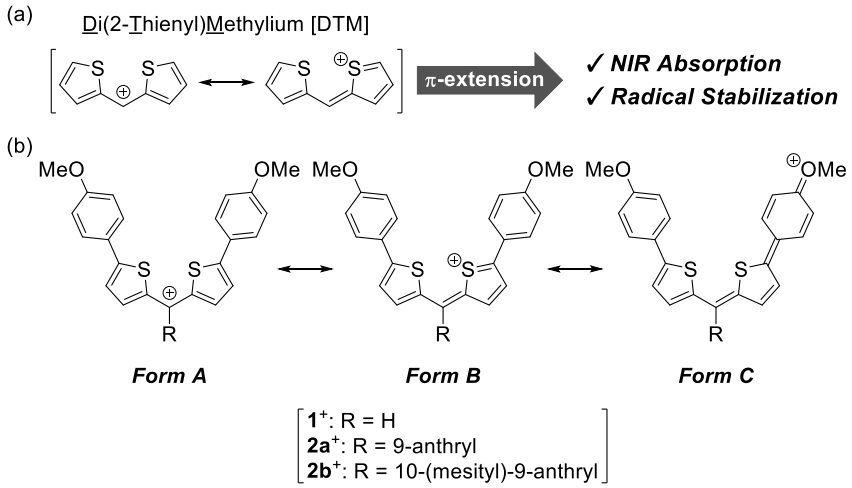

Upon 1e-reduction of $\mathbf{1}^+$, the resulting neutral radical $\mathbf{1}^{\bullet}$ would have a significant spin density at the central methine carbon, which is sterically less shielded to allow facile and quantitative dimerization to give a closed-shell dimer $\mathbf{1}_2$ (Scheme 2-2). When a bulky substituent, such as 9-anthryl or 10-(2,4,6-trimethylphenyl)-9-anthryl group,[43] is attached to the methine carbon as in $\mathbf{2}^+$, the neutral radical $\mathbf{2}^{\bullet}$ generated upon 1e-reduction would be stable enough to be used as a counterpart of EM. These are the central points of the molecular design concept for EM with a new π-extended DTM skeleton. The assumed stability of $\mathbf{2}^{\bullet}$ is also suggested by 11,11,12,12-tetrakis[5-(4-methoxyphenyl-2-thienyl)]anthraquinodimethane,[39] which the author's group recently isolated as a stable entity. It exists in fast equilibrium with its diradical form, which contains the subunit of $\mathbf{2}^{\bullet}$.

Scheme 2-2. Reduction processes of $\mathbf{1}^+$ and $\mathbf{2}^+$.

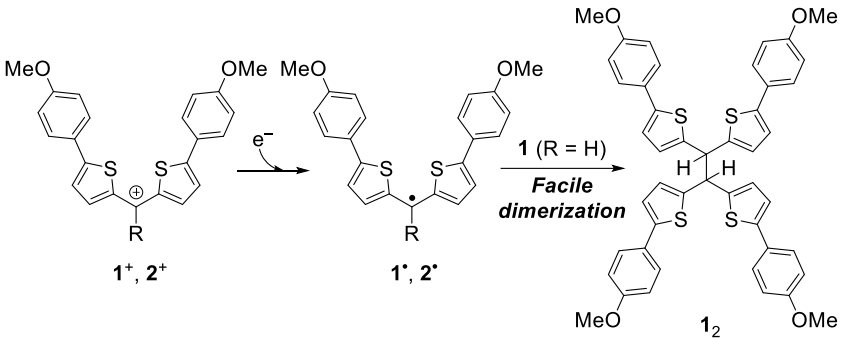

2-2-2. Preparation and Spectroscopic Properties of Cationic Salts of $\mathbf{1}^+$ and $\mathbf{2}^+$

2-Bromo-5-(4-methoxyphenyl)thiophene **4**,[44] which was prepared from 2-(4-methoxyphenyl)thiophene **3**, was treated with *n*BuLi in THF, and the resulting aryllithium was reacted with *N*,*N*-dimethylcarbamoyl chloride to give diarylketone **5** in 93% yield. Reduction of **5** with $LiAlH_4$ in THF gave **Pre-1** in 78% yield, from which cationic salt $\mathbf{1}^+BF_4^-$ was obtained upon treatment with aqueous HBF_4 in trifluoroacetic anhydride (TFAA) and isolated as a stable deep-green solid in 100% yield (Scheme 2-3).

Scheme 2-3. Preparation of $\mathbf{1}^+BF_4^-$.

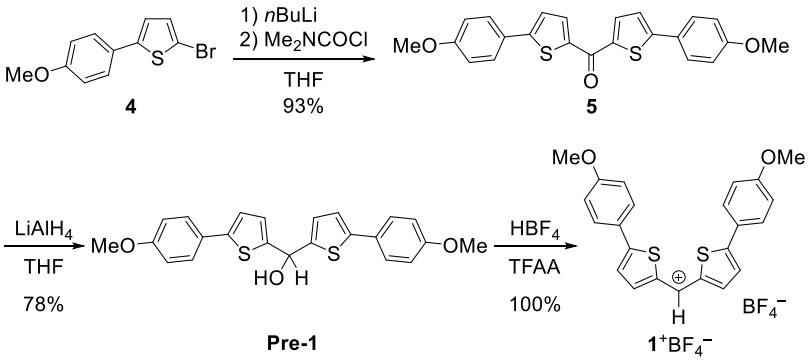

From bromide **4**, arylboronic acid pinacol ester **6** was derived in 89% yield over 2 steps, and then used for the Suzuki-Miyaura coupling reaction with 10-dibromomethylene-9-anthrone **7**[43] to give 10-diarylmethylene-9-anthrone **8** in 85% yield. Reduction of **8** with $NaBH_4$ in THF/EtOH gave **Pre-2a** in 94% yield. On the other hand, reaction of **8** with 2,4,6-trimethylphenyllithium (Mes-Li) in THF gave **Pre-2b** in 53% yield. Cationic salts $\mathbf{2a}^+BF_4^-$ and $\mathbf{2b}^+BF_4^-$ were prepared by treatment of the corresponding precursor alcohols **Pre-2a** and **Pre-2b** with HBF_4 in TFAA and isolated as stable deep-green solids in respective yields of 100% and 97% (Scheme 2-4).

Scheme 2-4. Preparation of **2a**$^{+}BF_4^{-}$ and **2b**$^{+}BF_4^{-}$.

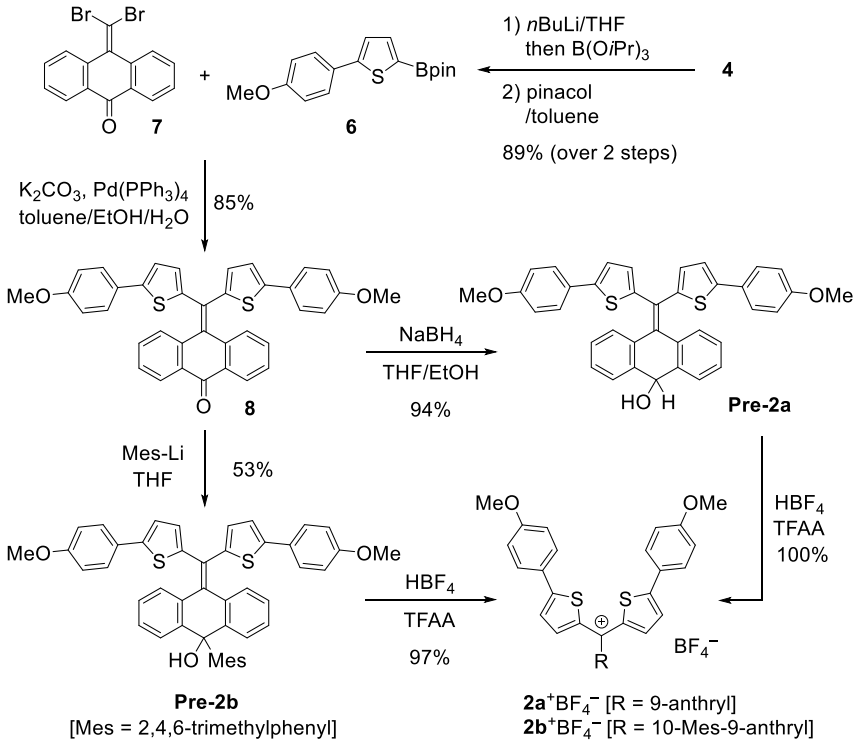

As designed, the newly prepared cationic salts exhibit strong absorptions in the NIR region with the end absorption reaching around 780 nm for **1**$^{+}BF_4^{-}$ and 850 nm for both **2a**$^{+}BF_4^{-}$ and **2b**$^{+}BF_4^{-}$ in MeCN [λ_{max} (log ε): 679 (4.95) for **1**$^{+}BF_4^{-}$, 703 (5.02) for **2a**$^{+}BF_4^{-}$, and 703 (5.02) for **2b**$^{+}BF_4^{-}$, respectively] (Figure 2-1). From the ^{13}C NMR of **1**$^{+}BF_4^{-}$, the alternation of positive charges was indicated along the polymethine chain of the DTM chromophore (Table 2-1), which is a characteristic feature of cyanine dyes.[45] The resonance contribution of Form C shown in Scheme 2-1b is indicated by the low-field shift of the signals assigned to the methoxyphenyl carbons at the meta (C_g) and ipso (C_i) positions of the OMe group, when compared to the non-charged reference compound (**1**$_2$), the generation of which will be shown later.

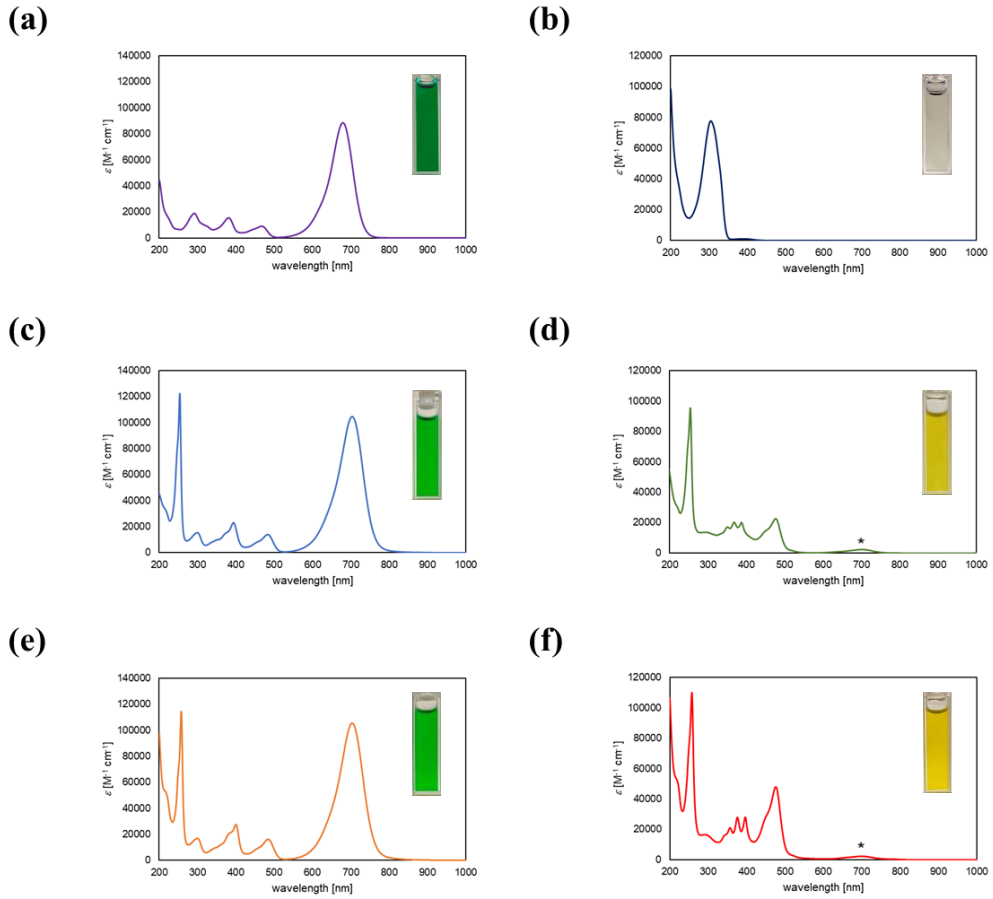

	λ_{max} [nm] (ε [M^{-1} cm^{-1}])
$\mathbf{1}^{+}BF_4^{-}$	292 (18300), 381 (15300), 467 (8900), 679 (88500)
$\mathbf{1}_2$	305 (78000)
$\mathbf{2a}^{+}BF_4^{-}$	254 (122000), 300 (15200), 393 (23000), 483 (13700), 703 (104000)
$\mathbf{2a}^{\bullet}$	254 (95000), 351 (17000), 368 (20000), 387 (20000), 476 (22600)
$\mathbf{2b}^{+}BF_4^{-}$	260 (118000), 305 (16000), 404 (28000), 493 (21000), 703 (105000)
$\mathbf{2b}^{\bullet}$	261 (119000), 359 (21000), 378 (28000), 399 (30000), 482 (63000)

Figure 2-1. UV-Vis-NIR spectra of (a) $\mathbf{1}^{+}BF_4^{-}$, (b) $\mathbf{1}_2$, (c) $\mathbf{2a}^{+}BF_4^{-}$, (d) $\mathbf{2a}^{\bullet}$, (e) $\mathbf{2b}^{+}BF_4^{-}$, and (f) $\mathbf{2b}^{\bullet}$ in MeCN. (*Slightly observed cation species due to an oxidation of radicals in the cuvette.)

Table 2-1. ^{13}C NMR chemical shifts[a,b] of $\mathbf{1}^+BF_4^-$ and the neutral reference compound ($\mathbf{1}_2$) in CD_3CN.

	$\mathbf{1}^+BF_4^-$	$\mathbf{1}_2$
a	147.82	50.19
b	140.13	145.96
c	154.03	127.82
d	130.03	122.66
e	175.20	143.81
f	125.10	127.72
g	131.69	127.65
h	116.62	115.39
i	166.13	160.40
j	56.88	56.04

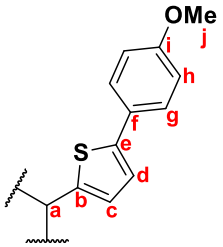

[a]Peaks were assigned based on 2D NMR spectroscopy [COSY (^1H-^1H), HSQC (^1H-^{13}C), HMBC (^1H-^{13}C). [b]Values are reported in reference to tetramethylsilane.

2-2-3. X-ray Structure of Cationic Salts of $\mathbf{1}^+$ and $\mathbf{2}^+$

According to X-ray analyses of the newly prepared cationic salts ($\mathbf{1}^+SbCl_6^-$, $\mathbf{2a}^+SbCl_6^-$, and $\mathbf{2b}^+BF_4^-$), the DTM units and two extra methoxyphenyl groups are located on nearly the same plane in all cases (Figure 2-2a,c,d), indicating effective conjugation over the four aromatic rings. The anthryl-type substituent at the methine carbon of the DTM unit is attached in a perpendicular manner in both $\mathbf{2a}^+$ and $\mathbf{2b}^+$, with twisting angles of 87.7° and 86.5°, respectively, showing only marginal electronic effects on the cationic π-skeleton.

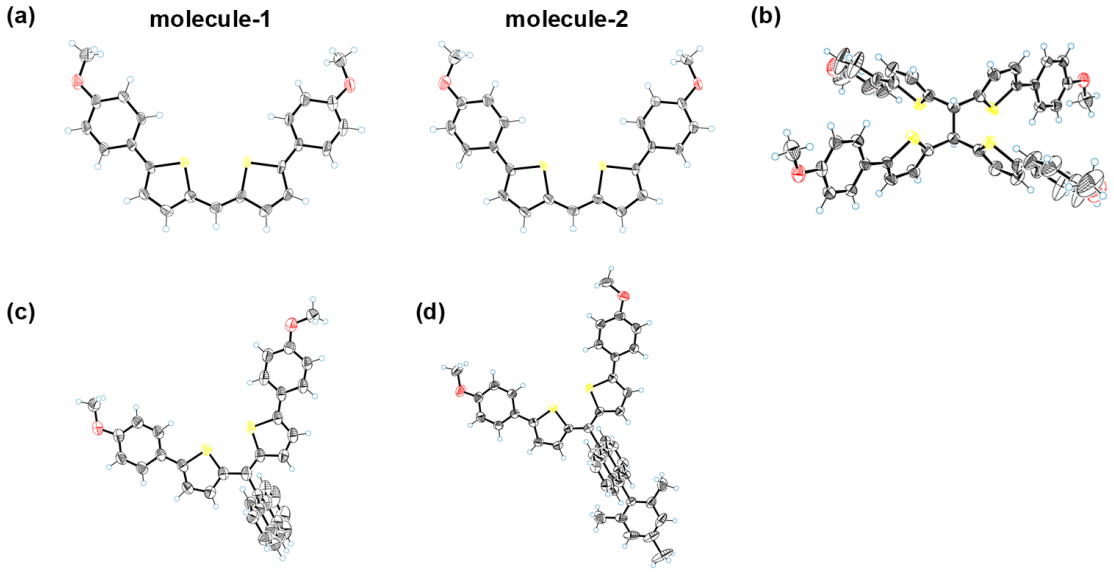

Figure 2-2. ORTEP drawings of (a) $\mathbf{1}^+$ (two crystallographically independent molecules), (b) $\mathbf{1}_2$, (c) $\mathbf{2a}^+$, and (d) $\mathbf{2b}^+$ in $\mathbf{1}^+SbCl_6^-$, $\mathbf{2a}^+SbCl_6^-$, and $\mathbf{2b}^+BF_4^-$ salts, respectively, obtained by X-ray analyses at 150 K.

The bond lengths were precisely determined for the salt of **2b**$^+$, and small estimated standard deviations of 0.002-0.003 Å allowed discussion of the significant disappearance of bond alternation (Table 2-2). When compared to the non-charged reference compound (**1**$_2$), bonds A, C, G and K are shortened while bonds B and D are elongated. Although the change in bond length is not clear for the aromatic hexagon (bonds H, I, and J), the above changes are in accord with the assumption of contribution from Form C shown in Scheme 2-1b. The significant difference between the two S-C bond lengths (shortened bond E and elongated bond F) can be explained by the contribution of Form B. By the geometrical analysis based on crystallography shown above, it is clear that the π-extended DTM units designed in this work have a typical cyanine-type π-electron conjugation.[45]

Table 2-2. Comparisons of bond lengths[a] in the DTM skeleton for cyanine (**2b**$^+$)[b] and the neutral reference compound (**1**$_2$)[c].

	2b$^+$	**1**$_2$	
A	1.406(2)	1.521(4)	1.507(5)
B	1.399(3)	1.348(5)	1.337(5)
C	1.374(3)	1.417(5)	1.419(6)
D	1.396(3)	1.363(5)	1.353(6)
E	1.721(2)	1.728(3)	1.730(4)
F	1.745(2)	1.728(3)	1.735(4)
G	1.447(3)	1.468(4)	1.474(5)
H	1.399(3) 1.400(3)	1.387(5) 1.410(4)	1.352(7) 1.378(6)
I	1.366(3) 1.382(3)	1.380(5) 1.387(5)	1.366(8) 1.388(7)
J	1.379(3) 1.387(3)	1.385(5) 1.388(5)	1.361(9) 1.367(8)
K	1.347(3)	1.373(4)	1.365(6)
L	1.447(3)	1.409(5)	1.430(10)

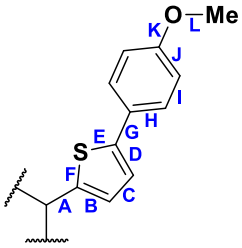

[a]Values were obtained by X-ray analyses at 150 K and are shown in Å. [b]Values for **2b**$^+$$BF_4^-$ salt (*C*2/*c*, Z = 4, molecule on the 2-fold axis). [c]Values for **1**$_2$•2CH_2Cl_2 (*P*2$_1$/*n*, Z = 2, molecule on the center of symmetry).

A noteworthy feature in these X-ray structures is the orientation of two thiophene rings in the DTM skeleton: both rings adopt a conformation with two S atoms facing each other (Form X in Scheme 2-5a). Such a conformation of Form X was also seen in the X-ray structures of other DTM derivatives,[38,39] so that terminal methoxyphenyl groups do not directly cause such a preference. Thus, the observed preference of Form X over Forms Y and Z could be explained by the general tendency of an all-trans preference[46–48] of the cyanine chains. Density functional theory (DFT) calculations[49] (B3LYP/6-31G*) indicated that Forms Y and Z are higher in energy by +1.09 and +3.13 kcal mol^{-1}, respectively. On the other hand, Form X is also a suitable

conformation for the transannular interaction[42,50,51] between two S atoms (Scheme 2-5b), which may also stabilize Form X but not Forms Y and Z.

Scheme 2-5. Conformation with two S atoms.

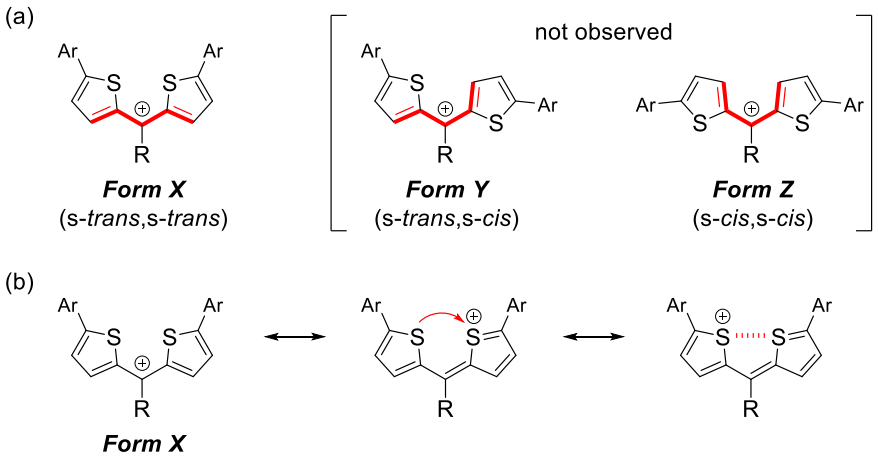

2-2-4. Redox and Electrochromic Behavior of $\mathbf{1}^+$

Voltammetric analysis of $\mathbf{1}^+BF_4^-$ in MeCN showed a cathodic peak at +0.12 V vs SCE. This reduction process to generate $\mathbf{1}^{\bullet}$ is electrochemically irreversible in the sense that the return peak corresponding to the oxidation of as-generated $\mathbf{1}^{\bullet}$ was absent in the first oxidation process (Figure 2-3a). Instead, a new peak appeared in the far anodic region (+0.68 V) at the second cycle, and the smaller current is due to dispersion. The latter peak was later assigned as the oxidation peak of σ-bonded dimer $\mathbf{1}_2$ (Scheme 2-2). Actually, upon treatment of $\mathbf{1}^+BF_4^-$ (0.04 M in MeCN) with Zn powder (20 equiv.), dimer $\mathbf{1}_2$ was isolated in 99% yield as a colorless solid, the structure of which was confirmed by X-ray analysis (Figure 2-2b and Table 2-2). The selective and quantitative dimerization of as-generated $\mathbf{1}^{\bullet}$ can be accounted for by the compact and semi-rigid skeleton of DTM with a sufficient spin density on the central methine carbon, as estimated by a DFT calculation [UB3LYP/6-31G*] (Figure 2-4). The newly formed C-C bond in dimer $\mathbf{1}_2$ has a normal bond length of 1.549(6) Å, which indicates negligible steric hinderance around this bond, thanks to the five-membered ring structure of thienyl groups.

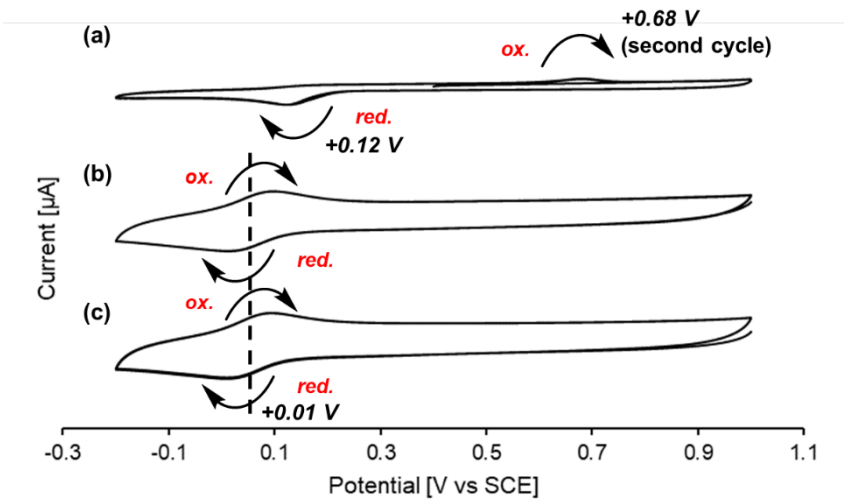

Figure 2-3. Cyclic voltammograms of (a) $\mathbf{1}^{+}BF_4^{-}$, (b) $\mathbf{2a}^{+}BF_4^{-}$, and (c) $\mathbf{2b}^{+}BF_4^{-}$ (1 mM) in MeCN containing 0.1 M Et_4NClO_4 as a supporting electrolyte (*E*/V vs SCE, scan rate 100 mV/s, Pt electrodes).

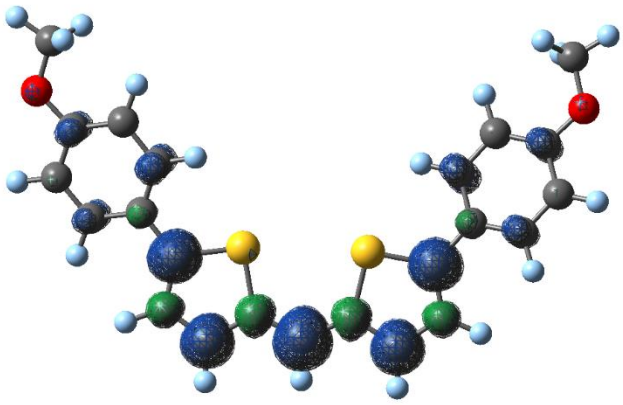

Figure 2-4. Spin density of $\mathbf{1}^{\bullet}$ calculated by a DFT method (UB3LYP/6-31G*) with an isovalue of 0.0035.

By considering that the oxidation process of $\mathbf{1}_2/\mathbf{1}^{+}$ is electrochemically irreversible (Figure 2-3a), mesolysis[52] of the central C-C bond would occur after 1e-oxidation of $\mathbf{1}_2$ (Scheme 2-6). The cleavage of the central C-C bond is an entropically favorable process and can be accounted for by DFT calculations of $\mathbf{1}_2$, for which the coefficients of HOMO-2 are certainly located on the central σ-bond (Figure 2-12). Since the generated $\mathbf{1}^{\bullet}$ is more easily oxidized than $\mathbf{1}_2$, subsequent 1e-oxidation would occur to form two molecules of $\mathbf{1}^{+}$. Actually, when $\mathbf{1}_2$ was treated with 2 equiv. of $(4\text{-}BrC_6H_4)_3N^{+\bullet}SbCl_6^{-}$ (magic blue, MB) in CH_2Cl_2, $\mathbf{1}^{+}SbCl_6^{-}$ was isolated in 98% yield.

Scheme 2-6. Oxidation process of $\mathbf{1}_2$.

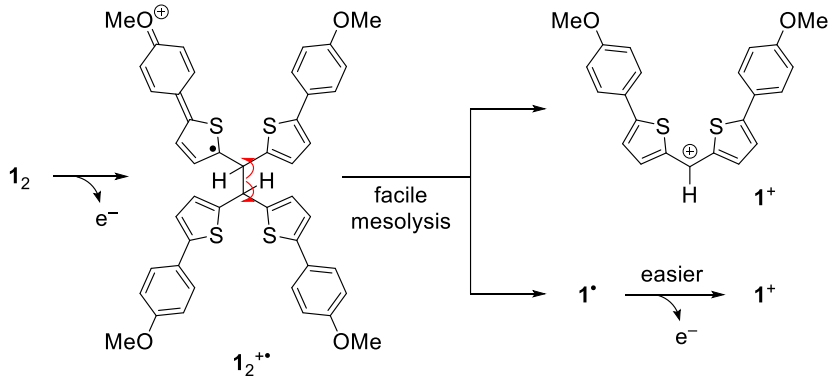

Based on the almost quantitative interconversion on a preparative scale and the large difference in the spectroscopic properties of $\mathbf{1}^+$ and $\mathbf{1}_2$ [λ_{max} (log ε): 306 (4.98)], electrochromic behavior was examined by following the reduction process of $\mathbf{1}^+$ and the oxidation process of as-prepared $\mathbf{1}_2$ by UV-Vis-NIR spectroscopy under the constant-current mode in MeCN (Figures 2-5). Isosbestic points were observed in both processes, showing clean interconversion between $\mathbf{1}^+$ and $\mathbf{1}_2$ as well as a negligible steady-state concentration of the intermediates ($\mathbf{1}^\bullet$ and $\mathbf{1}_2^{+\bullet}$). This is the first demonstration of electrochromism of an EM consisting of one cyanine dye, with a change in Vis-NIR absorption.

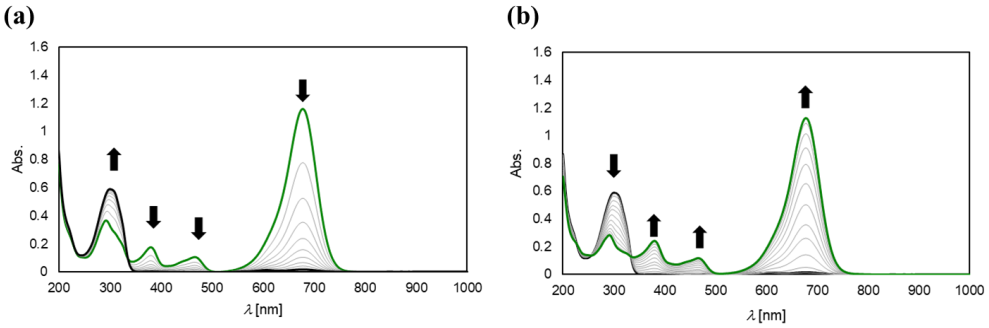

Figure 2-5. Changes in UV-Vis-NIR spectra of (a) $\mathbf{1}^+BF_4^-$ (13.1 μM) upon constant-current electrochemical reduction (5.0 μA, every 30 sec) and (b) as-prepared $\mathbf{1}_2$ upon constant-current electrochemical oxidation (20 μA, every 1 min), in MeCN containing 0.05 M Et_4NClO_4 as a supporting electrolyte.

2-2-5. Redox and Electrochromic Behavior of 2^+

In contrast to $\mathbf{1}^+BF_4^-$, the cyclic voltammograms of $\mathbf{2a}^+BF_4^-$ and $\mathbf{2b}^+BF_4^-$ showed a pair of reversible waves (Figure 2-3b,c) (half-wave potential: +0.01 and +0.01 V vs SCE, respectively), suggesting that the neutral radicals $\mathbf{2a}^\bullet$ and $\mathbf{2b}^\bullet$ are persistent in solution. To confirm the generations of neutral radical species, electron spin resonance (ESR) measurements were performed using reductive compounds obtained as brown solids from $\mathbf{2a}^+BF_4^-$ and $\mathbf{2b}^+BF_4^-$ by zinc powder in MeCN. The ESR spectra in CH_2Cl_2 showed three split lines with g = 2.0034 (Figure 2-6). The spectra of the solids obtained from $\mathbf{2a}^+BF_4^-$ and $\mathbf{2b}^+BF_4^-$ were explained by two equivalent ^{1}H nuclei with hyperfine coupling constants of $|a^H|$ = 0.51 and 0.48 mT, respectively. The experimental results indicated that the reductive species could be identified as neutral radical $\mathbf{2a}^\bullet$ and $\mathbf{2b}^\bullet$, since the DFT calculations showed the presence of large spin densities at the C3 positions of the both thienyl groups (Figure 2-7).[39] Further examination was conducted for the interconversion of $\mathbf{2b}^+$ and $\mathbf{2b}^\bullet$, for which the side reactions of the neutral radical are much less likely to occur.

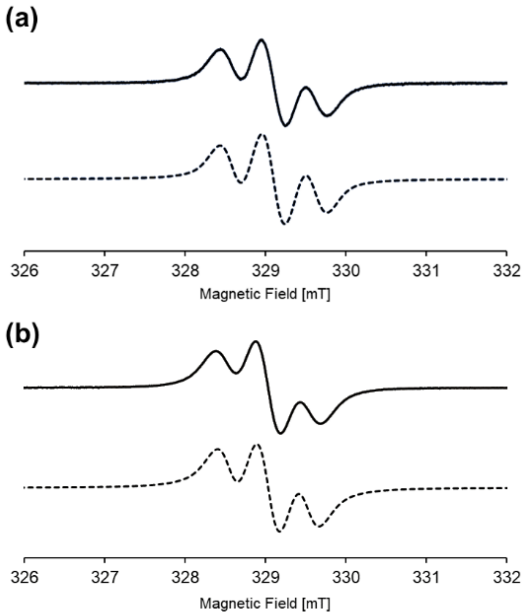

Figure 2-6. Observed (solid line) and simulated (dashed line) ESR spectra of (a) $\mathbf{2a}^\bullet$ and (b) $\mathbf{2b}^\bullet$ (1 mM) in CH_2Cl_2. Microwave frequency is 9.219848 GHz and 9.218638 GHz, respectively.

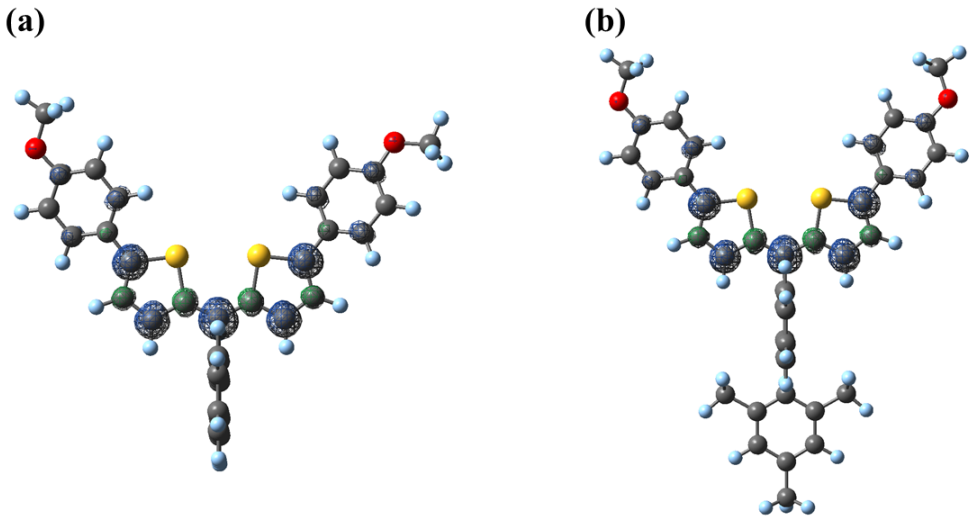

Figure 2-7. Spin density of (a) **2a**$^{\bullet}$ and (b) **2b**$^{\bullet}$ calculated by a DFT method (UB3LYP/6-31G*) with an isovalue of 0.0035.

The brown powder of **2b**$^{\bullet}$ obtained by Zn reduction in 98% yield is stable in solution and in the solid state. In accord with the reversible redox peaks, monocation was regenerated and isolated as $SbCl_6^-$ salt in 87% yield when the isolated solid of **2b**$^{\bullet}$ was treated with 1 equiv. of MB in CH_2Cl_2. Based on the clean interconversion on a preparative scale and the large difference in the spectroscopic properties of **2b**$^+$ and **2b**$^{\bullet}$ [λ_{max} (log ε): 477 (4.68)], electrochromic behavior was examined by following the reduction of **2b**$^+$ and the oxidation of as-prepared **2b**$^{\bullet}$ by UV-Vis-NIR spectroscopy (Figures 2-8). Isosbestic points were observed in both processes, showing clean interconversion between **2b**$^+$ and **2b**$^{\bullet}$. This is the first demonstration of electrochromism by the redox pair of a cationic cyanine dye and neutral radical, with a change in NIR absorption.

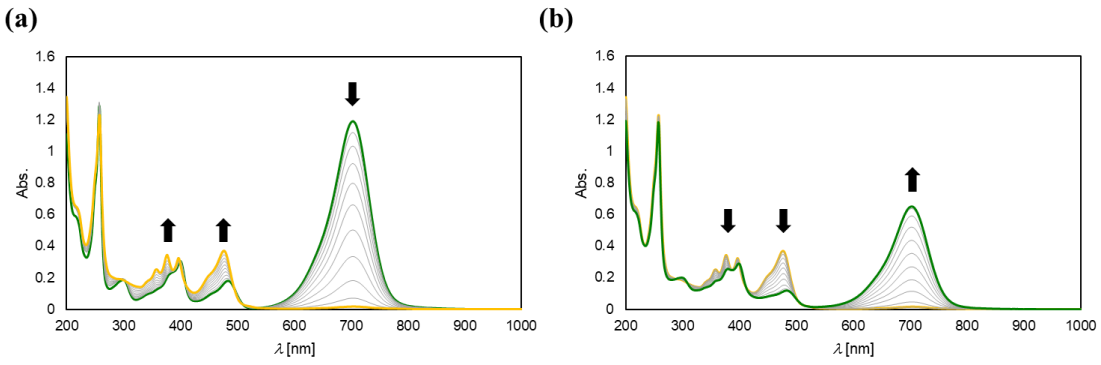

Figure 2-8. Changes in UV-Vis-NIR spectra of (a) **2b**$^+BF_4^-$ (13.5 μM) upon constant-current electrochemical reduction (20 μA, every 1 min) and (b) as-prepared **2b**$^{\bullet}$ upon constant-current electrochemical oxidation (20 μA, every 1 min), in MeCN containing 0.05 M Et_4NClO_4 as a supporting electrolyte.

2-3. Conclusion

In this work, the author newly designed π-extended DTM dyes $\mathbf{1}^+$ and $\mathbf{2}^+$ attached to two units of 4-methoxyphenyl groups at the 5,5'-positions. Based on ^{13}C NMR spectroscopy and X-ray analysis, alternation of positive charges along the polymethine chain as well as the significant disappearance of bond alternation were confirmed, which proves their cyanine-type conjugation. They exhibit strong absorption in the Vis-NIR region thanks to π-delocalization over the four aromatic rings. Through the stabilization effects on neutral radicals by a 5-(4-methoxyphenyl)-2-thienyl group, secondary radical $\mathbf{1}^{\bullet}$ selectively and cleanly converted into the dimer $\mathbf{1}_2$ even with a use of a diluted solution of 10^{-5} M, whereas tertiary radical $\mathbf{2b}^{\bullet}$ was isolated as a stable entity. With the redox pairs $\mathbf{1}_2/\mathbf{1}^+$ and $\mathbf{2b}^+/\mathbf{2b}^{\bullet}$, electrochromic interconversion was demonstrated. This work provides valuable guidelines for the molecular design of EM, which exhibits a change in absorption in the NIR region using only one unit of cyanine dye.

2-4. Experimental Section

2-4-1. General

All reactions were carried out under an argon atmosphere. All commercially available compounds were used without further purification unless otherwise indicated. Compounds **4**[53] and **7**[54] were synthesized according to the reported procedures. Dry MeCN was obtained by distillation from CaH_2 prior to use. Column chromatography was performed on silica gel 60N (KANTO KAGAKU, spherical neutral) of particle size 40–50 μm or Wakogel® 60N (neutral) of particle size 38-100 μm. ^{1}H and ^{13}C NMR spectra were recorded on a BRUKER Ascend™ 400 (^{1}H/400 MHz and ^{13}C/100 MHz) spectrometer or a JEOL ECA600 (^{1}H/600 MHz and ^{13}C/151 MHz) spectrometer. ESR spectra were recorded on a JEOL JES-FE2XG spectrometer. IR spectra were measured on a Shimadzu IRAffinity-1S spectrophotometer using the attenuated total reflection (ATR) mode. Mass spectra were recorded on a JEOL JMS-T100GCV spectrometer in FD mode (GC-MS&NMR Laboratory, Research Faculty of Agriculture, Hokkaido University). Melting points were measured on a Stanford Research Systems MPA100 Optimelt and are uncorrected. UV-Vis-NIR spectra were recorded on a Hitachi U-2910 spectrophotometer. Redox potentials (E^{ox} and E^{red}) were measured on a BAS ALS-612EX by cyclic voltammetry. Pt electrodes were used as the working (disk) and counter electrodes. The working electrode was polished using a water suspension of aluminum oxide (0.05 μm) before use. DFT calculations were performed with the Gaussian 16 W program package.[55] The geometries of the compounds were optimized by using the (U)B3LYP method in combination with the 6-31G(d) basis set. Single-crystal X-ray structure analyses were performed by a Rigaku XtaLAB Synergy (Cu-Kα radiation, λ = 1.54184 Å) with HyPix diffractometer. Using Olex2,[56] the structure was solved with the SHELXT[57] structure solution program using Intrinsic Phasing and refined with the SHELXL[58] refinement package using Least Squares minimization. All the hydrogen atoms were located at the calculated positions and refined with riding.

2-4-2. Preparations

Synthesis of dithienylketone 5

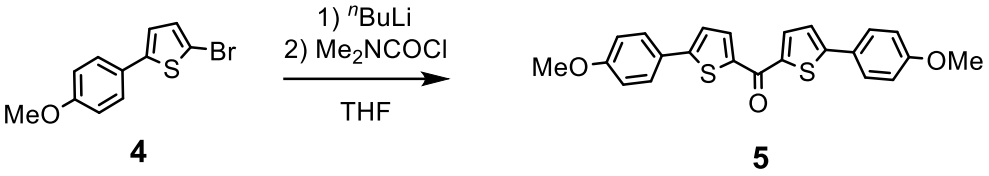

To a solution of 2-bromo-5-(4-methoxyphenyl)thiophene **4** (1.76 g, 6.53 mmol) in dry THF (30 mL) was added ^{n}BuLi (1.58 M in hexane, 4.35 mL, 6.87 mmol) dropwise over 15 min at -78 °C. After stirring at -78 °C for 1 h, *N*, *N*-dimethylcarbamoyl chloride (0.30 mL, 3.26 mmol) was added to the suspension at -78 °C. The reaction mixture was stirred for 10 min at -78 °C and for another 25 h at 26 °C, then quenched with 1M-HCl aq. The precipitates were collected by filtration, washed with Et_2O and EtOH, and dried in vacuo to give ketone **5** as a yellow solid in 93% yield.

Mp 259-260 °C; ^{1}H NMR (400 MHz, 1,1,2,2-tetrachloroethane-d_2): δ/ppm = 7.92 (2H, d, J = 3.6 Hz), 7.70 (4H, d, J = 8.6 Hz), 7.35 (2H, d, J = 3.8 Hz), 7.02 (4H, d, J = 8.6 Hz), 3.91 (6H, s); ^{13}C NMR (100 MHz, 1,1,2,2-tetrachloroethane-d_2): δ/ppm = 178.09, 160.48, 152.60, 140.65, 134.41, 127.86, 126.03, 123.20, 114.76, 55.71; IR (ATR): ν/cm^{-1} = 3389, 2954, 2837, 2544, 2495, 1603, 1579, 1532, 1507, 1468, 1433, 1338, 1308, 1290, 1253, 1205, 1179, 1134, 1111, 1064, 1025, 958, 834, 826, 819, 805, 786, 725, 677, 631; LR-MS (FD) m/z (%): 408.02 (13), 407.02 (29), 406.02 (bp, M^{+}); HR-MS (FD) Calcd. for $C_{23}H_{18}O_3S_2$: 406.06974; Found: 406.06815.

Synthesis of pre-1

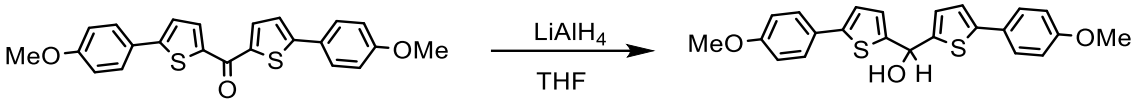

5 **Pre-1**

To a solution of ketone **5** (1.20 g, 2.95 mmol) in dry THF (150 mL) was added $LiAlH_4$ (336 mg, 8.85 mmol) at 0 °C. After stirring at 23 °C for 2 h, the reaction was quenched with water (100 mL) at 0 °C. The mixture was filtered through a Celite pad with EtOAc as eluent, and the filtrate was extracted with EtOAc. The combined organic layers were washed with water, brine, and dried over anhydrous sodium sulfate. After filtration, the organic solvent was evaporated under reduced pressure. The resulting solid was washed with Et_2O (10 mL) using an ultrasonic bath. The precipitates were collected by filtration and washed with Et_2O (5.0 mL) to give alcohol **Pre-1** as a white solid in 78% yield.

Mp 206-208 °C (decomp.); ^{1}H NMR (400 MHz, $CDCl_3$): δ/ppm = 7.51 (4H, dd, *J* = 2.1, 4.6 Hz), 7.07 (2H, d, *J* = 3.7 Hz), 7.01 (2H, dd, *J* = 0.90, 3.7 Hz), 6.90 (4H, dd, *J* = 2.1, 6.7Hz), 6.25 (1H, d, *J* = 4.3 Hz), 3.83 (6H, s), 2.53 (1H, d, *J* = 4.4 Hz); ^{13}C NMR (100 MHz, $CDCl_3$): δ/ppm = 159.47, 145.34, 144.76, 127.30, 127.22, 126.14, 121.67, 114.44, 69.09, 55.51; IR (ATR) : *v*/cm^{-1} = 3570, 3375, 2836, 1605, 1571, 1544, 1511, 1467, 1440, 1414, 1363, 1313, 1282, 1248, 1180, 1110, 1047, 1030, 996, 958, 881, 831, 820, 800, 757, 656, 631; LR-MS (FD) m/z (%): 410.13 (13), 409.13 (28), 408.13 (bp, M^+); HR-MS (FD) Calcd. for $C_{23}H_{20}O_3S_2$: 408.08539; Found: 408.08713.

Synthesis of pinacol borane 6

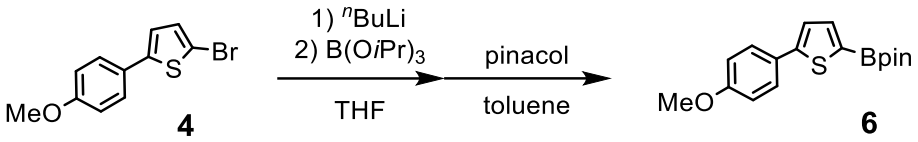

To a solution of **4** (7.48 g, 27.8 mmol) in dry THF (224mL) was added ^{n}BuLi (1.55 M in hexane, 21.2 mL, 33.3 mmol) dropwise over 30 min at -78 °C. After stirring at -78 °C for 1.5 h, triisopropyl borate (12.7 mL, 55.6 mmol) was added to the suspension at -78 °C. The mixture was stirred for 1 h at -78 °C and for another 1 h at 24 °C. After quenching with saturated NH_4Cl aq., the mixture was stirred for 30 min at 24 °C. The organic layer was collected and the aqueous layer was extracted with EtOAc three times. The combined organic layers were washed with water and brine, and dried over anhydrous sodium sulfate. After filtration, the solvent was concentrated under reduced pressure to give a crude product as a green solid.

To a solution of the crude product in toluene (334 mL) was added pinacol (3.94 g, 33.3 mmol) at 24 °C and the mixture was stirred for 16 h. After diluting with water, the organic layer was collected and the aqueous layer was extracted with EtOAc three times. The combined organic layers were washed with water and brine, and dried over anhydrous sodium sulfate. After filtration, the solvent was concentrated under reduced pressure and the resulting residue was dried in vacuo to give compound **6** as a pale green solid in 89 % yield.

Mp 108-109 °C; ^{1}H NMR (400 MHz, $CDCl_3$): δ/ppm = 7.57 (2H, d, *J* = 8.7 Hz), 7.57 (1H, d, *J* = 3.6 Hz), 7.27 (1H, d, *J* = 3.6 Hz), 6.91 (2H, d, *J* = 8.7 Hz), 3.83 (3H, s), 1.36 (12H, s); ^{13}C NMR (100 MHz, $CDCl_3$): δ/ppm = 159.69, 151.46, 138.34, 127.57, 127.27, 123.64, 114.46, 84.17, 55.46, 24.89; IR (ATR) : ν/cm^{-1} = 3004, 2974, 2938, 2838, 2041, 1610, 1572, 1538, 1511, 1456, 1442, 1379, 1370, 1356, 1337, 1312, 1284, 1270, 1246, 1246, 1210, 1179, 1136, 1113, 1075, 1030, 1017, 961, 952, 851, 831, 818, 800, 777, 685, 674, 659, 631, 587, 536, 511, 494, 442, 419; LR-MS (FD) m/z (%): 318.14 (7), 317.14 (21), 316.14 (bp, M^{+}), 315.14 (24); HR-MS (FD) Calcd. for $C_{17}H_{21}BOS$: 315.13408; Found: 315.13298.

Synthesis of ketone 8

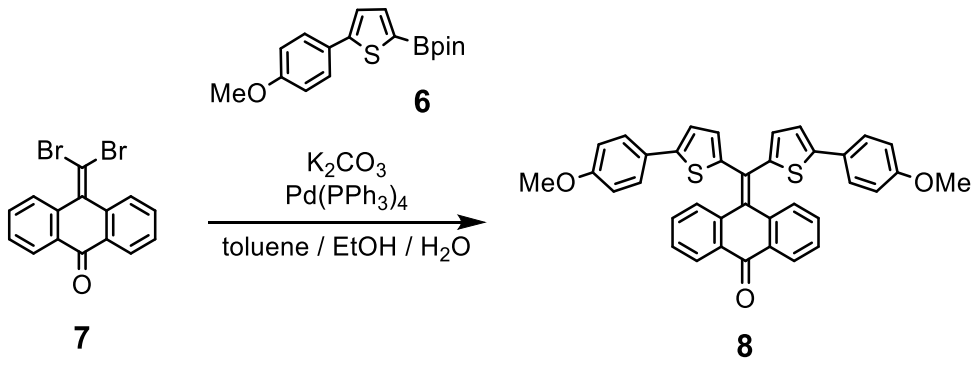

A mixture of 10-dibromomethylene-9-anthrone **7** (220 mg, 0.604 mmol), arylboronic acid pinacol ester **6** (572 mg, 1.81 mmol), K_2CO_3 (334 mg, 2.42 mmol), and $Pd(PPh_3)_4$ (70.0 mg, 60.4 μmol) in toluene (20 mL), EtOH (2.0 mL), and H_2O (2.0 mL) was refluxed for 9 h. After cooling to 23 °C, the mixture was diluted with water (40 mL) and extracted with EtOAc (60 mL × 3). The combined organic layers were washed with water and brine, and dried over anhydrous sodium sulfate. After filtration, the solution was evaporated under reduced pressure. The crude product was purified by a Al_2O_3 column using CH_2Cl_2/hexane = 1:2 containing 0.5% of Et_3N as eluent (R_f = 0.37) to give compound **8** as a black solid in 85% yield.

Mp 93-95 °C (decomp.); ^{1}H NMR (400 MHz, 1,1,2,2-tetrachloroethane-d_2): δ/ppm = 8.22 (2H, d, J = 7.2 Hz), 7.68 (2H, d, J = 7.9 Hz), 7.55 (4H, d, J = 8.8 Hz), 7.45 (2H, t, J = 7.5 Hz), 7.34 (2H, t, J = 7.1 Hz), 7.16 (2H, d, J = 3.7 Hz), 6.96-6.94 (6H, m), 3.87 (6H, s); ^{13}C NMR (100 MHz, $CDCl_3$): δ/ppm = 185.65, 159.64, 146.95, 143.26, 139.21, 133.72, 132.61, 131.29, 131.04, 130.46, 128.76, 127.91, 127.09, 126.84, 126.71, 122.22, 114.45, 55.49; IR (ATR): ν/cm^{-1} = 3065, 2834, 1661, 1633, 1593, 1571, 1534, 1503, 1458, 1433, 1288, 1247, 1175, 1111, 1029, 956, 931, 890, 828, 793, 777, 694, 617; LR-MS (FD) m/z (%): 585.17 (6), 584.17 (19), 583.17 (43), 582.17 (bp, M^+); HR-MS (FD) Calcd. for $C_{37}H_{26}O_3S_2$: 582.13234; Found: 582.13403.

Synthesis of Pre-2a

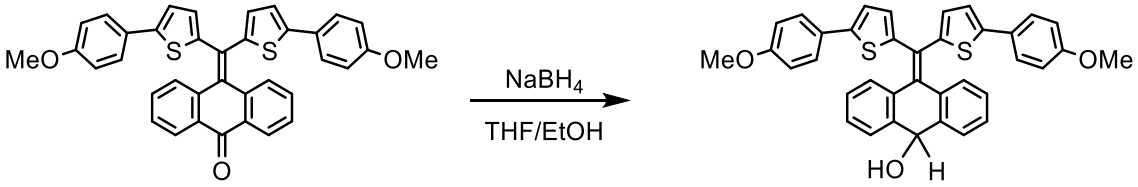

8 **Pre-2a**

To a solution of **8** (150 mg, 0.257 mmol) in THF (10 mL) and EtOH (10 mL) was added $NaBH_4$ (41.0 mg, 1.08 mmol) at 24 °C. After stirring at 24 °C for 15 h, the mixture was diluted with water (20 mL) and extracted with EtOAc (60 mL × 3). The combined organic layers were washed with water and brine, and dried over anhydrous sodium sulfate. After filtration, the solution was evaporated under reduced pressure. The crude product was washed with a mixed solvent of hexane (10 mL) and CH_2Cl_2 (3.0 mL) using an ultrasonic bath. The precipitates were collected by filtration and washed with hexane (10 mL) to give alcohol **Pre-2a** as a yellow solid in 94% yield.

Mp 124-128 °C (decomp.); ^{1}H NMR (400 MHz, $CDCl_3$): δ/ppm = 7.65 (2H, d, J = 7.6 Hz), 7.46-7.44 (6H, m), 7.25-7.23 (2H, m), 7.06 (2H, t, J = 7.5 Hz), 7.01 (2H, d, J = 3.6 Hz), 6.89-6.85 (6H, m), 5.72 (1H, d, J = 7.7 Hz), 3.81 (6H, s), 2.26 (1H, d, J = 7.8 Hz); ^{13}C NMR (100 MHz, $CDCl_3$): δ/ppm = 159.33, 144.95, 142.08, 140.71, 136.95, 136.04, 129.50, 128.32, 127.33, 127.19, 127.02, 126.60, 125.41, 124.00, 121.72, 114.35, 70.65, 55.47; IR (ATR): ν/cm^{-1} = 3397, 3062, 3030, 2997, 2834, 2550, 2047, 1765, 1607, 1572, 1537, 1501, 1450, 1440, 1417, 1378, 1334, 1308, 1288, 1247, 1199, 1176, 1126, 1111, 1093, 1030, 952, 891, 829, 800, 751, 732, 667, 650; LR-MS (FD) m/z (%): 587.18 (6), 586.16 (20), 585.17 (44), 584.16 (bp, M^+); HR-MS (FD) Calcd. for $C_{37}H_{28}O_3S_2$: 584.14799; Found: 584.14891.

Synthesis of Pre-2b

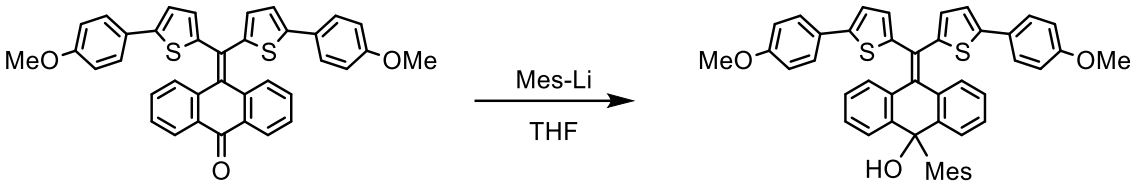

8 **Pre-2b**

To a solution of 2-bromomesitylene (0.300 mL, 2.06 mmol) in dry THF (5.0 mL) was added ^{n}BuLi (1.56 M in hexane, 1.26 mL, 1.96 mmol) dropwise over 3 min at -78 °C. After stirring at -78 °C for 0.5 h, a solution of ketone **8** (300 mg, 0.515 mmol) in dry THF (7.0 mL) was added to the suspension and stirred for 1 h at 24 °C. The reaction was quenched by water (20 mL), and the resulting mixture was extracted with EtOAc (60 mL × 3). The combined organic layers were washed with water and brine, and dried over anhydrous sodium sulfate. After filtration, the solution was evaporated under reduced pressure. The crude product was purified by a silica-gel column using EtOAc /hexane = 1:4 as eluent (R_f = 0.29) to give compound **Pre-2b** as a yellow solid in 53% yield.

Mp 120-122 °C (decomp.); ^{1}H NMR (400 MHz, $CDCl_3$): δ/ppm = 7.51 (2H, d, *J* = 7.5 Hz), 7.45 (4H, d, *J* = 8.8 Hz), 7.05-7.00 (8H, m), 6.86 (6H, t, *J* = 4.4 Hz), 6.82 (2H, d, *J* = 3.7 Hz), 3.81 (6H, s) , 2.41 (1H, s) , 2.32 (3H, s) , 1.93 (6H, s); ^{13}C NMR (100 MHz, $CDCl_3$): δ/ppm = 159.30, 144.91, 144.33, 143.03, 138.33, 138.21, 136.91, 136.44, 135.38, 131.72, 129.18, 128.74, 127.51, 127.31, 127.02, 126.53, 126.14, 125.45, 121.78, 114.34, 80.84, 55.47, 24.39, 20.76; IR (ATR): ν/cm^{-1} = 3565, 3485, 2931, 2833, 2544, 2293, 2049, 1880, 1756, 1607, 1572, 1537, 1505, 1460, 1439, 1378, 1288, 1246, 1175, 1111, 1030, 951, 901, 852, 828, 801, 767, 737, 686, 661, 644, 636, 618; LR-MS (FD) m/z (%): 706.22 (4), 705.22 (10), 704.22 (25), 703.22 (54), 702.21 (bp, M^+); HR-MS (FD) Calcd. for $C_{46}H_{38}O_3S_2$: 702.22624; Found: 702.22498.

Synthesis of $1^{+}BF_4^{-}$

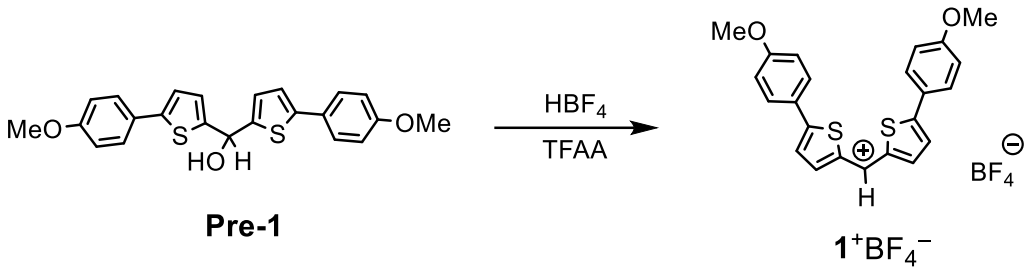

Pre-1 $\qquad$ $\mathbf{1}^{+}BF_4^{-}$

To a solution of alcohol **Pre-1** (16.9 mg, 41.3 μmol) in trifluoroacetic anhydride (2.0 mL) was added 42%-HBF_4 aq. (0.03 mL, 207 μmol) at 0 °C. After stirring at 23 °C for 1 h, the addition of dry Et_2O (7.0 mL) led to precipitation of the cation salt. The precipitates were collected and washed with dry Et_2O (7.0 mL× 2), and dried *in vacuo* to give $\mathbf{1}^{+}BF_4^{-}$ as a green solid in 100% yield.

Mp 171-172 °C; ^{1}H NMR (600 MHz, CD_3CN): δ/ppm = 8.43 (1H, s), 8.00 (2H, s), 7.74 (4H, d, J = 5.6 Hz), 7.64 (2H, s), 6.94 (4H, d, J = 5.5 Hz), 3.85 (6H, s); ^{13}C NMR (151 MHz, CD_3CN): δ/ppm = 175.20, 166.13, 154.03, 147.82, 140.13, 131.69, 130.03, 125.10, 116.62, 56.88; IR (ATR, with KBr): ν/cm^{-1} = 3089, 3015, 2943, 2847, 2366, 1598, 1553, 1454, 1412, 1310, 1262, 1178, 1150, 1115, 1100, 1046, 1016, 955, 827, 798, 707, 686, 651, 627, 596; LR-MS (FD) m/z (%): 393.05 (14), 392.05 (32), 391.05 (bp, M^{+}); HR-MS (FD) Calcd. for $C_{23}H_{19}O_2S_2$: 391.08265; Found: 391.08164.

Synthesis of $2a^{+}BF_4^{-}$

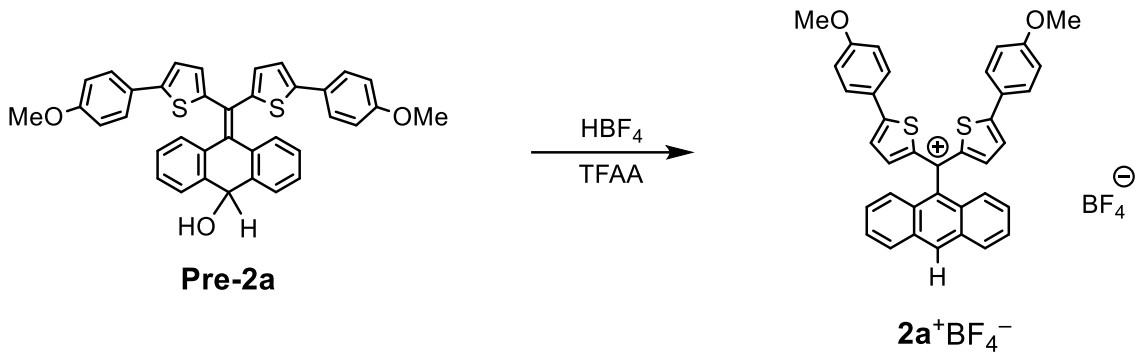

Pre-2a $\qquad$ $\mathbf{2a}^{+}BF_4^{-}$

To a solution of alcohol **Pre-2a** (24.2 mg, 41.3 μmol) in trifluoroacetic anhydride (2.0 mL) was added 42%-HBF_4 aq. (0.03 mL, 207 μmol) at 0 °C. After stirring at 22 °C for 1 h, the addition of dry Et_2O (7.0 mL) led to precipitation of the cation salt. The precipitates were collected and washed with dry Et_2O (7.0 mL× 2), and dried *in vacuo* to give $\mathbf{2a}^{+}BF_4^{-}$ as a purple solid in 100% yield.

Mp 151-156 °C (decomp.); ^{1}H NMR (400 MHz, CD_3CN): δ/ppm = 8.96 (1H, s), 8.27 (2H, d, J = 8.5 Hz), 7.94 (4H, br-s), 7.81 (4H, d, J = 8.6 Hz), 7.63-7.54 (6H, m), 7.12 (4H, d, J = 8.5 Hz) , 3.94 (6H, s); ^{13}C NMR could not be recorded due to its poor solubility.: IR (ATR, with KBr): ν/cm^{-1} = 3195, 3106, 2843, 2587, 1591, 1522, 1496, 1460, 1446, 1415, 1356, 1307, 1260, 1146, 1072, 1012, 961, 796, 760, 738, 714, 688, 648, 630, 608; LR-MS (FD) m/z (%): 570.10 (6), 569.10 (20), 568.10 (45), 567.10 (bp, M^+); HR-MS (FD) Calcd. for $C_{37}H_{27}O_2S_2$: 567.14525; Found: 567.14495.

Synthesis of $2b^{+}BF_4^{-}$

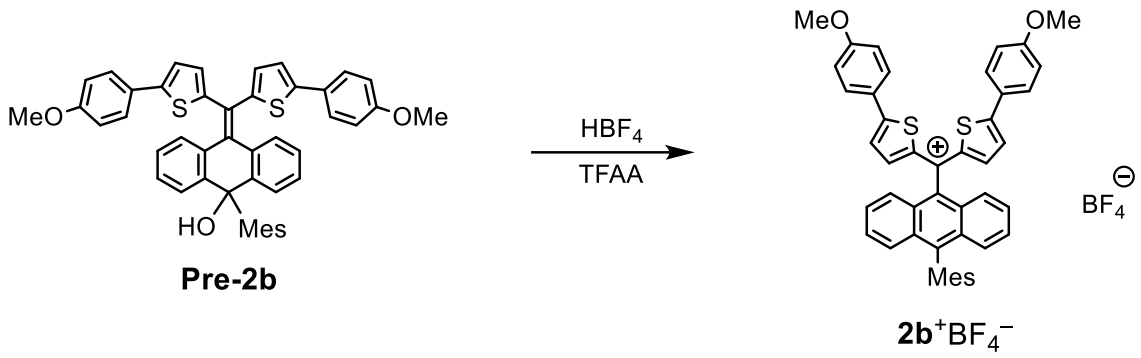

Pre-2b **$2b^{+}BF_4^{-}$**

To a solution of alcohol **Pre-2b** (29.0 mg, 41.3 μmol) in trifluoroacetic anhydride (2.0 mL) was added 42%-HBF_4 aq. (0.03 mL, 207 μmol) at 0 °C. After stirring at 25 °C for 1 h, the addition of dry Et_2O (7.0 mL) led to precipitation of the cation salt. The precipitates were collected and washed with dry Et_2O (7.0 mL× 2), and dried *in vacuo* to give **$2b^{+}BF_4^{-}$** as a green solid in 97% yield.

Mp 186-189 °C (decomp.); ^{1}H NMR (400 MHz, CD_3CN): δ/ppm = 7.98 (4H, br-s), 7.90-7.84 (5H, m), 7.60-7.47 (7H, m), 7.25 (2H, s), 7.14 (4H, d, J = 8.6 Hz), 3.95 (6H, s), 2.51 (3H, s), 1.84 (6H, s); ^{13}C NMR could not be recorded due to its poor solubility.; IR (ATR, with KBr): ν/cm^{-1} = 3104, 3075, 2949, 2914, 2844, 2626, 1762, 1592, 1560, 1523, 1498, 1466, 1438, 1354, 1304, 1264, 1145, 1067, 1052, 1012, 953, 907, 870, 842, 819, 797, 763, 725, 698, 683, 673, 650, 610; LR-MS (FD) m/z (%): 688.16 (9), 687.16 (24), 686.16 (55), 685.16 (bp, M^+); HR-MS (FD) Calcd. for $C_{46}H_{37}O_2S_2$: 685.22350; Found: 685.22537.

Synthesis of $\mathbf{1}_2$

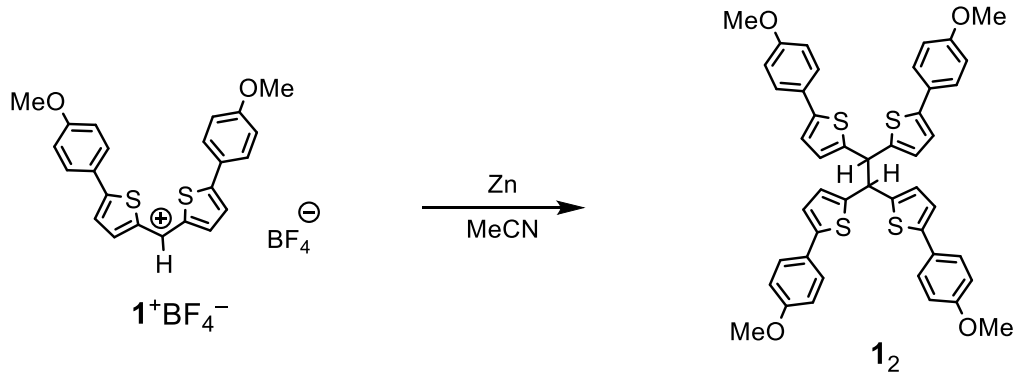

To a solution of $\mathbf{1}^+BF_4^-$ (100 mg, 0.209 mmol) in dry MeCN (5.0 mL) was added Zn powder (273 mg, 4.18 mmol). After stirring at 23 °C for 10 min, the mixture was diluted with water (10 mL) and extracted with CH_2Cl_2 (20 mL × 3). The combined organic layers were washed with water and brine, and dried over anhydrous sodium sulfate. After filtration, the solution was evaporated under reduced pressure. The crude product was washed with hexane (5.0 mL) using an ultrasonic bath. The precipitates were collected by filtration and washed with hexane (5.0 mL) to give σ-dimer $\mathbf{1}_2$ as a white solid in 99% yield.

Mp 182-183 °C; ^{1}H NMR (600 MHz, CD_3CN): δ/ppm = 7.44 (8H, d, J = 8.8 Hz), 6.99 (4H, d, J = 3.6 Hz), 6.96 (4H, d, J = 3.9 Hz), 6.89 (8H, d, J = 8.9 Hz), 5.30 (2H, s), 3.77 (12H, s); ^{13}C NMR (151 MHz, CD_3CN): δ/ppm = 160.40, 145.96, 143.81, 127.82, 127.72, 127.65, 122.66, 115.39, 56.04, 50.19 ; IR (ATR): ν/cm^{-1} = 3069, 3001, 2956, 2902, 2833, 1605, 1570, 1546, 1507, 1460, 1438, 1417, 1288, 1247, 1175, 1109, 1029, 953, 828, 793, 753, 719, 694, 650, 630, 592; LR-MS (FD) m/z (%): 786.21 (4), 785.22 (13), 784.22 (32), 783.22 (51), 782.22 (92, M^+), 394.12 (11), 393.12 (31), 392.12 (99), 391.11 (bp); HR-MS (FD) Calcd. for $C_{46}H_{38}O_4S_4$: 782.16529; Found: 782.16669.

Oxidation of $\mathbf{1}_2$

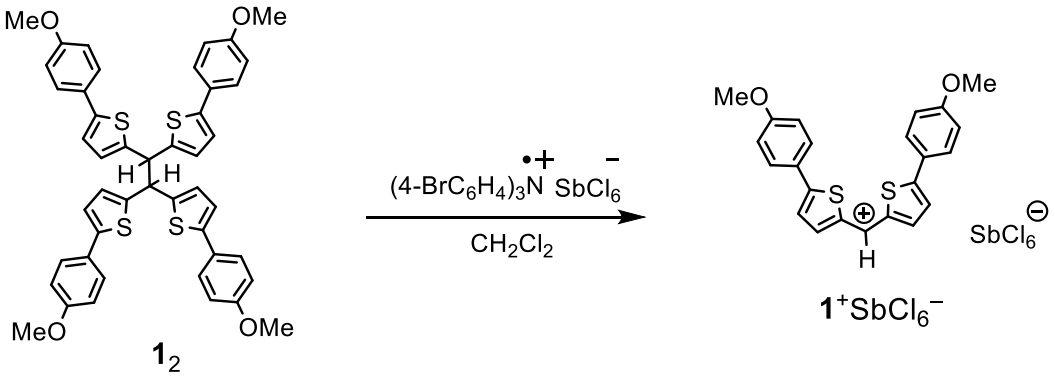

To a solution of σ-dimer $\mathbf{1}_2$ (32.3 mg, 41.3 μmol) in dry CH_2Cl_2 (3.0 mL) was added tris(4-bromophenyl)aminium hexachloroantimonate (67.4 mg, 82.6 μmol). After stirring at 23 °C for 1 h, the addition of dry Et_2O (7.0 mL) led to precipitation of the cation salt. The precipitates were collected and washed with dry Et_2O (7.0 mL× 2), and dried *in vacuo* to give $\mathbf{1}^+SbCl_6^-$ as a green solid in 98% yield.

Mp 213-214 °C; ^{1}H NMR and ^{13}C NMR spectra are identical to those of $\mathbf{1}^+BF_4^-$; IR (ATR, with KBr): ν/cm^{-1} = 3190, 3091, 3023, 2973, 2938, 2841, 2624, 2580, 2362, 1591, 1551, 1517, 1450, 1398, 1356, 1309, 1264, 1169, 1139, 1073, 1019, 953, 890, 832, 794, 746, 704, 689, 656, 624, 608; LR-MS (FD) m/z (%): 393.08 (14), 392.09 (29), 391.09 (bp, M^+); HR-MS (FD) Calcd. for $C_{23}H_{19}O_2S_2$: 391.08265; Found: 391.08220.

Reduction of $2a^+BF_4^-$

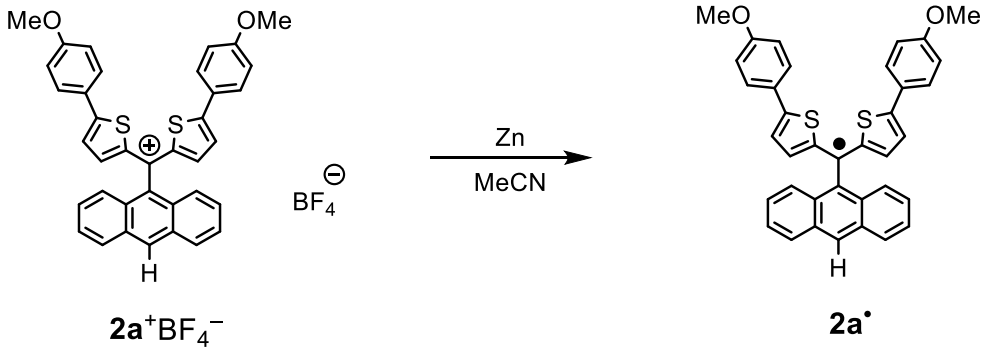

$2a^+BF_4^-$ $2a^{\bullet}$

To a solution of $2a^+BF_4^-$ (80.0 mg, 122 μmol) in degassed dry MeCN (5.0 mL) was added Zn powder (160 mg, 2.44 mmol) at 24 °C. After stirring at 24 °C for 20 min, the mixture was diluted with water (10 mL) and extracted with degassed CH_2Cl_2 (20 mL × 2). The combined organic layers were washed with water and dried over anhydrous sodium sulfate. After filtration, the solvent was evaporated under reduced pressure and the resulting residue was dried in vacuo to give $2a^{\bullet}$ as a brown solid in 96% yield.

Mp 133-139 °C (decomp.); IR (ATR): ν/cm^{-1} = 3054, 2956, 2931, 2834, 2554, 2292, 2050, 1599, 1576, 1538, 1501, 1436, 1373, 1289, 1248, 1174, 1162, 1110, 1084, 1029, 956, 887, 827, 792, 735, 657, 627, 612; LR-MS (FD) m/z (%): 570.11 (7), 569.11 (21), 568.11 (50), 567.11 (bp, M^+); HR-MS (FD) Calcd. for $C_{37}H_{27}O_2S_2$: 567.14525; Found: 567.14659.

Reduction of $2b^{+}BF_4^{-}$

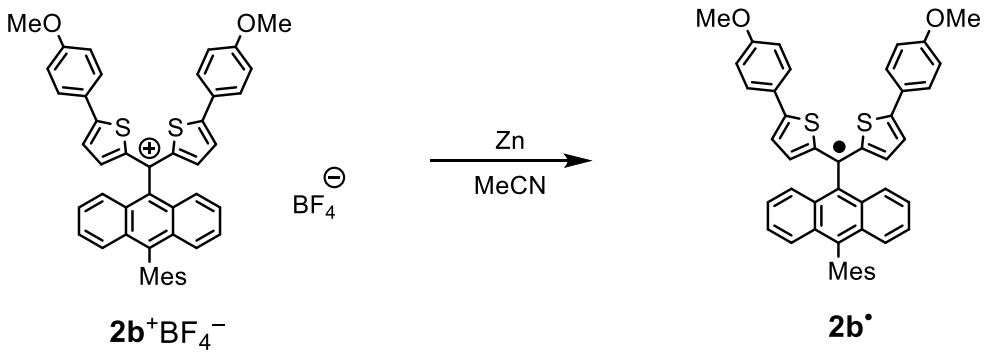

$2b^{+}BF_4^{-}$ $2b^{\bullet}$

To a solution of $2b^{+}BF_4^{-}$ (50.0 mg, 64.7 μmol) in degassed dry MeCN (5.0 mL) was added Zn powder (84.0 mg, 1.29 mmol) at 26 °C. After stirring at 26 °C for 20 min, the mixture was diluted with water (10 mL) and extracted with degassed CH_2Cl_2 (20 mL × 2). The combined organic layers were washed with water and dried over anhydrous sodium sulfate. After filtration, the solvent was evaporated under reduced pressure and the resulting residue was dried in vacuo to give $2b^{\bullet}$ as a brown solid in 97% yield.

Mp 171-173 °C (decomp.); IR (ATR): ν/cm^{-1} = 3067, 2996, 2932, 2912, 2835, 2047, 1729, 1656, 1598, 1568, 1517, 1481, 1461, 1437, 1373, 1305, 1287, 1245, 1177, 1157, 1111, 1081, 1067, 1023, 958, 908, 852, 820, 778, 759, 656, 612; LR-MS (FD) m/z (%): 688.16 (10), 687.16 (26), 686.16 (54), 685.16 (bp, M^{+}); HR-MS (FD) Calcd. for $C_{46}H_{37}O_2S_2$: 685.22350; Found: 685.22447.

Synthesis of $2a^{+}SbCl_6^{-}$

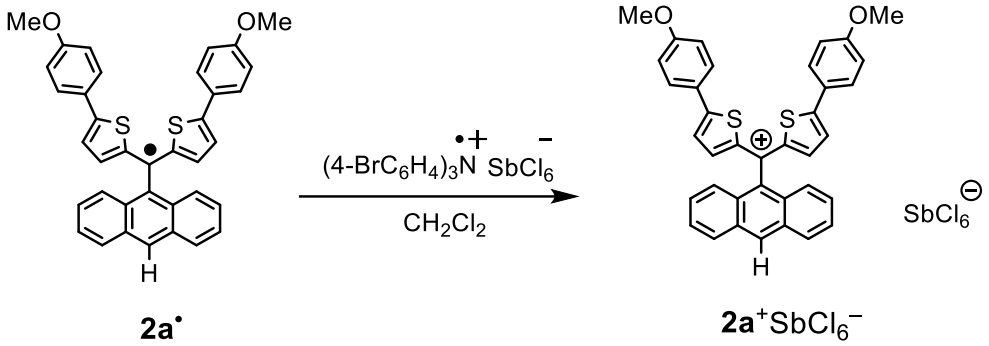

2a• **$2a^{+}SbCl_6^{-}$**

To a solution of monoradical **2a•** (21.0 mg, 37.0 μmol) in dry CH_2Cl_2 (0.60 mL) was added tris(4-bromophenyl)aminium hexachloroantimonate (30.2 mg, 37.0 μmol). After stirring at 23 °C for 1 h, the addition of dry Et_2O (5.0 mL) led to precipitation of the cation salt. The precipitates were collected and washed with dry Et_2O (5.0 mL× 2), and dried *in vacuo* to give **2a**$^{+}SbCl_6^{-}$ as a green solid in 84% yield.

Mp 147-149 °C (decomp.); ^{1}H NMR spectra are identical to those of **2a**$^{+}BF_4^{-}$; IR (ATR, with KBr): ν/cm^{-1} = 3195, 3100, 2939, 2839, 2578, 1593, 1561, 1521, 1496, 1458, 1438, 1415, 1363, 1309, 1263, 1152, 1116, 1073, 1018, 954, 912, 893, 863, 834, 796, 781, 760, 736, 724, 697, 649, 629; LR-MS (FD) m/z (%): 570.15 (6), 569.15 (19), 568.18 (43), 567.15 (bp, M^+); HR-MS (FD) Calcd. for $C_{37}H_{27}O_2S_2$: 567.14525; Found: 567.14501.

Synthesis of $2b^{+}SbCl_6^{-}$

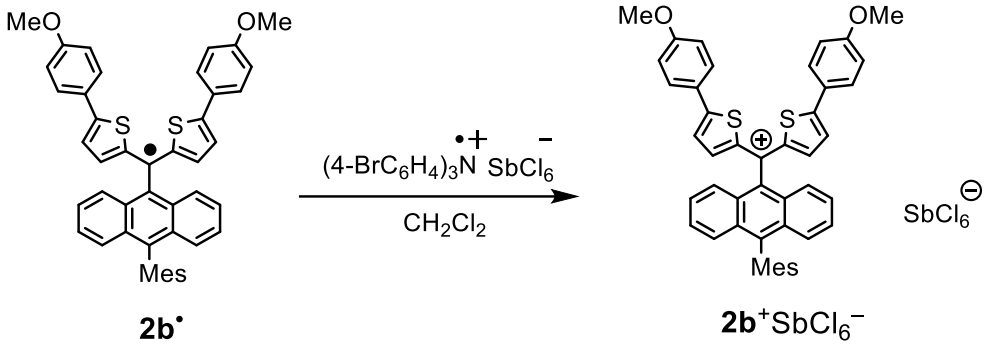

2b• **$2b^{+}SbCl_6^{-}$**

To a solution of monoradical **2b•** (25.5 mg, 37.2 μmol) in dry CH_2Cl_2 (1.0 mL) was added tris(4-bromophenyl)aminium hexachloroantimonate (30.4 mg, 37.2 μmol). After stirring at 26 °C for 1 h, the addition of dry Et_2O (7.0 mL) led to precipitation of the cation salt. The precipitates were collected and washed with dry Et_2O (7.0 mL× 2), and dried *in vacuo* to give $\mathbf{2b}^{+}SbCl_6^{-}$ as a green solid in 84% yield.

Mp 184-186 °C (decomp.); ^{1}H NMR spectra are identical to those of $\mathbf{2b}^{+}BF_4^{-}$; IR (ATR, with KBr): $\tilde{\nu}$/cm^{-1} = 3102, 2938, 2838, 1593, 1560, 1521, 1496, 1459, 1438, 1418, 1364, 1306, 1262, 1199, 1152, 1076, 1019, 955, 907, 867, 835, 777, 761, 722, 701, 681, 648, 608; LR-MS (FD) m/z (%): 688.23 (9), 687.23 (25), 686.23 (54), 685.22 (bp, M^+); HR-MS (FD) Calcd. for $C_{46}H_{37}O_2S_2$: 685.22350; Found: 685.22300.

2-4-3. X-ray Analysis

Table 2-3. Crystal data of $\mathbf{1}^{+}SbCl_6^{-}$, $\mathbf{1}_2$, $\mathbf{2a}^{+}SbCl_6^{-}$, and $\mathbf{2b}^{+}BF_4^{-}$.

Compounds	$\mathbf{1}^{+}SbCl_6^{-}$	$\mathbf{1}_2 \cdot 2CH_2Cl_2$	$\mathbf{2a}^{+}SbCl_6^{-}$	$\mathbf{2b}^{+}BF_4^{-}$
Solvent system	CH_3CN/Et_2O	CH_2Cl_2/hexane	THF/Et_2O	CH_2Cl_2/Et_2O
Empirical formula	$C_{23}H_{19}O_2S_2Cl_6Sb$	$C_{48}H_{42}O_4S_4Cl_4$	$C_{37}H_{27}Cl_6O_2S_2Sb$	$C_{46}H_{37}BF_4O_2S_2$
Formula weight	725.95	952.85	902.15	772.68
Temperature/K	150	150	150	149.9(8)
Crystal system	monoclinic	monoclinic	triclinic	monoclinic
Space group	$P2_1/n$	$P2_1/n$	P-1	$C2/c$
a/Å	7.33280(19)	14.4899(4)	12.0058(4)	7.6994(3)
b/Å	30.8921(6)	6.18632(15)	13.2394(6)	24.1031(7)
c/Å	24.6939(5)	26.3182(7)	14.5586(6)	20.7579(7)
α/°	90	90	111.773(4)	90
β/°	95.737(2)	103.357(3)	97.651(3)	95.179(3)
γ/°	90	90	108.146(4)	90
Volume/Å^3	5565.8(2)	2295.33(11)	1959.36(15)	3836.5(2)
Z	8	2	2	4
ρ_{calc} g/cm^3	1.733	1.379	1.529	1.338
μ/mm^{-1}	14.743	4.391	10.599	1.745
Color and shape	dark blue needle	colorless plate	dark green plate	dark green plate
Crystal size/mm^3	0.2 × 0.03 × 0.01	0.6 × 0.1 × 0.05	0.2 × 0.1 × 0.03	0.03 × 0.008 × 0.006
Reflections	34014	12479	31192	11766
R_{int}	0.0979	0.0228	0.0999	0.0232
Data/restraints/para	11157/0/620	4562/0/283	7860/0/438	3512/150/321
GOF	1.047	1.049	1.04	1.039
R_1 [I>=2σ(I)]	0.0997	0.0779	0.0892	0.0495
wR_2 [I>=2σ(I)]	0.2648	0.2248	0.2335	0.1252
R_1 [all data]	0.1161	0.0820	0.1031	0.0628
wR_2 [all data]	0.2807	0.2295	0.2466	0.1331
Largest diff.peak/hole/e Å^{-3}	2.64/-2.83	0.87/-0.95	3.08/-2.59	0.28/-0.20
Solvent mask	None	None	Used for the analysis	None
CCDC No.	2280693	2280694	2280695	2280696

2-4-4. DFT Calculations

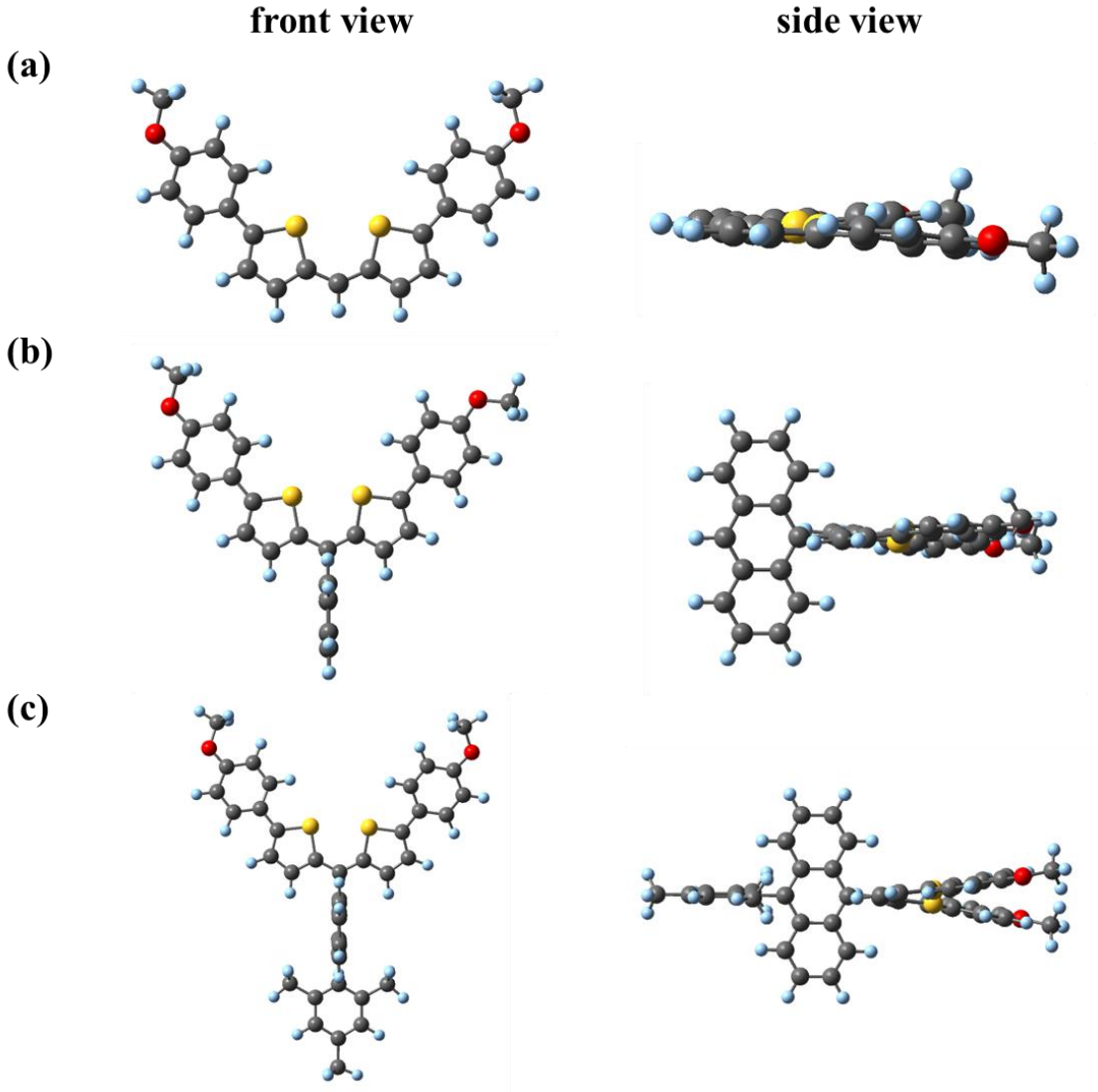

Figure 2-9. Optimized structures of (a) $\mathbf{1}^+$, (b) $\mathbf{2a}^+$, and (c) $\mathbf{2b}^+$ based on DFT calculations at the B3LYP/6-31G(d) level.

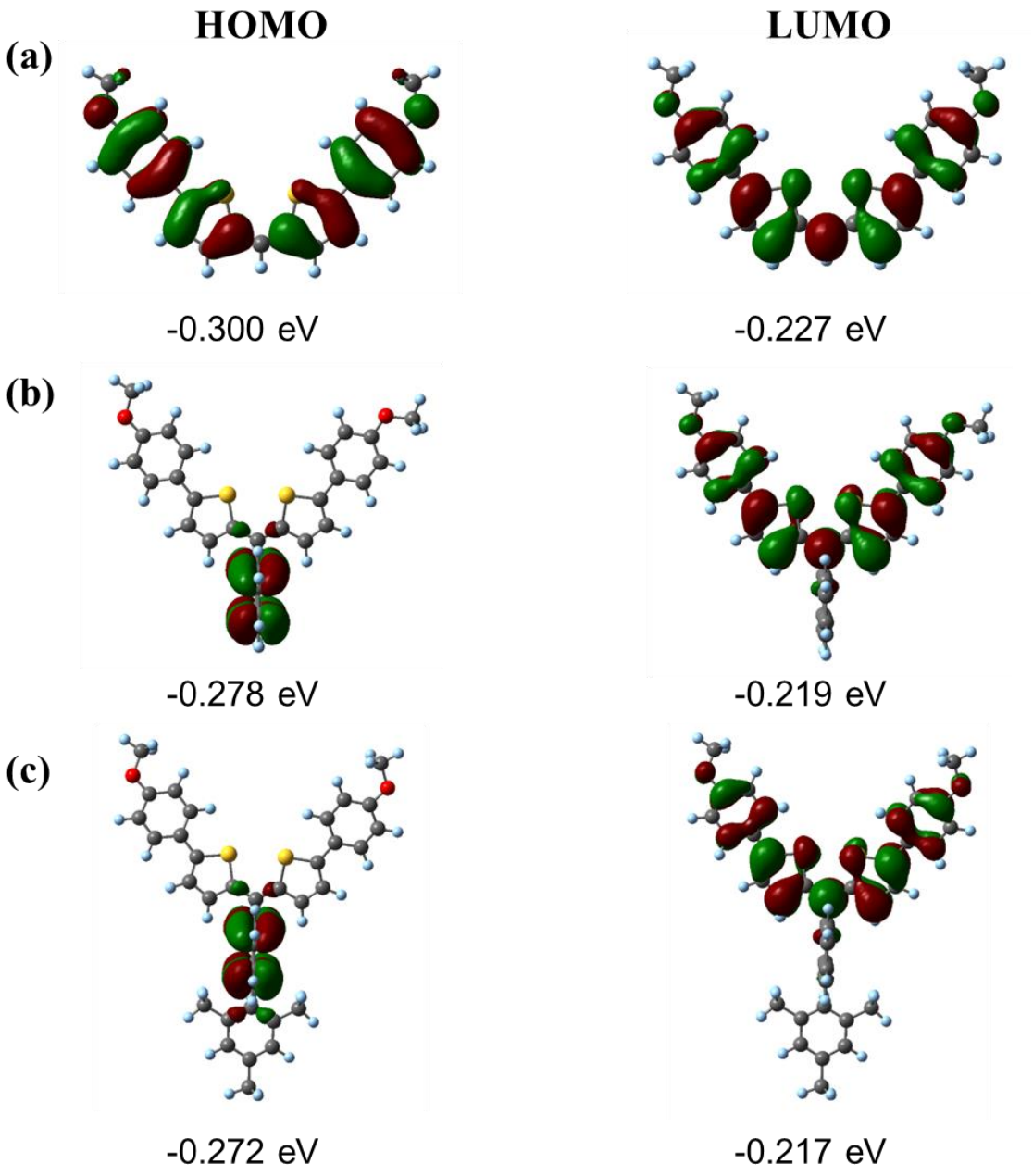

Figure 2-10. Molecular orbitals of (a) $\mathbf{1}^{+}$, (b) $\mathbf{2a}^{+}$, and (c) $\mathbf{2b}^{+}$ based on DFT calculations at the B3LYP/6-31G(d) level.

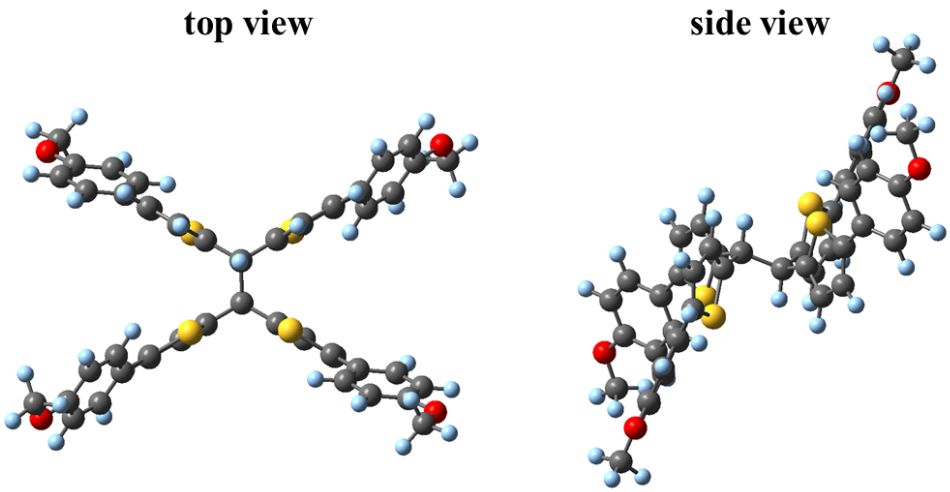

Figure 2-11. Optimized structures of $\mathbf{1}_2$ based on DFT calculations at the B3LYP/6-31G(d) level.

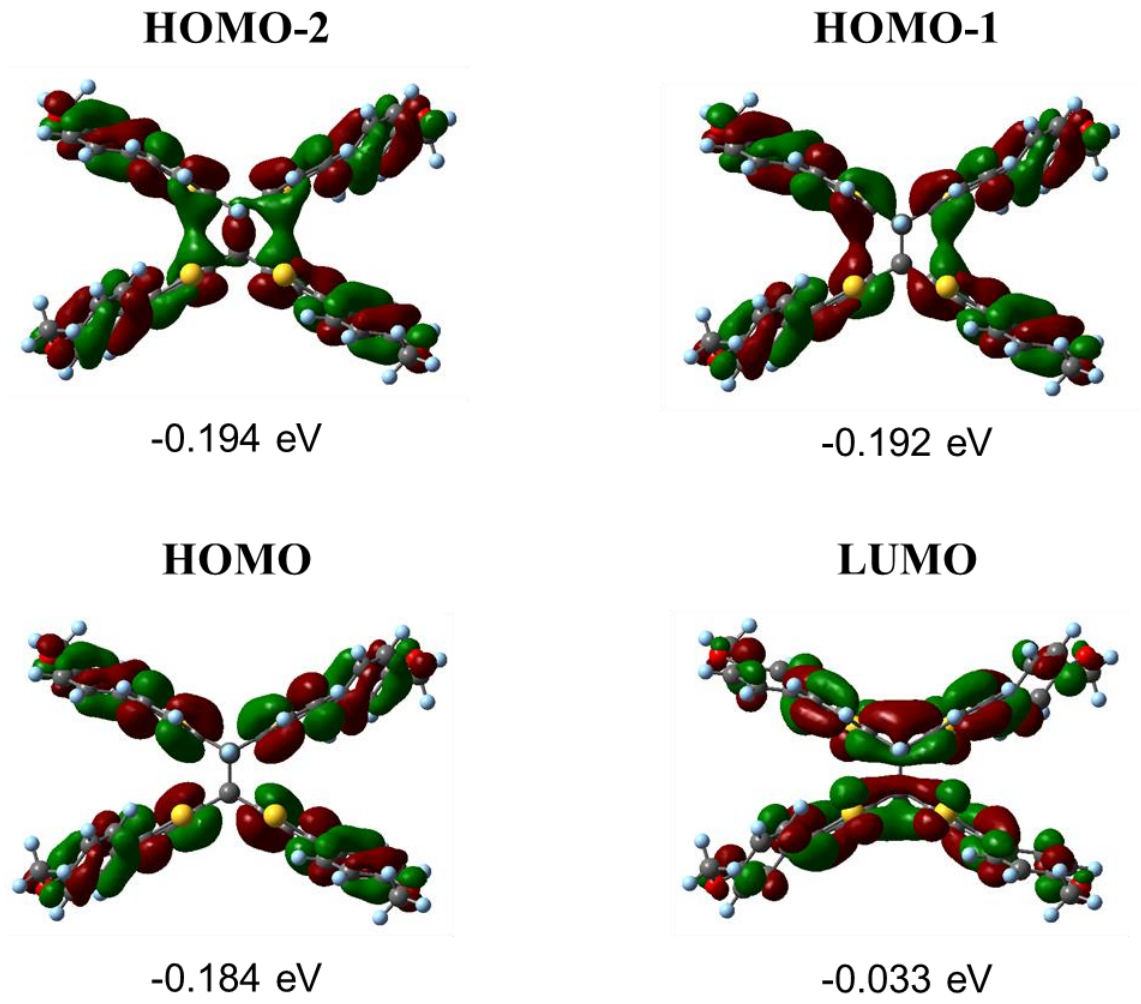

Figure 2-12. Molecular orbitals of $\mathbf{1}_2$ based on DFT calculations at the B3LYP/6-31G(d) level.

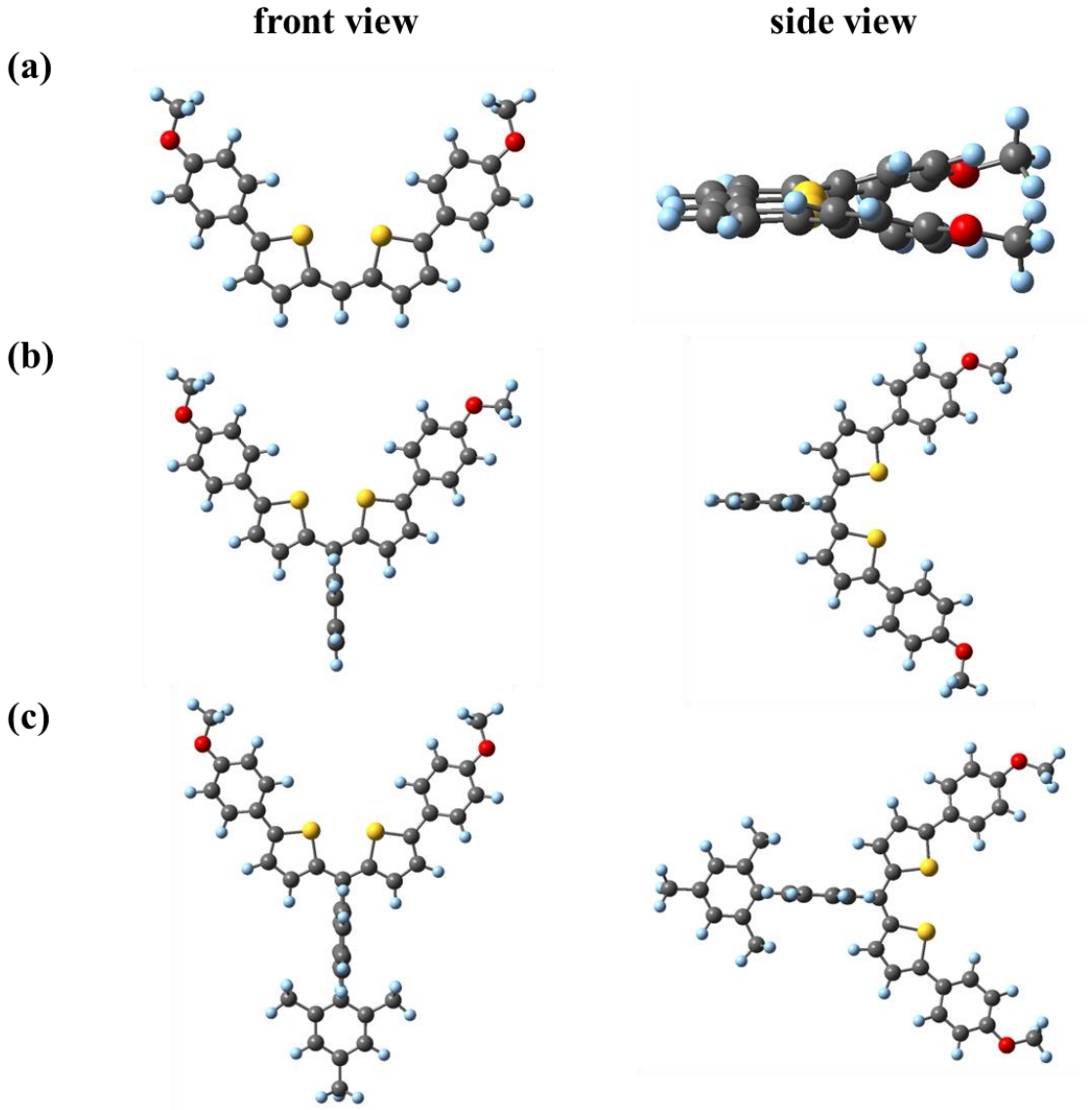

Figure 2-13. Optimized structures of (a) **1**$^{\bullet}$, (b) **2a**$^{\bullet}$, and (c) **2b**$^{\bullet}$ based on DFT calculations at the UB3LYP/6-31G(d) level.

2-5. References

[1] A. Mishra, R. K. Behera, P. K. Behera, B. K. Mishra, G. B. Behera, *Chem. Rev.* **2000**, *100*, 1973.

[2] B. A. Armitage, *in Topics in Current Chemistry*, **2005**, Vol. 253, pp. 55–76.

[3] B. Le Guennic, D. Jacquemin, *Acc. Chem. Res.* **2015**, *48*, 530.

[4] J. L. Bricks, A. D. Kachkovskii, Y. L. Slominskii, A. O. Gerasov, S. V. Popov, *Dye. Pigment.* **2015**, *121*, 238.

[5] W. Sun, S. Guo, C. Hu, J. Fan, X. Peng, *Chem. Rev***. 2016**, *116*, 7768.

[6] H. A. Shindy, *Dye. Pigment.* **2017**, *145*, 505.

[7] P. Monk, R. Mortimer, D. Rosseinsky, *Electrochromism and Electrochromic Devices*, Cambridge University Press, Cambridge, **2007**.

[8] D. R. Rosseinsky, P. M. S. Monk, R. J. Mortimer, *Electrochromic Materials and Devices*, ed. by Roger J. Mortimer, David R. Rosseinsky, Paul M. S. Monk, Wiley-VCH, Weinheim, Germany, **2013**.

[9] S. Mujawar, P. Patil, *Electrochromism in Pristine and Doped Niobium Oxide Thin Films: Spray Pyrolytic Synthesis of Niobium Oxide Thin Films for Smart Window Application*, LAP LAMBERT Academic Publishing, **2016**.

[10] T. Suzuki, Y. Sakano, Y. Tokimizu, Y. Miura, R. Katoono, K. Fujiwara, N. Yoshioka, N. Fujii, H. Ohno, Chem. Asian J. 2014, 9, 1841.

[11] C. Zhu, X. Ji, D. You, T. L. Chen, A. U. Mu, K. P. Barker, L. M. Klivansky, Y. Liu, L. Fang, *J. Am. Chem. Soc.* **2018**, *140*, 18173.

[12] D. T. Christiansen, A. L. Tomlinson, J. R. Reynolds, *J. Am. Chem. Soc.* **2019**, *141*, 3859.

[13] P. W. Antoni, T. Bruckhoff, M. M. Hansmann, *J. Am. Chem. Soc.* **2019**, *141*, 9701.

[14] Y. Ishigaki, T. Harimoto, K. Sugimoto, L. Wu, W. Zeng, D. Ye, T. Suzuki, *Chem. – An Asian J.* **2020**, *15*, 1147.

[15] P. Rietsch, S. Sobottka, K. Hoffmann, A. A. Popov, P. Hildebrandt, B. Sarkar, U. Resch-Genger, S. Eigler, *Chem. – A Eur. J.* **2020**, *26*, 17361.

[16] R. Rausch, M. I. S. Röhr, D. Schmidt, I. Krummenacher, H. Braunschweig, F. Würthner, *Chem. Sci.* **2021**, *12*, 793.

[17] Y. Ishigaki, T. Harimoto, K. Sugawara, T. Suzuki, *J. Am. Chem. Soc.* **2021**, *143*, 3306.

[18] B. Sk, M. Sarkar, K. Singh, A. Sengupta, A. Patra, *Chem. Commun.* **2021**, *57*, 13590.

[19] P. W. Antoni, C. Golz, M. M. Hansmann, *Angew. Chem. Int. Ed.* **2022**, *61*, e202203064.

[20] T. Harimoto, T. Suzuki, Y. Ishigaki, *Chem. – A Eur. J.* **2023**, *29*, e202203899.

[21] P. W. Antoni, C. Golz, M. M. Hansmann, *Angew. Chem. Int. Ed.* **2022**, *61*, e202203064.

[22] J. R. Lenhard, A. D. Cameron, *J. Phys. Chem.* **1993**, *97*, 4916.

[23] S. Ito, N. Morita, Eur. *J. Org. Chem.* **2009**, 4567.
[24] S. Hünig, M. Kemmer, H. Wenner, I. F. Perepichka, P. Bäuerle, A. Emge, G. Gescheid, *Chem. – A Eur. J.* **1999**, *5*, 1969.
[25] S. Hünig, M. Kemmer, H. Wenner, F. Barbosa, G. Gescheidt, I. F. Perepichka, P. Bäuerle, A. Emge, K. Peters, *Chem. – A Eur. J.* **2000**, *6*, 2618.
[26] S. Hünig, A. Langels, M. Schmittel, H. Wenner, I. F. Perepichka, K. Peters, Eur. *J. Org. Chem.* **2001**, 1393.
[27] T. Shoji, J. Higashi, S. Ito, T. Okujima, N. Morita, *Eur. J. Org. Chem.* **2011**, 584.
[28] S. Ito, T. Kubo, N. Morita, T. Ikoma, S. Tero-Kubota, A. Tajiri, *J. Org. Chem.* **2003**, 68, 9753.

[29] S. Ito, K. Akimoto, J. Kawakami, A. Tajiri, T. Shoji, H. Satake, N. Morita, *J. Org. Chem.* **2007**, *72*, 162.
[30] S. Ito, R. Sekiguchi, A. Mizushima, K. Kudo, J. Kawakami, T. Shoji, *Arkivoc* **2018**, *ii*, 145.
[31] S. Hünig, C. A. Briehn, P. Bäuerle, A. Emge, *Chem. – A Eur. J.* **2001**, *7*, 2745.
[32] S. Hünig, S. Aldenkortt, P. Bäuerle, C. A. Briehn, M. Schäferling, I. F. Perepichka, D. Stalke, B. Walfort, Eur. *J. Org. Chem.* **2002**, 1603.
[33] H. John, C. Briehn, J. Schmidt, S. Hünig, J. Heinze, *Angew. Chem. Int. Ed.* **2007**, *46*, 449.
[34] A. Gosset, L. Wilbraham, Š. N. Lachmanová, R. Sokolová, G. Dupeyre, F. Tuyèras, P. Ochsenbein, C. Perruchot, H.-P. J. de Rouville, H. Randriamahazaka, L. Pospíšil, I. Ciofini, M. Hromadová, P. P. Lainé, *J. Am. Chem. Soc.* **2020**, *142*, 5162.
[35] T. Suzuki, T. Takeda, E. Ohta, K. Wada, R. Katoono, H. Kawai, K. Fujiwara, *Chem. Rec.* **2015**, *15*, 280.
[36] T. Suzuki, H. Tamaoki, J. Nishida, H. Higuchi, T. Iwai, Y. Ishigaki, K. Hanada, R. Katoono, H. Kawai, K. Fujiwara, T. Fukushima, *in Organic Redox Systems*, John Wiley & Sons, Inc, Hoboken, NJ, **2015**, pp. 13–37.
[37] T. Suzuki, Y. Ishigaki, M. Takata, J. Nishida, T. Fukushima, *Heterocycles* **2021**, *102*, 419.
[38] T. Suzuki, H. Shiohara, M. Monobe, T. Sakimura, S. Tanaka, Y. Yamashita, T. Miyashi, *Angew. Chem. Int. Ed. Engl.* **1992**, *31*, 455.
[39] Y. Ishigaki, T. Hashimoto, K. Sugawara, S. Suzuki, T. Suzuki, *Angew. Chem. Int. Ed.* **2020**, *59*, 6581.
[40] J. Nakayama, A. Ishii, Y. Yamada, M. Sugino, M. Hoshino, *Tetrahedron Lett.* **1990**, *31*, 2627.
[41] B. Abarca, G. Asensio, R. Ballesteros, T. Varea, *J. Org. Chem.* **1991**, *56*, 3224.
[42] T. Varea, M. Medio-Simón, B. Abarca, R. Ballesteros, G. Asensio, S. García-Granda, E. Pérez-Carreño, F. Gómez-Beltrán, J. Chem. Soc., *Chem. Commun.* **1993**, 1476.
[43] T. Nishiuchi, S. Aibara, T. Kubo, *Angew. Chem. Int. Ed.* **2018**, *57*, 16516.
[44] R. Samae, P. Surawatanawong, U. Eiamprasert, S. Pramjit, L. Saengdee, P. Tangboriboonrat,

S. Kiatisevi, *Eur. J. Org. Chem.* **2016**, 3536.
[45] S. Dähne, D. Leupold, *Angew. Chem. Int. Ed. Engl.* **1966**, *5*, 984.
[46] N. Katayama, Y. Ozaki, S. Yasui, K. Iriyama, *J. Mol. Struct.* **1992**, *274*, 171.
[47] Y. Fujimoto, N. Katayama, Y. Ozaki, S. Yasui, K. Iriyama, *J. Mol. Struct.* **1992**, *274*, 183.
[48] I. Baraldi, A. Carnevali, F. Momicchioli, G. Ponterini, Spectrochim. *Acta Part A Mol. Spectrosc.*, **1993** *49*, 471.
[49] M. J. Frisch, G. W. Trucks, H. B. Schlegel, G. E. Scuseria, M. A. Robb, J. R. Cheeseman, G. Scalmani, V. Barone, G. A. Petersson, X. Nakatsuji, H.; Li, M. Caricato, A. V. Marenich, J. Bloino, B. G. Janesko, R. Gomperts, B. Mennucci, H. P. Hratchian, J. V. Ortiz, A. F. Izmaylov, J. L. Sonnenberg, D. Williams-Young, F. Ding, F. Lipparini, F. Egidi, J. Goings, B. Peng, A. Petrone, T. Henderson, D. Ranasinghe, V. G. Zakrzewski, J. Gao, N. Rega, G. Zheng, W. Liang, M. Hada, M. Ehara, K. Toyota, R. Fukuda, J. Hasegawa, M. Ishida, T. Nakajima, Y. Honda, O. Kitao, H. Nakai, T. Vreven, K. Throssell, J. A. J. Montgomery, J. E. Peralta, F. Ogliaro, M. J. Bearpark, J. J. Heyd, E. N. Brothers, K. N. Kudin, V. N. Staroverov, T. A. Keith, R. Kobayashi, J. Normand, K. Raghavachari, A. P. Rendell, J. C. Burant, S. S. Iyengar, J. Tomasi, M. Cossi, J. M. Millam, M. Klene, C. Adamo, R. Cammi, J. W. Ochterski, R. L. Martin, K. Morokuma, O. Farkas, J. B. Foresman, D. J. Fox, *Gaussian 16, Revision B.01*, Gaussian, Inc., Wallingford CT, **2016**.
[50] F. Wudl, G. Srdanov, B. Rosenau, D. Wellman, K. Williams, S. D. Cox, *J. Am. Chem. Soc.* **1988**, *110*, 1316.
[51] C. T. Pedersen, Phosphorus. *Sulfur. Silicon Relat. Elem.* **1991**, *58*, 17.
[52] P. Maslak, W. H. Chapman, T. M. Vallombroso, B. A. Watson, *J. Am. Chem. Soc.* **1995**, *117*, 12380.
[53] Y. Ishigaki, T. Hashimoto, K. Sugawara, S. Suzuki, T. Suzuki, *Angew. Chem. Int. Ed.* **2020**, *59*, 6581.
[54] T. Nishiuchi, S. Aibara, T. Kubo, *Angew. Chem. Int. Ed.* **2018**, *57*, 16516.
[55] M. J. Frisch, G. W. Trucks, H. B. Schlegel, G. E. Scuseria, M. A. Robb, J. R. Cheeseman, G. Scalmani, V. Barone, G. A. Petersson, X. Nakatsuji, H.; Li, M. Caricato, A. V. Marenich, J. Bloino, B. G. Janesko, R. Gomperts, B. Mennucci, H. P. Hratchian, J. V. Ortiz, A. F. Izmaylov, J. L. Sonnenberg, D. Williams-Young, F. Ding, F. Lipparini, F. Egidi, J. Goings, B. Peng, A. Petrone, T. Henderson, D. Ranasinghe, V. G. Zakrzewski, J. Gao, N. Rega, G. Zheng, W. Liang, M. Hada, M. Ehara, K. Toyota, R. Fukuda, J. Hasegawa, M. Ishida, T. Nakajima, Y. Honda, O. Kitao, H. Nakai, T. Vreven, K. Throssell, J. A. J. Montgomery, J. E. Peralta, F. Ogliaro, M. J. Bearpark, J. J. Heyd, E. N. Brothers, K. N. Kudin, V. N. Staroverov, T. A. Keith, R. Kobayashi, J. Normand, K. Raghavachari, A. P. Rendell, J. C. Burant, S. S. Iyengar, J. Tomasi, M. Cossi, J. M. Millam, M. Klene, C. Adamo, R. Cammi, J. W. Ochterski, R. L. Martin, K. Morokuma, O. Farkas, J. B. Foresman, D. J. Fox, *Gaussian*

16, Revision B.01, Gaussian, Inc., Wallingford CT, **2016**.

[56] O. V. Dolomanov, L. J. Bourhis, R. J. Gildea, J. A. K. Howard, H. Puschmann, *J. Appl. Crystallogr.* **2009**, *42*, 339.

[57] G. M. Sheldrick, *Acta Crystallogr. Sect. A Found. Adv.* **2015**, *71*, 3.

[58] G. M. Sheldrick, *Acta Crystallogr. Sect. C Struct. Chem.* **2015**, *71*, 3

Chapter 3

Incorporation of Cationic Nitrogen into Cyclopenta-Fused PAHs (CP-PAHs): Synthesis of Cationic Azaacenaphthylene as a New Class of Strong π-Electron Acceptors for Organic NIR Dyes

3-1. Introduction

Organic π-conjugated dyes, which have near-infrared (NIR) absorptions, have much attention due to the potential applications in optical materials, such as an expansion of light-harvesting range for organic solar cells,[1] NIR-transmitting optical filters for security marking,[2,3] and so on.

For the development of NIR-absorbing dyes, to achieve a large red-shift of absorption properties reaching the NIR region (700 - 2500 nm), an extension of the π-conjugated systems is the most straightforward method, however, is often accompanied by decreased chemical stability and low solubility, thus limiting their investigation for applications.[4-6] Therefore, utilizing an intramolecular charge-transfer (ICT) interaction by the linking of donor (D) and acceptor (A) units is a promising strategy and is widely used for developing organic NIR dyes.[4] In this case, the control of the frontier orbital levels is very important to make HOMO-LUMO gap (ΔE_{CT}) narrow enough to absorb lights in the NIR region (Figure 3-1).

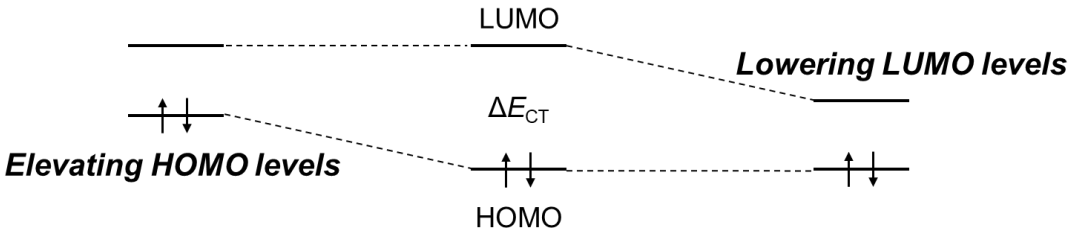

Figure 3-1. Two types of strategies for narrowing the HOMO-LUMO gap.

To attain the narrower HOMO-LUMO gap for the design of D-A type NIR dyes, there are mainly two approaches, e.g., lowering LUMO levels and/or elevating HOMO levels. Considering that the π-conjugated systems intrinsically have an electron-donating character, the former is considered more difficult than the latter, so the creation of highly π-electron-accepting units makes great advances for the development of NIR dyes. However, the design concept of most electron-accepting organic units has mainly relied on introducing electron-withdrawing groups, for example, the introduction of imide groups into the aromatic core such as perylenebisimide (PBI)[7-9] and the incorporation of 1,2-diimine skeleton into π-conjugated systems such as chalcogenadiazoles.[10-13]

On the other hand, the doping of cationic nitrogen into π-conjugated systems is also effective for the design of π-electron-accepting units. Such cationic aromatic rings are classified as azonia aromatic heterocycles (AZAHs)[14] and have a high electron affinity, thanks to the introduced cationic quaternary nitrogen into π-systems. In addition, cationic organic dyes have an advantage of tunability for the structure in crystalline states and for solubility in organic solvents by counter anion exchange, unlike neutral organic dyes. However, the applications of AZAHs for D-A type chromophores are limited to a few examples utilizing the quinolizinium system as an acceptor unit reported by Vaquero and co-workers,[15,16] and the photo-absorption edge of them is extending to 600 nm, but does not reach the NIR region. Therefore, the more electron-accepting AZAHs are desired for attaining NIR-absorbing properties, but most synthesized AZAHs are thus far quinolizinium derivatives, composed only of hexagonal rings, except for [2.3.3]cyclizine[17] reported by Leaver's group and pyrazole or imidazole containing AZAHs.[18,19]

In this work, the author focused on unsaturated pentagon rings annulated PAHs, which are the so-called cyclopenta-fused polyaromatic hydrocarbons (CP-PAHs),[20] with the expectation that a cationic nitrogen-doped CP-PAH could overcome the photo-absorption limit of AZAH-substituted cationic dyes. Based on the intrinsically electron-accepting nature of the pentagonal ring,[21] CP-PAHs generally have lower LUMO compared to other PAHs consisting only of hexagonal rings, so cationic nitrogen-doped CP-PAHs are expected to have higher electron-accepting properties than conventional AZAHs. Under this concept using CP-PAH skeletons, we newly designed cationic azaacenaphthylene (CAA), which is the new family of cationic nitrogen-doped CP-PAH, and developed the synthetic methods for cationic D-A type chromophores with CAA skeleton as an acceptor unit. For the newly synthesized CAA derivatives, the photo-absorption edge reached the NIR region around 1000 nm, and additionally, clean tri-color halochromism was observed based on the different electronic states of the two donor units.

3-2. Results and Discussion

3-2-1. Molecular Design

As mentioned in **3-1**, acenaphthylene was selected as a parent structure for cationic nitrogen doping. Acenaphthylene is classified as CP-PAHs, and also known as a part of a fullerene C_{60}, which is the highly electron-accepting hydrocarbon.[22,23] In this case, three isomers can be designed based on the position of quaternary nitrogen doping into the acenaphthylene skeleton. According to the density functional theory (DFT) calculations, it was expected that the CAA containing quinoline moiety has the lowest LUMO level than other CAAs (Figure 3-1).

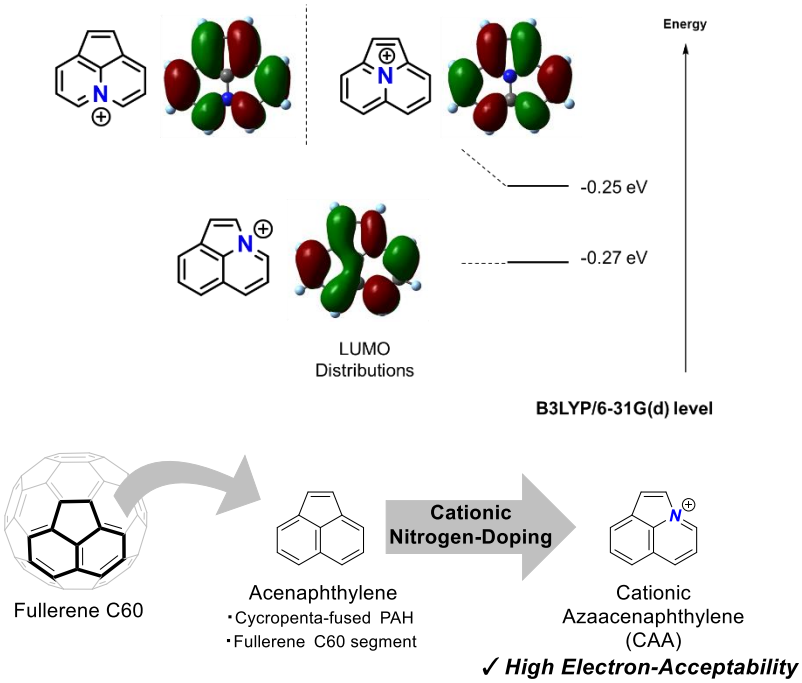

Figure 3-2. Concept for the design of CAA and calculated LUMO levels of CAA isomers.

In order to evaluate the π-electron acceptability of CAA in D-A type chromophore by comparison with AZAH substituted organic dye reported by Vaquero's group, 4-dimethylaminophenyl and 4-methoxyphenyl group, both of which were also used as donor units in Vaquero's work,[16] were employed as donor units and connected into CAA at the K-region. Thus, CAA-attached CP-PAHs **12-N** and **12-O** were designed for constructing the novel NIR-absorbing dyes.

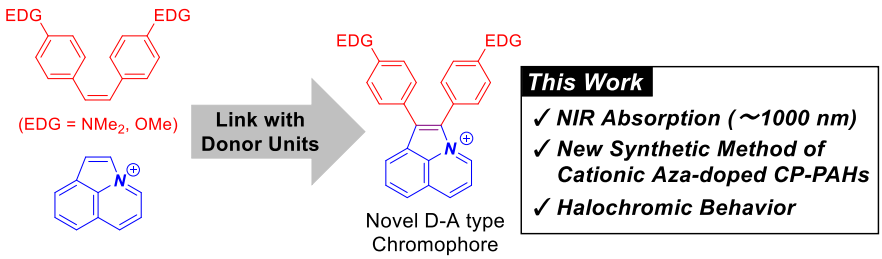

Figure 3-3. Design concept for the CAA attached novel NIR dyes.

3-2-2. Preparations and X-ray Analyses of Cationic Salts of 12-N$^+$ and 12-O$^+$

The newly designed cation **12**$^+$ was synthesized by protonation/dehydration of ether **11**, which were formed by two-electron oxidation of ethene **10** and following etherification.

Firstly, by Wittig-Horner reaction of **9-N**/*n*BuLi or **9-O**/*n*BuLi with 8-quinolinecarboxaldehyde in THF, triarylethenes **10-N** and **10-O** were obtained in 81% and 73% yields, respectively. Then, two-electron oxidation of **10-N** and **10-O** with appropriate oxidants in CH_2Cl_2 followed by treatment with TBAF·$3H_2O$ in MeCN to give **11-N** and **11-O** in 33% and 12% yields, respectively (Scheme 3-1). Although characterization of ether **11** was difficult due to the existence of the diastereomeric mixture and its instability in solution, the X-ray structure of one of the diastereomers for **11-N** was successfully determined by single-crystal X-ray diffraction analysis (Figure 3-4).

As a control experiment, when the oxidation of **10-N** was carried out using 1.5 equiv. of iodine, **11-N** was obtained only in 9.7% yield, and 26% of ethene **10-N** was recovered (Scheme 3-2). This result suggests that the transformation from **10** to **11** proceeds in two-electron oxidation manner. Based on these experimental results, the estimated reaction mechanism is shown in Scheme 3-3. Upon the first one-electron oxidation of **10**, the corresponding radical cation was generated, at which nucleophilic attack from the nitrogen atom of the quinoline unit to the cation center to give the distonic radical cation **10**$^{\bullet+}$. Next, the second one-electron oxidation of **10**$^{\bullet+}$ proceeded to form dication **10**$^{2+}$ and 1,2-migration of the aryl group occurred to give quinoidal dication, which immediately tautomerized to the protonated form of **12**$^+$. Lastly, deprotonation and etherification proceeded in the presence of TBAF·$3H_2O$ in MeCN solution to give precursor ether **11**.

Scheme 3-1 Preparation of **11-N** and **11-O**

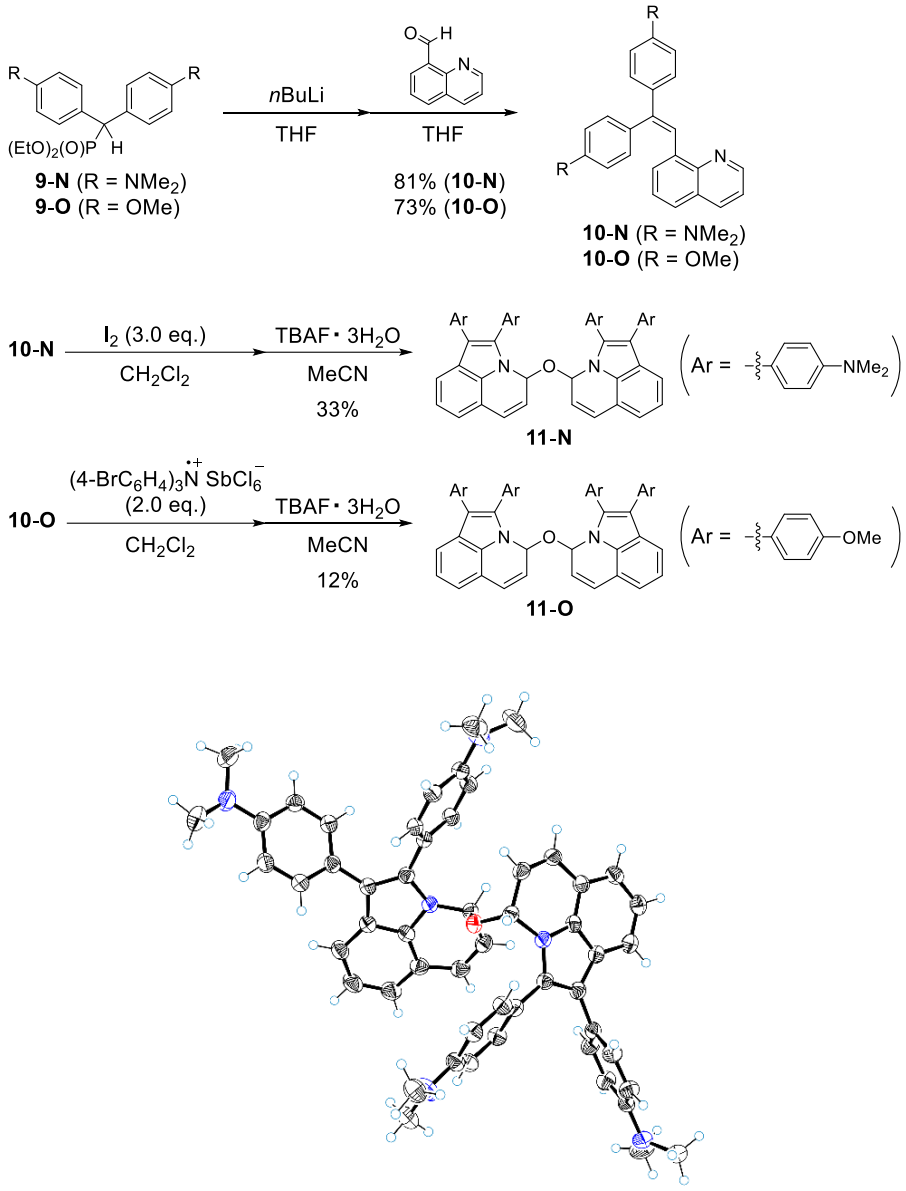

Figure 3-4. ORTEP drawings of **11-N** obtained by X-ray analysis at 150 K.

Scheme 3-2 Control experiment of the synthesis of **11-N** under one-electron oxidation condition.

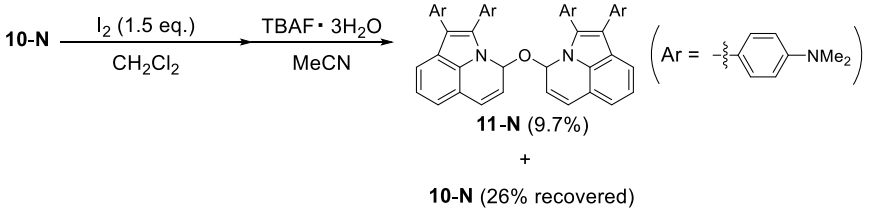

Scheme 3-3 Estimated reaction mechanism of transformation from **10** to **11**.

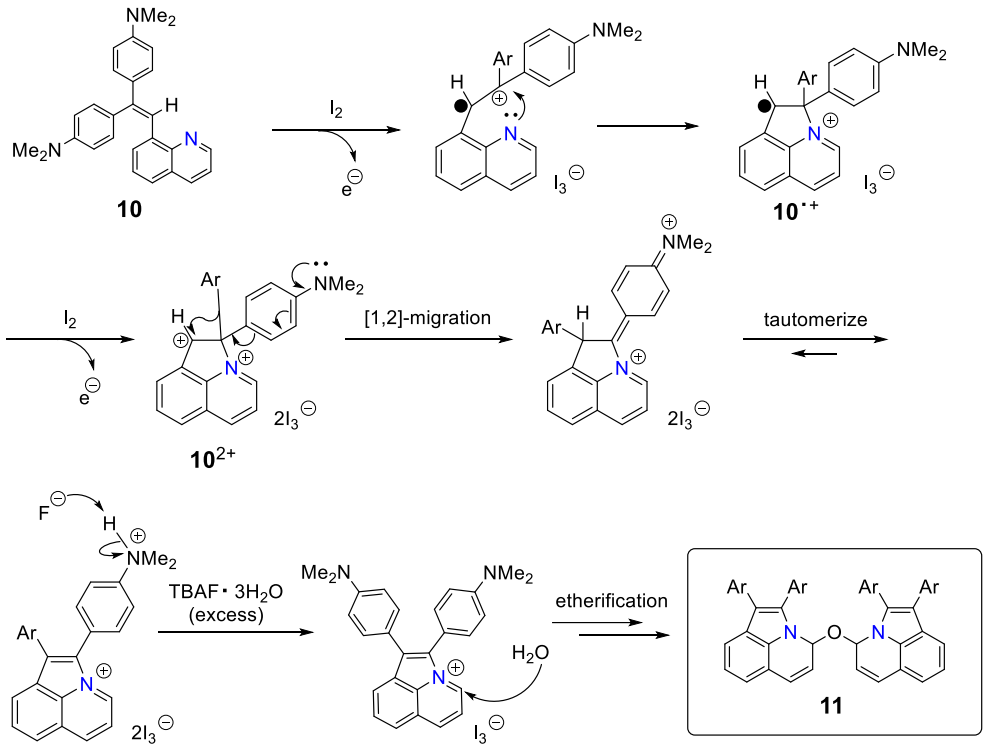

Upon treatment of THF solutions of ethers **11-N** and **11-O** with aqueous HBF_4 or HPF_6, the corresponding cations, **12-N**$^+$ and **12-O**$^+$, were isolated in moderate to good yields as stable dark purple solids and red-purple solids, respectively (Scheme 3-4). This transformation from ethene **9** to cation **12**$^+$ is not classified to any conventional methodology of the synthesis of AZAHs and this synthetic approach is expected to be widely applied for the cationic nitrogen doping into more π-extended or any functional group substituted CP-PAHs because the substrates, 8-quinolyl diarylethene derivatives **10**, are easily prepared by well-known olefination reactions.

Scheme 3-4 Preparation of **12-N**$^+$ and **12-O**$^+$.

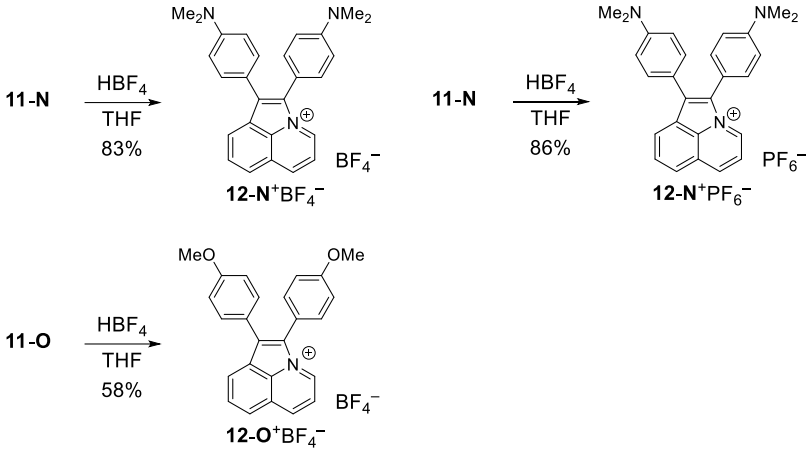

Next, X-ray analyses of single crystals obtained by a vapor diffusion method, for both **12-N**$^+$$PF_6^-$ and **12-O**$^+$$BF_4^-$, were conducted to confirm their structures (Figure 3-5). In the crystalline state, the dimethylaniline unit, which is close to the cationic nitrogen, was attached to the CAA plane with larger twisted angles than another dimethylaniline unit on the opposite side of the cationic nitrogen. Hence, by considering that the two donor units are in different electronic states, the donor far from the cationic nitrogen is more effectively π-conjugated with CAA moiety.

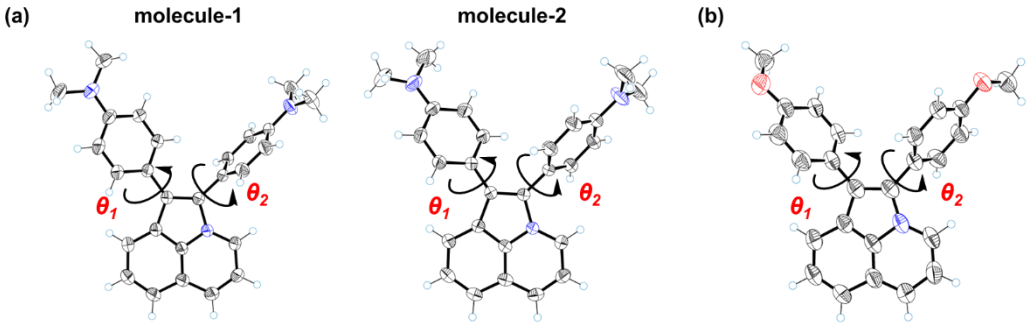

		θ_1 [°]	θ_2 [°]
(a)	**mol 1**	24.4(4)	70.0(3)
	mol 2	28.0(4)	63.1(3)
(b)		41.1(9)	58.6(3)

Figure 3-5. ORTEP drawings of (a) **12-N**$^+$$PF_6^-$ (two crystallographically independent molecules) and (b) **12-O**$^+$$BF_4^-$ salts obtained by X-ray analyses at 150 K. Counterions are omitted for clarity.

3-2-3. (TD-)DFT Calculations of 12-N^+ and 12-O^+

To investigate the distributions of frontier orbitals, the author carried out DFT calculations of cation **12-N**$^+$ and **12-O**$^+$, respectively (Figure 3-6). In both cases, the LUMO distributions are mainly located on the acenaphthylene skeleton thanks to the high electron affinity of CAA core, and the HOMO/HOMO-1 distributions are located on the stilbene unit. This result suggests that **12-N**$^+$ could exhibit longer-wavelength absorption based on the ICT from donating aniline units to the accepting CAA moiety, so UV-Vis-NIR spectra were simulated by TD-DFT calculations for **12-N**$^+$ and **12-O**$^+$, respectively (Figure 3-7). The simulated UV-Vis-NIR spectrum of **12-N**$^+$ widely spreads over the Vis-NIR region, and especially for the ICT band, the absorption was expected to greatly exceed 1000 nm. Even in the simulation of UV-Vis-NIR spectrum of **12-O**$^+$, the NIR absorption based on the ICT interaction was expected, but the whole spectrum was blue-shifted compared to that of **12-N**$^+$ because the HOMO level of **12-O**$^+$ with methoxyphenyl groups is lower than that of **12-N**$^+$ with dimethylaminophenyl groups, which are more electro-donating than methoxyphenyl groups.

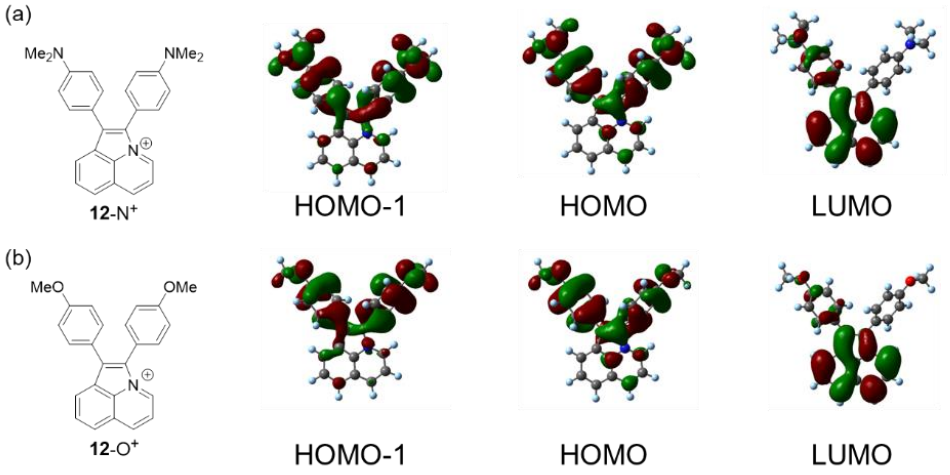

Figure 3-6. Frontier orbitals of (a) **12-N**$^+$ and (b) **12-O**$^+$ calculated at the B3LYP/6-31G(d) level.

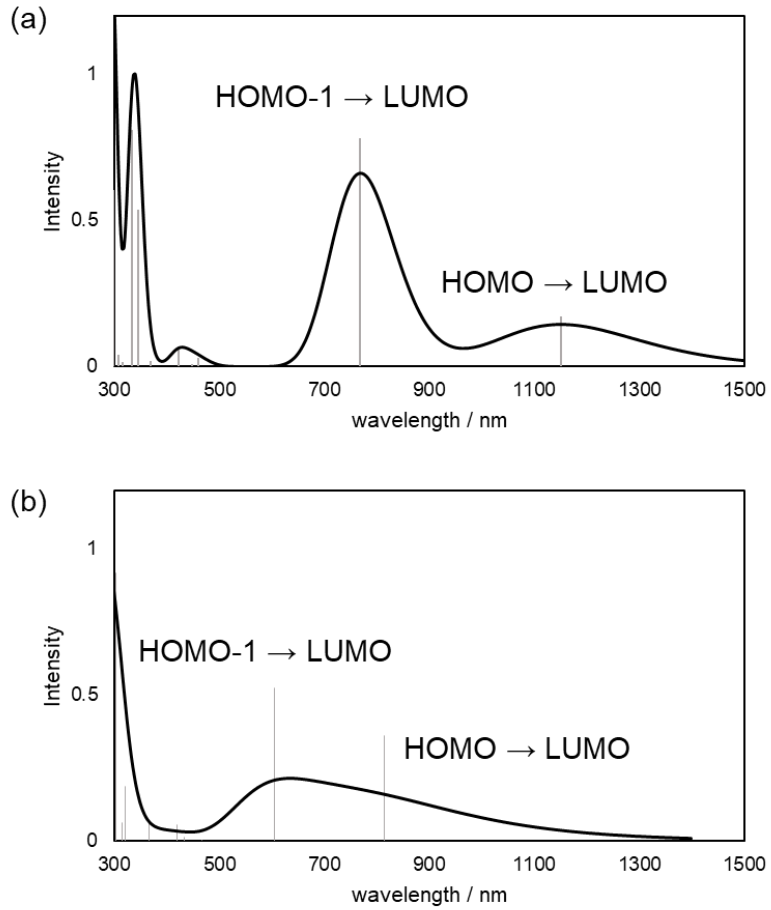

Figure 3-7. Simulated UV-Vis-NIR spectra of (a) **12-N**$^+$ and (b) **12-O**$^+$ calculated by TD-DFT at the B3LYP/6-31G(d) level.

3-2-4. Spectroscopic Properties of Cationic Salts of 12-N$^+$ and 12-O$^+$

Cation salt **12-N**$^+BF_4^-$ showed absorption maxima at 713 nm, 570 nm, and 310 nm in CH_2Cl_2 and at 627 nm, 510 nm, and 308 nm in MeCN, respectively (Figure 3-8). As expected in TD-DFT calculation, the NIR-absorption edge of **12-N**$^+BF_4^-$ reached around 1000 nm in both cases. The observed large red-shift from 627 nm in MeCN to 713 nm in CH_2Cl_2 suggested that cation salt **12-N**$^+BF_4^-$ would exhibit the negative solvatochromism, which is generally caused by a stabilization of charged species at the ground state in polar solvents. Thus, the author investigated solvent effects of photo-absorption of **12-N**$^+BF_4^-$ (Figure 3-9).

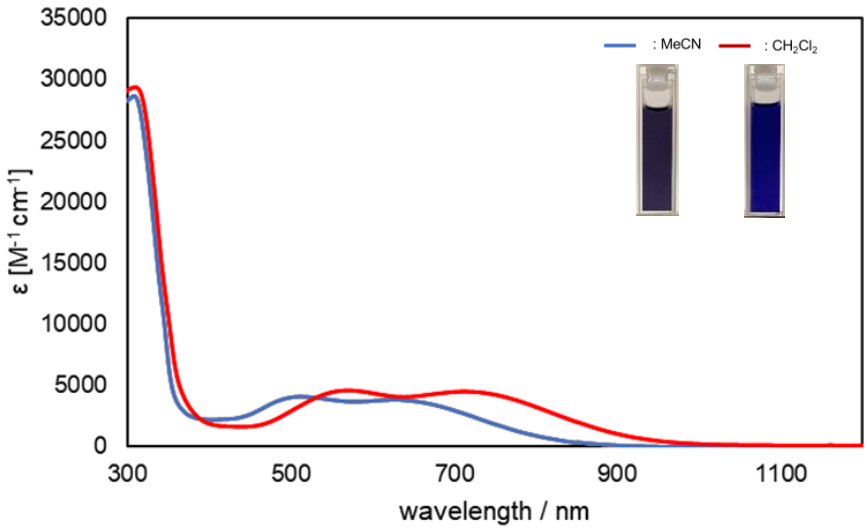

	λ_{max} [nm] (ε [M^{-1} cm^{-1}])
CH_2Cl_2	310 (29000), 570 (4500), 713 (4400)
MeCN	308 (29000), 510 (4000), 627 (3800)

Figure 3-8. UV-Vis-NIR spectra of **12-N**$^+$$BF_4^-$ in CH_2Cl_2 (red) and in MeCN (blue).

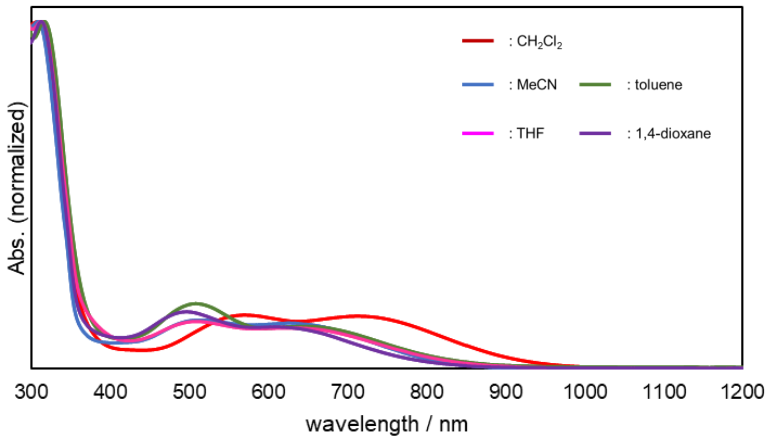

Figure 3-9. UV-Vis-NIR spectra of **12-N**$^+$$BF_4^-$ in CH_2Cl_2 (red) and non-halogenated solvents.

However, **12-N**$^+$$BF_4^-$ showed almost the same spectra in non-halogenated solvents, regardless of their polarity contrary to expectations (Figure 3-9). For further investigations of solvent effects of absorption properties of **12-N**$^+$$BF_4^-$, UV-Vis-NIR absorption spectra of **12-N**$^+$$BF_4^-$ were measured in various chlorinated solvents as shown in Figure 3-10. As a result, **12-N**$^+$$BF_4^-$ showed the largest red-shifted absorptions in 1,2-dichlorobenzene and 1,1,2,2-tetrachloroethane, both of which have a similar structure where two chloride atoms are bridged

by two carbon atoms. On the other hand, **12-N**$^{+}$$BF_4^{-}$ showed blue-shifted absorption spectra in both 1,3-dichlorobenzene and chloroform compared to that in CH_2Cl_2. According to the literature,[24,25] some D-A type dyes containing a cationic nitrogen atom show a red-shifted absorption specifically in halogenated solvents. The mechanism of the specific solvatochromic behavior in halogenated solvents has been still unclear, but the stabilization of D-A-conjugated systems by halogenated solvents at the excited state is one possibility.[25]

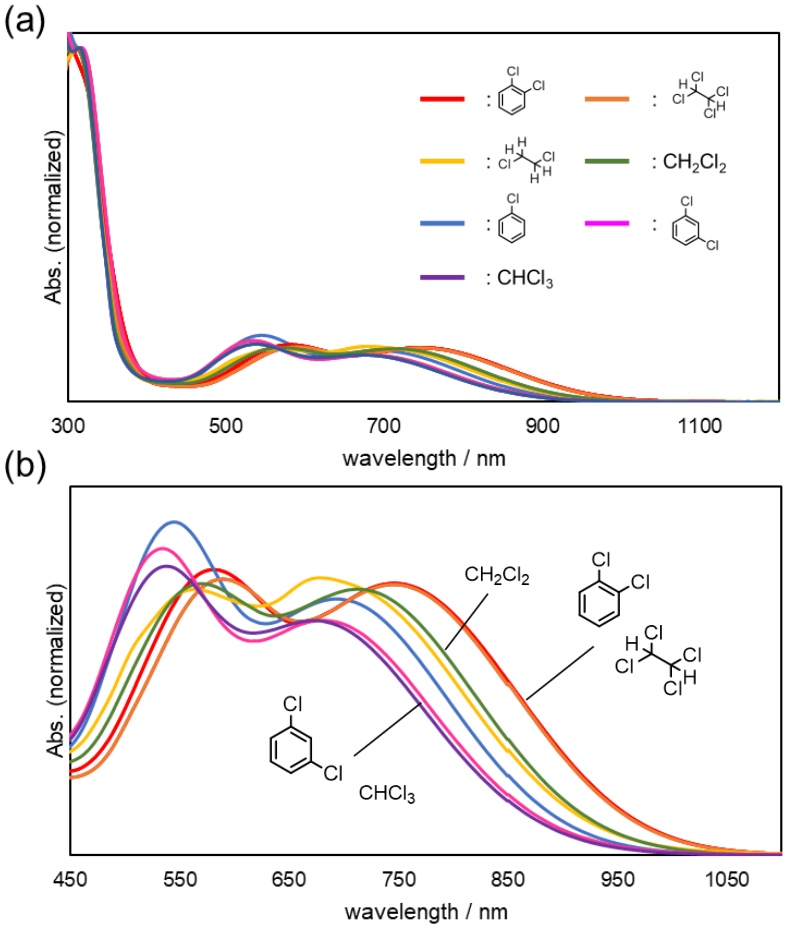

Figure 3-10. (a) UV-Vis-NIR and (b) Vis-NIR spectra of **12-N**$^{+}$$BF_4^{-}$ in chlorinated solvents.

Due to the less donating ability of methoxyphenyl groups, cation salt **12-O**$^{+}$$BF_4^{-}$ showed absorption maxima at 544 nm, 401 nm, and 340 nm in CH_2Cl_2 and at 511 nm and 336 nm in MeCN, respectively (Figure 3-11). Unlike **12-N**$^{+}$$BF_4^{-}$, the absorption spectra were blue-shifted in both solvents from simulated those (Figure 3-7b), but the absorption bands appeared in the whole visible region (< 700 nm). For **12-O**$^{+}$$BF_4^{-}$, red-shifted absorption spectra were observed specifically in chlorinated solvents as the same as **12-N**$^{+}$$BF_4^{-}$, but the extent of a red-shift was less than **12-N**$^{+}$$BF_4^{-}$. (Figure 3-12).

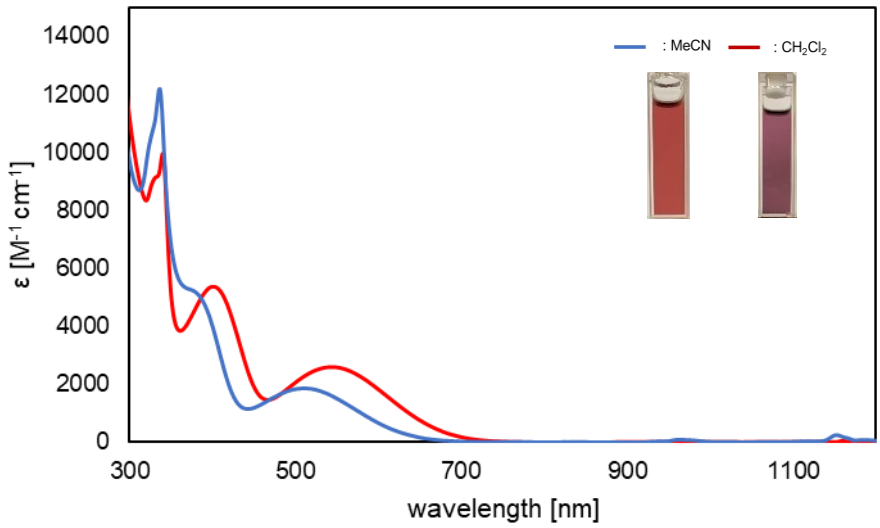

	λ_{max} [nm] (ε [M^{-1} cm^{-1}])
CH_2Cl_2	340 (9900), 401 (5400), 544 (2600)
MeCN	336 (12200), 511 (1800)

Figure 3-11. UV-Vis-NIR spectra of **12-O**$^{+}BF_4^{-}$ in CH_2Cl_2 (red) and in MeCN (blue).

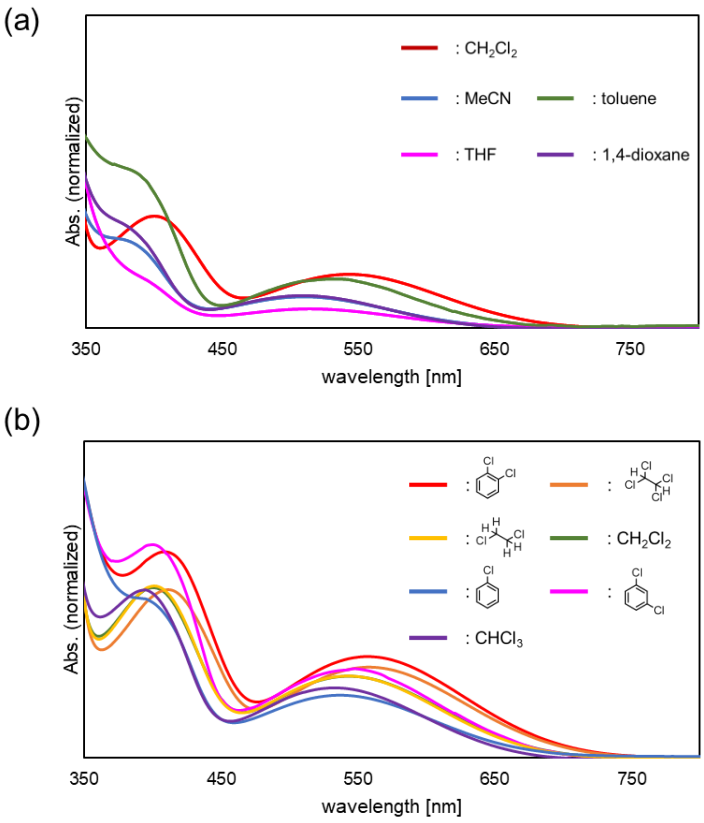

Figure 3-12. Vis-NIR spectra of **12-O**$^{+}BF_4^{-}$ (a) in CH_2Cl_2 (red) and non-halogenated solvents and (b) in chlorinated solvents.

Considering that previously reported quinolizinium-based D-A-type dyes by Vaquero and co-workers utilize the same donor units as **12**$^+$ but only absorb the light up to 600 nm at most, these results shown in this study suggest the higher π-electron acceptability of CAA **12-N**$^+$$BF_4^-$ than that of conventional quinolizinium-based cationic acceptors.

3-2-5. Redox Behavior of 12-N$^+$ and 12-O$^+$

Cyclic voltammetry measurements of cation salts **12-N**$^+$$BF_4^-$ and **12-O**$^+$$BF_4^-$ in CH_2Cl_2 and MeCN were carried out to investigate their redox behaviors and correlations between HOMO-LUMO gap and solvent polarity.

Voltammetric analysis of **12-N**$^+$$BF_4^-$ showed a one-electron reduction peak corresponding to the CAA moiety at -1.14 V vs Fc/Fc^+ in CH_2Cl_2. In MeCN, such a reduction peak anodically shifted and appeared at -0.81 V, indicating that the LUMO level can be lowered in the polar solvent. This reduction process to generate neutral species **12-N**$^{\bullet}$ is electrochemically irreversible in the sense that the return peaks were absent in both solvents (Figure 3-13a). Instead, new peaks appeared in the far anodic region (+0.03 V in CH_2Cl_2 and -0.08 V in MeCN), and the smaller current than the corresponding reduction peak is probably due to dispersion. The latter peak was estimated as the oxidation peak of the corresponding σ-bonded dimer of **12-N**$^{\bullet}$. In contrast to the irreversible reduction process of **12-N**$^+$$BF_4^-$, (quasi-)reversible one-electron oxidation processes were observed at $E_{1/2}$ = +0.50 V and +0.47 V in CH_2Cl_2 and MeCN, respectively (Figure 3-13a). According to the DFT calculation of **12-N**$^+$ (Figure 3-6), the oxidation process is corresponding to the electron transfer from the bis(dimethylamino)stilbene moiety, on which the coefficients of HOMO were mainly located. In addition, (quasi-)reversible processes indicated that one-electron oxidized species **12-N**$^{2+\bullet}$$BF_4^-$ is considered to be stable at least under voltammetric conditions.

In the case of **12-O**$^+$$BF_4^-$, voltammetric analysis showed a one-electron reduction peak corresponding to the CAA moiety at -0.83 V vs Fc/Fc^+ and -0.74 V in CH_2Cl_2 and MeCN, respectively, with no return peaks in both solvents (Figure 3-13b). This result indicates that there is almost no change in the LUMO level regardless of the solvent polarity for **12-O**$^+$. The new peak estimated as the oxidation peak of the corresponding σ-bonded dimer was not observed in both solvents, unlike the case of **12-N**$^+$$BF_4^-$. In the anodic region, one-electron oxidation peaks were observed at +1.29 V and +1.25 V in CH_2Cl_2 and MeCN, respectively, however, the return peaks were absent in both solvents (Figure 3-13b). Therefore, **12-O**$^{2+\bullet}$$BF_4^-$ generated by the one-electron oxidation is considered unstable in solution probably due to the less donating ability of methoxyphenyl groups, as opposed to **12-N**$^{2+\bullet}$$BF_4^-$ with dimethylaminophenyl groups.

These results indicate that both **12-N**$^+$$BF_4^-$ and **12-O**$^+$$BF_4^-$ are electrochemically amphoteric due to their D-A type structures. The HOMO-LUMO gap of **12-N**$^+$$BF_4^-$ is narrower

than that of **12-O**$^{+}BF_4^{-}$, which is supported by the observed red-shift in the UV-Vis-NIR spectra between **12-N**$^{+}BF_4^{-}$ and **12-O**$^{+}BF_4^{-}$.

However, the difference in the HOMO-LUMO gap between the CH_2Cl_2 and MeCN solutions did not support the solvent effects in photo-absorption of **12-N**$^{+}BF_4^{-}$ and **12-O**$^{+}BF_4^{-}$, especially in the case of **12-N**$^{+}BF_4^{-}$. This might be the reason that the molecules of cation **12**$^{+}$ are surrounded not only by solvents but also by a large amount of supporting electrolytes under the condition of cyclic voltammetry measurements, so the interactions among organic cations, organic solvents, and counter anions are not the same as under that of UV-Vis-NIR spectroscopic measurements.

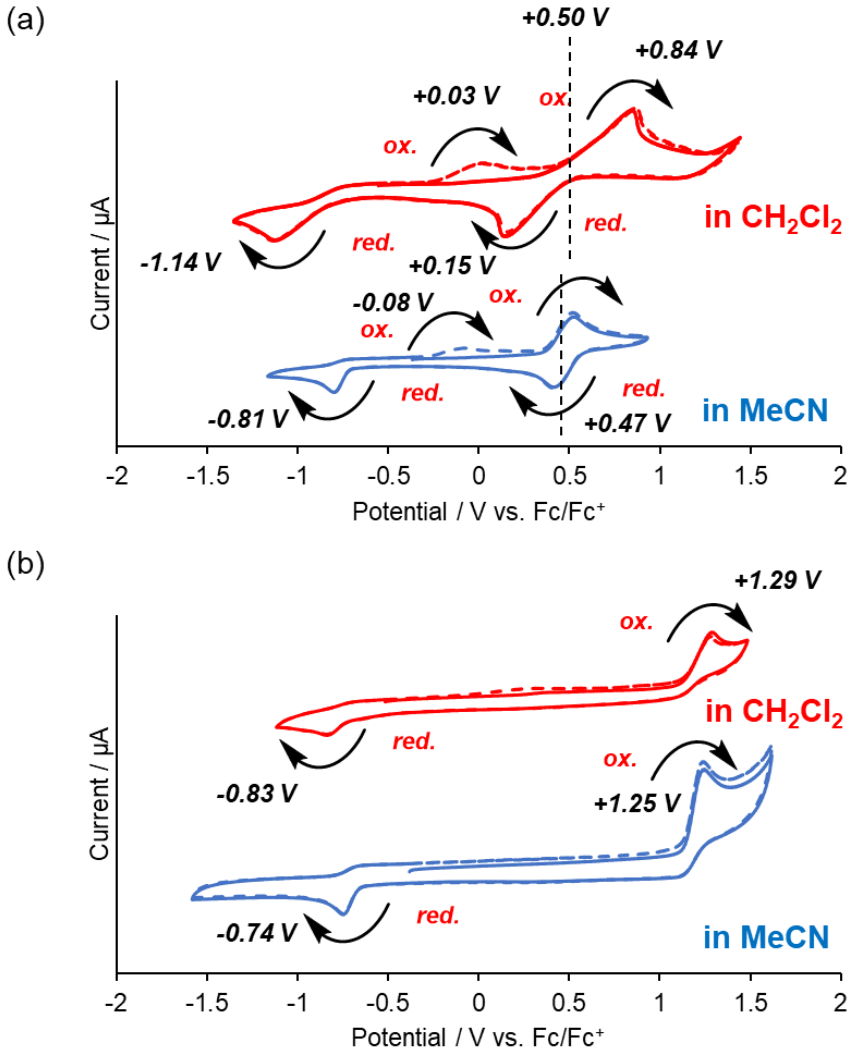

Figure 3-13. Cyclic voltammograms of (a) **12-N**$^{+}BF_4^{-}$ and (b) **12-O**$^{+}BF_4^{-}$ in CH_2Cl_2 (red, 0.1 M n-$Bu_4N^{+}BF_4^{-}$) and in MeCN (blue, 0.1 M $Et_4N^{+}ClO_4^{-}$). Scan rate: 500 mV s^{-1}. The second cycles are shown by a dotted line.

3-2-6. Halochromic Behavior of 12-N$^+$

Due to the high basicity of cation **12**$^+$ bearing electron-donative heteroatoms, **12-N**$^+$ with the higher donating dimethylaniline units, especially, is expected to be easily protonated by Brønsted acids. Based on the NIR absorption attributed to the ICT from the electron-rich stilbene unit to the electron-poor CAA unit, **12-N**$^+$ has the potential to be applied for halochromic materials accompanying the ON/OFF switching of absorptions in the NIR region because the protonation would cause lowering the HOMO level. Furthermore, double protonation of **12-N**$^+$ is estimated to proceed in a stepwise manner because the two dimethylamino groups are in different electronic states due to its unsymmetric structure of **12-N**$^+$ as revealed by X-ray. Thus, tri-color halochromism based on three-state interconversion among **12-N**$^+$, monoprotonated adduct, and diprotonated adduct could be realized (Scheme 3-4).

Scheme 3-4 Stepwise protonation/deprotonation of **12-N**$^+$.

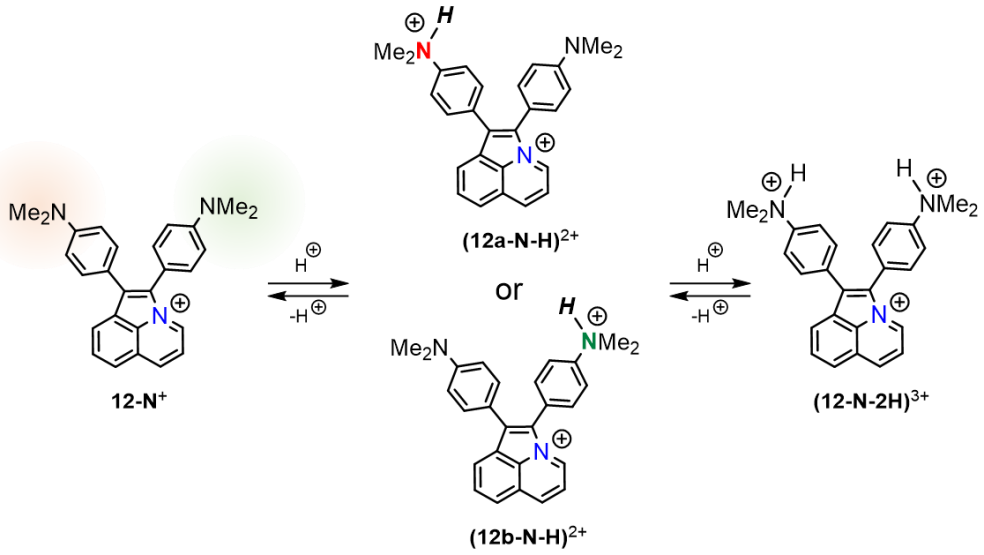

Firstly, an NMR experiment was conducted to investigate the reversibility of protonation/deprotonation processes using **12-N**$^+$$BF_4^-$ in MeCN (Figure 3-14). When an excess amount of trifluoroacetic acid was added to an acetonitrile-d_3 (CD_3CN) solution of **12-N**$^+$$BF_4^-$ in an NMR tube, quantitative transformation from **12-N**$^+$ to diprotonated adduct (**12-N-2H**)$^{3+}$ was observed. The original cation **12-N**$^+$ was completely reproduced by the addition of an excess amount of triethylamine to the as-generated trication (**12-N-2H**)$^{3+}$ in CD_3CN. According to these results, since oligocations generated by protonation of **12-N**$^+$$BF_4^-$ are stable enough in solution, both protonation/deprotonation of **12-N**$^+$ proceed quantitively with high reversibility.

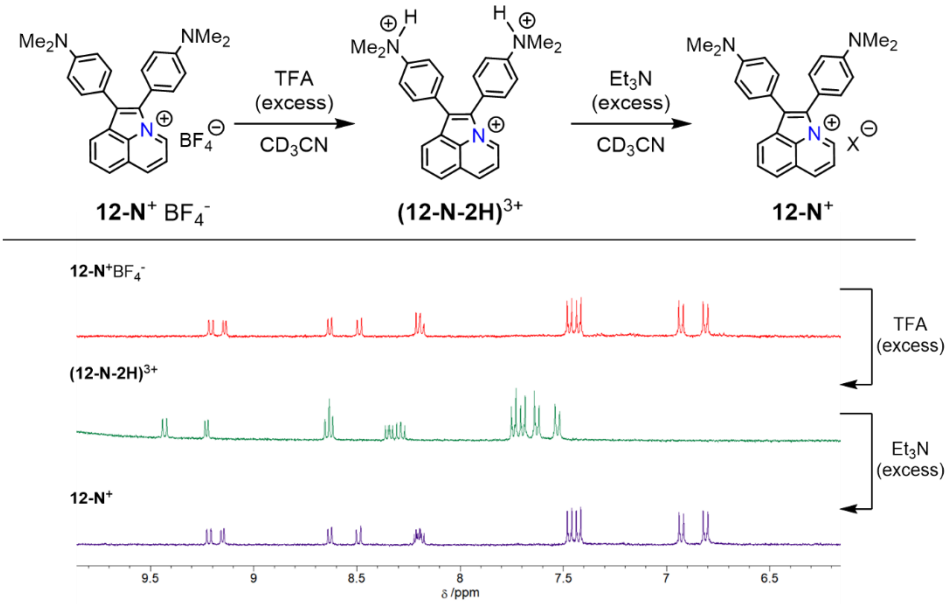

Figure 3-14. Changes in ^{1}H NMR spectrum of **12-N**$^{+}$$BF_4^{-}$ in acetonitrile-d_3 upon the addition of an excess amount of TFA and followed by the addition of an excess amount of triethylamine.

Based on the quantitative interconversion of **12-N**$^{+}$$BF_4^{-}$ with acid/base in solution on the NMR scale, halochromic behavior was then examined by following the protonation/deprotonation processes of **12-N**$^{+}$/(**12-N-2H**)$^{3+}$ by UV-Vis-NIR spectroscopy in MeCN (Figure 3-15). Isosbestic points were observed in both processes, showing clean interconversion between **12-N**$^{+}$ and (**12-N-2H**)$^{3+}$. As expected, the color changes of both processes occurred via the same intermediary state showing blue. To gain further insight into whether the intermediary protonated adduct is (**12a-N-H**)$^{2+}$ or (**12b-N-H**)$^{2+}$, DFT calculations were conducted at B3LYP/6-31G(d) level for each molecule. The author found that (**12a-N-H**)$^{2+}$ protonated on the opposite side of cationic quaternary nitrogen in the CAA unit has a slightly lower Gibbs energy, meaning that (**12a-N-H**)$^{2+}$, which is slightly more stable than another conformer (**12b-N-H**)$^{2+}$, may be observed. Therefore, this study revealed that **12-N**$^{+}$ can be used not only as an NIR-absorbing dye but also as a tri-color halochromic system.

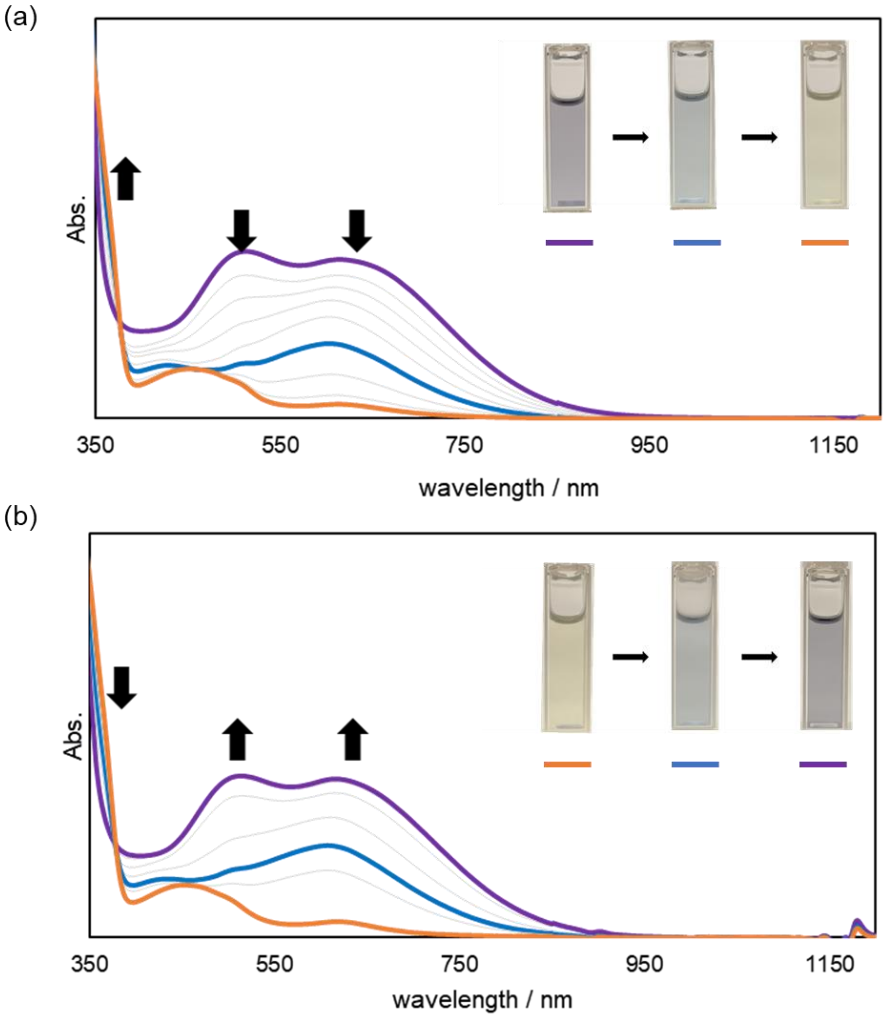

Figure 3-15. Changes in the UV-Vis-NIR absorption spectra of (a) **12-N**$^{+}BF_4^{-}$ in MeCN (6.0×10^{-5} M) with increasing concentrations of TFA [(0.0, 1.5, 3.0, 6.0, 12, 30, 60, 120, 180) $\times 10^{-3}$ M] and (b) as-prepared (**12-N-2H**)$^{3+}$ in MeCN (6.0×10^{-5} M) with increasing concentrations of Et_3N [(0.0, 30, 60, 90, 120, 180, 360) $\times 10^{-3}$ M]. The insets show the photograph of solutions during the experiments.

3-3. Conclusion

In this work, the author developed the synthetic method for CAA, the new family of AZAHs. Upon two-electron oxidation of 8-quinolyl diarylethene derivatives **10**, the CAA skeleton was efficiently formed via the intramolecular nucleophilic attack to the carbenium center from the nitrogen atom on the quinoline skeleton and 1,2-migration of an aromatic ring followed by deprotonation to produce the desired cation **12-N**$^+$. Additionally, newly synthesized D-A type cationic dyes, **12-N**$^+$$BF_4^-$ and **12-O**$^+$$BF_4^-$, exhibit large red-shifted absorptions compared to the conventional quinolizinium-based D-A π-conjugated dyes bearing the same donor units as **12**$^+$. Especially in the case of **12-N**$^+$$BF_4^-$, the longer-wavelength absorption was achieved and its edge reached around 1000 nm. These results were based on the higher π-electron acceptability of the CAA unit than that of the previously reported AZAHs consistiing only of hexagonal rings. The UV-Vis-NIR spectrum of **12-N**$^+$$BF_4^-$ and **12-O**$^+$$BF_4^-$ was specifically affected by chlorinated solvents, which is similar to the case of the reported cationic organic dyes containing a cationic nitrogen atom. With the stepwise protonation of two donor units in **12-N**$^+$$BF_4^-$, clean tri-color halochromism was observed. This work demonstrated that the incorporation of cationic nitrogen into CP-PAHs is effective for the construction of a highly π-electron-accepting unit to develop NIR-absorbing D-A-type dyes with a minimal skeleton.

3-4. Experimental Section

3-4-1. General

All reactions were carried out under an argon atmosphere. All commercially available compounds were used without further purification unless otherwise indicated. Compounds 8-quinolinecarboxaldehyde[26], **9-N**[27] and **9-O**[28] were synthesized according to the reported procedures. Dry MeCN was obtained by distillation from CaH_2 prior to use. Column chromatography was performed on silica gel 60N (KANTO KAGAKU, spherical neutral) of particle size 40–50 μm or Wakogel® 60N (neutral) of particle size 38-100 μm. ^1H and ^{13}C NMR spectra were recorded on a BRUKER Ascend™ 400 (^1H/400 MHz and ^{13}C/100 MHz) spectrometer or a JEOL ECA600 (^1H/600 MHz and ^{13}C/151 MHz) spectrometer. IR spectra were measured on a Shimadzu IRAffinity-1S spectrophotometer using the attenuated total reflection (ATR) mode. Mass spectra were recorded on a JEOL JMS-T100GCV spectrometer in FD mode (GC-MS&NMR Laboratory, Research Faculty of Agriculture, Hokkaido University). Melting points were measured on a Stanford Research Systems MPA100 Optimelt and are uncorrected. UV-Vis-NIR spectra were recorded on a JASCO V-770 spectrophotometer. Redox potentials (E^{ox} and E^{red}) were measured on a BAS ALS-612EX by cyclic voltammetry. Pt electrodes were used as the working (disk) and counter electrodes. The working electrode was polished using a water suspension of aluminum oxide (0.05 μm) before use. DFT calculations were performed with the Gaussian 16 W program package.[29] The geometries of the compounds were optimized by using the B3LYP method in combination with the 6-31G(d) basis set. Single-crystal X-ray structure analyses were performed by a Rigaku XtaLAB Synergy (Cu-Kα radiation, λ = 1.54184 Å) with HyPix diffractometer. Using Olex2,[30] the structure was solved with the SHELXT[31] structure solution program using Intrinsic Phasing and refined with the SHELXL[32] refinement package using Least Squares minimization. All the hydrogen atoms were located at the calculated positions and refined with riding.

3-4-2. Preparations

Synthesis of 10-N

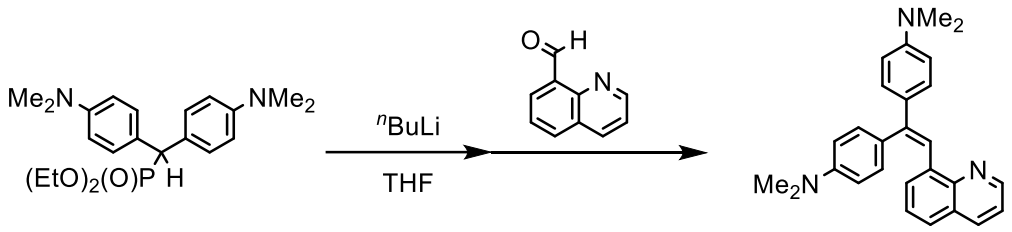

9-N **10-N**

To a solution of phosphonate **9-N** (6.83 g, 17.5 mmol) in dry THF (120 mL) was added ^{n}BuLi (2.69 M in hexane, 6.50 mL, 17.5 mmol) dropwise over 3 min at -78 °C. After stirring at -78 °C for 1 h, 8-quinolinecarboxaldehyde (2.50 g, 15.9 mmol) in dry THF (40 mL) was added to the reaction mixture at -78 °C. The resulting solution was stirred for 30 min at -78 °C and for another 2.5 h at 28 °C, then the reaction was quenched with water (100 mL). The organic layer was collected and the aqueous layer was extracted with CH_2Cl_2 (250 mL × 2). The combined organic layers were washed with water and brine, and dried over anhydrous sodium sulfate. After filtration, the solution was evaporated under reduced pressure. The crude product was purified by a silica gel column (diameter, 5.0 cm, height, 30 cm) using EtOAc/hexane (3:7, v/v) as eluent (R_f = 0.44) to give compound **10-N** (5.05 g) as a yellow solid in 81% yield.

Mp 164-165 °C; ^{1}H NMR (400 MHz, $CDCl_3$): δ/ppm = 8.94 (1H, dd, *J* = 1.8, 4.2 Hz), 8.10 (1H, dd, *J* = 1.8, 8.3 Hz), 7.80 (1H, s), 7.54 (1H, d, *J* = 6.8 Hz), 7.34 (1H, dd, 4.2, 8.2 Hz), 7.35-7.30 (3H, m), 7.21 (1H, t, 7.8 Hz), 7.09 (2H, d, *J* = 8.8 Hz), 6.68 (2H, d, *J* = 8.9 Hz), 6.61 (2H, d, *J* = 8.8 Hz), 2.97 (6H, s), 2.95 (6H, s); ^{13}C NMR (100 MHz, $CDCl_3$): δ/ppm = 150.18, 149.67, 149.32, 147.37, 144.37, 137.61, 136.35, 132.97, 131.87, 129.95, 129.44, 129.10, 128.39, 126.17, 125.54, 120.95, 120.18, 112.22, 112.00, 40.68, 40.57; IR (ATR): ν/cm^{-1} = 3046, 3029, 2994, 2886, 2800, 1607, 1586, 1566, 1516, 1493, 1478, 1442, 1361, 1337, 1320, 1264, 1253, 1234, 1219, 1201, 1189, 1174, 1163, 1147, 1123, 1081, 1071, 1058, 1040, 1026, 942, 903, 879, 821, 810, 792, 766, 752, 729, 715, 671, 619, 575, 542, 516; LR-MS (FD) m/z (%): 395.22 (5), 394.21 (31), 393.21 (bp, M^+); HR-MS (FD) Calcd. for $C_{27}H_{27}N_3$: 393.22050; Found: 393.22232.

Synthesis of X 11-N

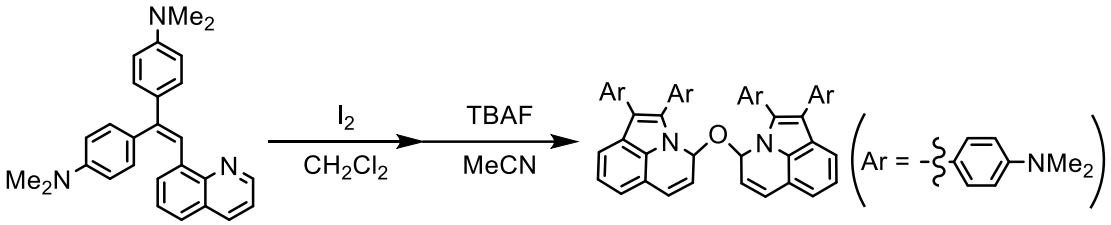

10-N **11-N**

To a solution of **10-N** (2.36 g, 6.00 mmol) in degassed CH_2Cl_2 (60 mL) was added I_2 (4.57 g, 18.0 mmol) at 27 °C. After stirring at 27 °C for 18 h, the solvents were evaporated under reduced pressure. The resulting solids were dissolved in MeCN (96 mL) and TBAF・$3H_2O$ (9.47 g, 30 mmol) in MeCN (24 mL) was added at 0 °C. After stirring for 1 h at 27 °C, the reaction mixture was diluted with Sat. aqueous $Na_2S_2O_3$ (20 mL) and water (80 mL), and extracted with CH_2Cl_2 (200 mL × 3). The combined organic layers were washed with water, and dried over anhydrous sodium sulfate. After filtration, the solution was evaporated under reduced pressure. The crude product was purified by an alumina column (diameter, 4.0 cm, height, 20 cm) using EtOAc/hexane (3:7, v/v) as eluent (R_f = 0.24) to give ether **11-N** (798 mg) as a yellow solid in 33% yield. Compound **11-N** was obtained as a mixture of diastereomers and its ratio could not be determined.

Mp 137-140 °C (decomp.); ^{1}H NMR (400 MHz, acetone-d_6): δ/ppm = 7.62-7.57 (2H, m), 7.41 (2H, d, J = 8.9 Hz), 7.34 (2H, d, J = 8.9 Hz), 7.23 (2H, d, J = 9.0 Hz), 7.21 (2H, d, J = 8.9 Hz), 7.13-7.09 (4H, m), 6.95 (1H, d, J = 9.8 Hz), 6.78-6.70 (9H, m), 6.40 (1H, d, J = 4.2 Hz), 6.35-6.32 (1H, m), 6.16 (1H, dd, J = 5.2, 10 Hz), 6.03 (1H, dd, J = 4.6, 9.8 Hz), 2.99 (12H, s), 2.93 (12H, s); IR (ATR): ν/cm^{-1} = 3036, 2885, 2798, 2360, 1612, 1559, 1526, 1500, 1487, 1458, 1443, 1399, 1347, 1325, 1281, 1244, 1225, 1194, 1166, 1126, 1093, 1054, 1044, 993, 944, 822, 803, 743, 651, 629, 572, 557, 526; The measurement of ^{13}C NMR spectroscopy was difficult because compound **11-N** is unstable in solution. Compound **11-N** was decomposed under the condition of FD-MS.

Synthesis of 12-$N^+BF_4^-$

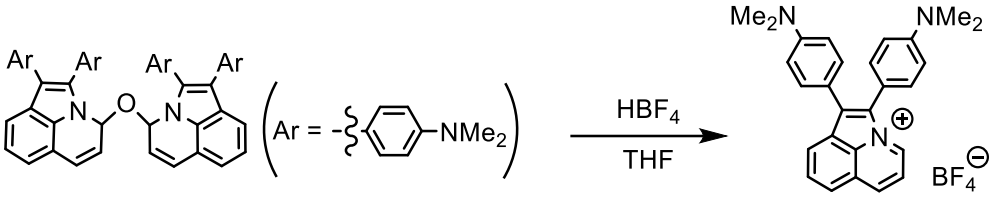

11-N **12-$N^+BF_4^-$**

To a solution of ether **11-N** (320 mg, 0.400 mmol) in dry THF (10 mL) was added 42% aqueous HBF_4 (0.120 mL, 0.800 mmol) at 0 °C. After stirring at 26 °C for 15 min, the addition of dry CH_2Cl_2 (6.0 mL) and dry Et_2O (100 mL) led to precipitation of the cation salt. The precipitates were collected and washed with dry Et_2O (100 mL× 2), and dried *in vacuo* to give **12-$N^+BF_4^-$** (316 mg) as a dark purple solid in 83% yield.

Mp >400 °C; ^{1}H NMR (600 MHz, $CDCl_3$): δ/ppm = 9.28 (1H, d, *J* = 3.9 Hz), 9.23 (1H, d, *J* = 5.4 Hz), 8.49 (1H, d, *J* = 4.7 Hz), 8.45-8.43 (2H, m), 8.10 (1H, t, *J* = 5.3 Hz), 7.39 (4H, d, *J* = 5.8 Hz), 6.83 (2H, d, *J* = 5.6 Hz), 6.73 (2H, d, *J* = 5.7 Hz), 3.06 (6H, s), 3.03 (6H, s); ^{13}C NMR (151 MHz, $CDCl_3$): δ/ppm = 151.67, 150.92, 146.10, 139.47, 137.22, 134.26, 132.31, 132.19, 131.61, 131.07, 130.96, 130.90, 130.17, 125.72, 125.53, 117.04, 112.90, 112.56, 111.54, 40.27, 40.23; IR (ATR): ν/cm^{-1} = 3093, 2897, 2804, 1668, 1648, 1605, 1511, 1447, 1419, 1363, 1348, 1269, 1227, 1195, 1157, 1050, 1034, 942, 829, 801, 765, 657, 630, 600, 571, 554, 519; LR-MS (FD) m/z (%): 394.21 (21), 393.21 (81), 392.21 (bp, M^+); HR-MS (FD) Calcd. for $C_{27}H_{26}N_3$: 392.21267; Found: 392.21112.

Synthesis of 12-N$^+$PF$_6^-$

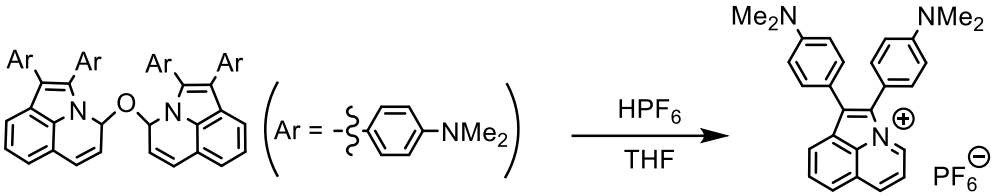

11-N **12-N$^+$PF$_6^-$**

To a solution of ether **11-N** (280 mg, 0.350 mmol) in dry THF (8.0 mL) was added 60% aqueous HPF_6 (0.104 mL, 0.707 mmol) at 0 °C. After stirring at 26 °C for 15 min, the addition of dry CH_2Cl_2 (5.0 mL) and dry Et_2O (60 mL) led to precipitation of the cation salt. The precipitates were collected and washed with dry Et_2O (60 mL), and dried *in vacuo* to give **12-N**$^+PF_6^-$ (324 mg) as a purple solid in 86% yield.

Mp 172-177 °C (decomp.); ^{1}H NMR and ^{13}C NMR spectra are identical to those of **12-N**$^+BF_4^-$; IR (ATR): $\tilde{\nu}$/cm^{-1} = 3100, 2807, 1611, 1506, 1448, 1421, 1368, 1348, 1267, 1233, 1191, 1158, 1126, 1062, 1017, 998, 944, 837, 799, 772, 652, 598, 556; LR-MS (FD) m/z (%): 394.18 (6), 393.18 (34), 392.17 (bp, M$^+$); HR-MS (FD) Calcd. for $C_{27}H_{26}N_3$: 392.21267; Found: 392.21290.

Synthesis of 10-O

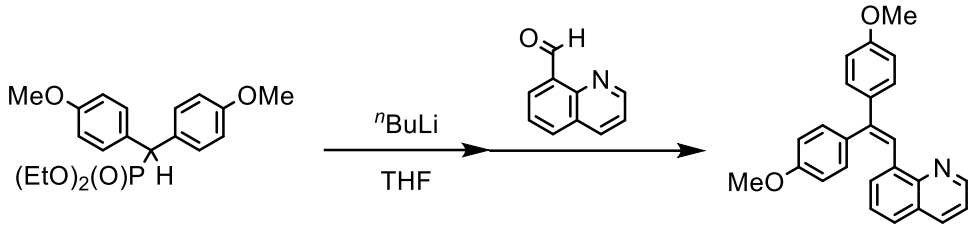

9-N **10-O**

To a solution of phosphonate **9-N** (3.61 g, 9.90 mmol) in dry THF (50 mL) was added ^{n}BuLi (1.56 M in hexane, 6.35 mL, 9.90 mmol) dropwise over 3 min at -78 °C. After stirring at -78 °C for 1 h, 8-quinolinecarboxaldehyde (1.41 g, 9.00 mmol) in dry THF (40 mL) was added to the reaction mixture at -78 °C. The resulting solution was stirred for 30 min at -78 °C and for another 2.5 h at 23 °C, then the reaction was quenched with water (90 mL). The organic layer was collected and the aqueous layer was extracted with CH_2Cl_2 (150 mL × 2). The combined organic layers were washed with water and brine, and dried over anhydrous sodium sulfate. After filtration, the solution was evaporated under reduced pressure. The crude product was purified by a silica gel column (diameter, 5.0 cm, height, 25 cm) using EtOAc/hexane (3:7, v/v) as eluent (R_f = 0.49) to give compound **10-O** (2.41 g) as a pale yellow solid in 73% yield.

Mp 128-129 °C; ^{1}H NMR (400 MHz, $CDCl_3$): δ/ppm = 8.94 (1H, dd, *J* = 1.8, 4.2 Hz), 8.10 (1H, dd, *J* = 1.8, 8.3 Hz), 7.89 (1H, s), 7.57 (1H, dd, *J* = 1.6, 7.8 Hz), 7.39 (1H, dd, 4.2, 8.2 Hz), 7.36 (2H, d, *J* = 8.9 Hz), 7.25-7.17 (2H, m), 7.12 (2H, d, 8.8 Hz), 6.85 (2H, d, *J* = 8.9 Hz), 6.78 (2H, d, *J* = 8.8 Hz), 3.81 (3H, s), 3.79 (3H, s); ^{13}C NMR (100 MHz, $CDCl_3$): δ/ppm = 159.17, 158.70, 149.29, 147.07, 142.93, 136.56, 136.47, 136.16, 132.95, 131.77, 129.91, 129.28, 128.10, 126.15, 125.84, 122.66, 120.91, 113.67, 113.30, 55.06, 54.92; IR (ATR): ν/cm^{-1} = 3059, 2999, 2953, 2932, 2907, 2834, 1605, 1590, 1507, 1492, 1462, 1451, 1439, 1416, 1385, 1361, 1353, 1319, 1304, 1280, 1258, 1241, 1180, 1172, 1116, 1107, 1083, 1035, 1028, 953, 874, 826, 808, 799, 787, 761, 739, 730, 681, 637, 619, 581, 544, 522, 507; LR-MS (FD) m/z (%): 369.10 (5), 368.10 (29), 367.10 (bp, M^+); HR-MS (FD) Calcd. for $C_{25}H_{21}NO_2$: 367.15723; Found: 367.15849.

Synthesis of 11-O

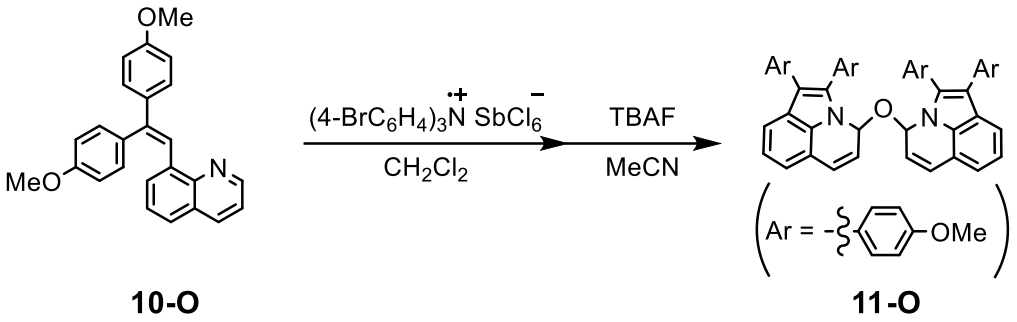

10-O **11-O**

To a solution of **10-O** (1.47 g, 4.00 mmol) in degassed CH_2Cl_2 (120 mL) was added tris(4-bromophenyl)aminium hexachloroantimonate (6.53 g, 8.00 mmol) at 23 °C. After stirring at 23 °C for 1 h, the solvents were evaporated under reduced pressure. The resulting solids were dissolved in MeCN (80 mL) and TBAF・$3H_2O$ (6.31 g, 20 mmol) in MeCN (20 mL) was added at 0 °C. After stirring for 1 h at 23 °C, the reaction mixture was diluted with water (150 mL), and extracted with CH_2Cl_2 (150 mL × 2). The combined organic layers were washed with water, and dried over anhydrous sodium sulfate. After filtration, the solution was evaporated under reduced pressure. The crude product was purified by an alumina column (diameter, 4.0 cm, height, 20 cm) using EtOAc/hexane (1:4, v/v) as eluent (R_f = 0.35) to give ether **11-O** (179 mg) as a yellow solid in 12% yield.

Mp 104-107 °C (decomp.); ^{1}H NMR (400 MHz, $CDCl_3$): δ/ppm = 7.71-7.69 (2H, m), 7.44 (4H, d, *J* = 8.8 Hz), 7.29 (4H, d, *J* = 8.9 Hz), 7.19-7.18 (4H, m), 7.01 (2H, d, *J* = 9.7 Hz), 6.94 (4H, d, *J* = 8.8 Hz), 6.86 (4H, d, *J* = 8.9 Hz), 6.43 (2H, dd, *J* = 4.3, 9.3 Hz), 6.15 (2H, dd, *J* = 4.4, 9.6 Hz), 3.85 (6H, s), 3.81 (6H, s); IR (ATR): *ν*/cm^{-1} = 3047, 2955, 2932, 2833, 2365, 1610, 1577, 1551, 1517, 1497, 1487, 1459, 1441, 1400, 1378, 1322, 1288, 1241, 1175, 1108, 1093, 1026, 972, 928, 835, 805, 744, 651, 627, 582, 562, 529; The measurement of ^{13}C NMR spectroscopy was difficult because compound **11-O** is unstable in solution. Compound **11-O** was decomposed under the condition of FD-MS.

Synthesis of 12-O$^+$BF$_4^-$

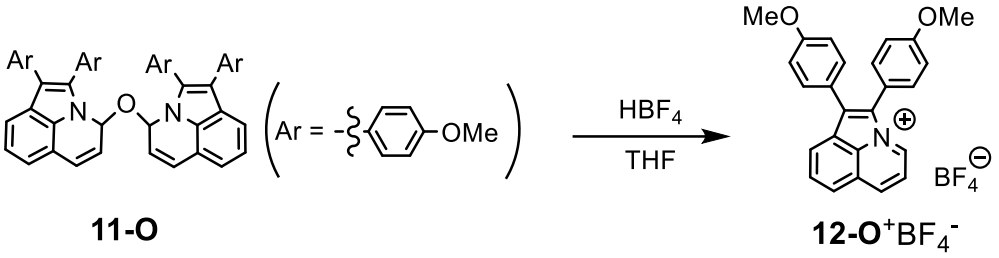

11-O **12-O$^+$BF$_4^-$**

To a solution of ether **11-O** (70.0 mg, 93.5 μmol) in dry THF (2.0 mL) was added 42% aqueous HBF_4 (0.140 mL, 0.935 mmol) at 0 °C. After stirring at 22 °C for 15 min, the addition of dry CH_2Cl_2 (1.0 mL) and dry Et_2O (15.0 mL) led to precipitation of the cation salt. The precipitates were collected and washed with dry Et_2O (15.0 mL), and dried *in vacuo* to give **12-O** $^+BF_4^-$ (48.9 mg) as a red-purple solid in 58% yield.

Mp 193-196 °C (decomp.); ^{1}H NMR (400 MHz, CD_3CN): δ/ppm = 9.29 (1H, dd, *J* = 0.84, 8.2 Hz), 9.15 (1H, d, *J* = 5.9 Hz), 8.62 (1H, d, *J* = 7.1 Hz), 8.54 (1H, d, *J* = 7.7 Hz), 8.25-8.19 (2H, m), 7.53 (2H, d, *J* = 8.9 Hz), 7.50 (2H, d, *J* = 8.9 Hz), 7.16 (2H, d, *J* = 8.9 Hz), 7.04 (2H, d, *J* = 8.9 Hz), 3.90 (3H, s), 3.84 (3H, s); ^{13}C NMR (100 MHz, CD_3CN): δ/ppm = 162.69, 161.80, 148.06, 141.60, 138.97, 136.16, 134.12, 133.47, 132.72, 132.43, 132.03, 131.82, 131.45, 126.58, 125.58, 122.76, 116.09, 115.71, 56.39, 56.24; IR (ATR): ν/cm^{-1} = 3102, 3082, 2973, 2936, 2840, 2550, 1652, 1611, 1508, 1501, 1465, 1451, 1426, 1369, 1349, 1296, 1274, 1249, 1175, 1163, 1129, 1052, 1028, 1017, 955, 851, 836, 806, 788, 768, 734, 722, 657, 630, 586, 560, 521; LR-MS (FD) m/z (%): 368.12 (4), 367.12 (28), 366.12 (bp, M$^+$); HR-MS (FD) Calcd. for $C_{25}H_{20}NO_2$: 366.14940; Found: 366.15107.

3-4-3. X-ray Analyses

Table 3-1. Crystal data of **11**-N, **12**-$N^+PF_6^-$, and **12**-$O^+BF_4^-$.

Compounds	**11**-N	**12**-$N^+PF_6^-$	**12**-$O^+BF_4^-$
Solvent system	$CHCl_3$/hexane	CH_2Cl_2/Et_2O	CH_3CN /Et_2O
Empirical formula	$C_{57}H_{59}N_6O$	$C_{27}H_{26}F_6N_3P$	$C_{25}H_{20}BF_4NO_2$
Formula weight	844.10	537.48	453.23
Temperature/K	150	150	150
Crystal system	triclinic	triclinic	monoclinic
Space group	*P*-1	*P*-1	$P2_1/n$
a/Å	11.77507(17)	11.6291(2)	16.4244(6)
b/Å	12.48597(19)	15.0837(4)	7.8987(3)
c/Å	17.3233(2)	17.3533(3)	16.8043(6)
α/°	110.3080(14)	74.6776(19)	90
β/°	99.5921(12)	89.8157(16)	99.589(3)
γ/°	98.2907(13)	68.095(2)	90
Volume/Å^3	2298.31(6)	2708.29(11)	2149.57(15)
Z	2	4	4
ρ_{calc} g/cm^3	1.220	1.318	1.400
μ/mm^{-1}	0.566	1.452	0.944
Color and shape	yellow block	dark violet plate	dark red plate
Crystal size/mm^3	0.25 × 0.2 × 0.1	0.3 × 0.2 × 0.02	0.155 × 0.082 × 0.031
Reflections	42244	51213	14163
R_{int}	0.0264	0.0337	0.0296
Data/restraints/para	9304/0/586	11056/0/675	4320/228/403
GOF	1.052	1.070	1.078
R_1 [I>=2σ(I)]	0.0486	0.0596	0.0636
wR_2 [I>=2σ(I)]	0.1375	0.1666	0.1555
R_1 [all data]	0.0545	0.0646	0.0781
wR_2 [all data]	0.1419	0.1702	0.1648
Largest diff.peak/hole/e Å^{-3}	0.56/-0.22	0.57/-0.40	0.26/-0.24
Solvent mask	None	Used for the analysis	None

3-5. References

[1] G. Chen, H. Sasabe, T. Igarashi, Z. Hong, J. Kido, *J. Mater. Chem. A.* **2015**, *3*, 14517.

[2] S. Ghosh, S. Cherumukkil, C. H. Suresh, A. Ajayaghosh, *Adv. Mater.* **2017**, *29*, 1703783.

[3] H. Han, Y. J. Lee, J. Kyhm, J. S. Jeong, J. Han, M. K. Yang, K. M. Lee, Y. Choi, T. Yoon, H. Ju, S. Ahn, J. A. Lim. *Adv. Funct. Mater.* **2020**, *30*, 2006236.

[4] J. Fabian, H. Nakazumi, M. Matsuoka, *Chem. Rev.* **1992**, *92*, 1197.

[5] G. Qian, Z. Y. Wang, *Chem. Asian J.* **2010**, *5*, 1006.

[6] Weil, T. Vosch, J. Hofkens, K. Peneva, K. Müllen, *Angew. Chem. Int. Ed.* **2010**, *49*, 9068.

[7] H. Langhals, *Heterocycles* **1995**, *40*, 477.

[8] F. Würthner, *Chem. Commun.* **2004**, 1564.

[9] C. Huang, S. Barlow, S. R. Marder, *J. Org. Chem.* **2011**, *76*, 2386.

[10] K. Ono, S. Tanaka, Y. Yamashita, *Angew. Chem. Int. Ed.* **1994**, *33*, 1977.

[11] M. Karikomi, C. Kitamura, S. Tanaka, Y. Yamashita, *J. Am. Chem. Soc.* **1995**, *117*, 6791.

[12] C. Kitamura, S. Tanaka, Y. Yamashita, *Chem. Mater.* **1996**, *8*, 570.

[13] Y. Yamashita, K. Ono, M. Tomura, S. Tanaka, *Tetrahedron* **1997**, *53*, 10169.

[14] D. Sucunza, A. A. Cuadro, J. Alvarez-Builla, J. J. Vaquero, *J. Org. Chem.* **2016**, *81*, 10126.

[15] T. Cañeque, A. M. Cuadro, J. Alvarez-Builla, J. Pérez-Moreno, K. Clays, O. Castaño, J. L. Andrés, J. J. Vaquero, *Dyes Pigm.* **2014**, *101*, 116.

[16] T. Cañeque, A. M. Cuadro, R. Custodio, J. Alvarez-Builla, B. Batanero, P. Gómez-Sal, J. Pérez-Moreno, K. Clays, O. Castaño, J. L. Andrés, T. Carmona, F. Mendicuti, J. J. Vaquero, *Dyes Pigm.* **2017**, *144*, 17.

[17] D. Farquhar, T. T. Gough, D. Leaver, J. F. Miller, J. W. Dick, M. A. Jessep, *J. Chem. Soc., Perkin Trans. 1*, **1984**, 2553.

[18] Davies. D. L, Ellul. C. E, Macgregor. S. A, McMullin. C. L, Singh. K, *J. Am. Chem. Soc.* **2015**, *137*, 9659.

[19] P. Bosch, G. Marcelo, A. Matamoros-Recio, D. Sucunza, F. Mendicuti, A. Domingo, J. J. Vaquero, *Dyes Pigm.* **2021**, *192*, 109443.

[20] Chaolumen, M. Murata, A. Wakamiya, Y. Murata, *Org. Lett.* **2017**, *19*, 826.

[21] K. Yamamoto, Y. Ie, N. Tohnai, F. Kakiuchi, Y. Aso, *Sci. Rep.* **2018**, *8*, 17663.

[22] Q. Xie, E. Perez-Cordero, L. Echegoyen, *J. Am. Chem. Soc.* **1992**, *114*, 3978.

[23] Y. Chabre, D. Djurado, M. Armand, W. R. Romanow, N. Coustel, J. P. McCauley Jr., J. E. Fischer, A. B. Smith III, *J. Am. Chem. Soc.* **1992**, *114*, 764.

[24] T. Higashino, Y. Ooyama, *Chem. Lett.* **2021**, *50*, 1530.

[25]A. Tamoto, N. Aratani, H. Yamada, *J. Photochem. Photobiol. Chem.* **2018**, *358*, 441.

[26] Y. Xu, G. Yan, Z. Ren, G. Dong, *Nat. Chem.* **2015**, *7*, 829.

[27] S. Zheng, S. Barlow, T. C. Parker, S. R. Marder, *Tetrahedron. Lett.* **2003**, *44*, 7989.
[28] S. S. Prasad, D. K. Singh, I. Kim, *J. Org. Chem.* **2019**, *84*, 6323.
[29] M. J. Frisch, G. W. Trucks, H. B. Schlegel, G. E. Scuseria, M. A. Robb, J. R. Cheeseman, G. Scalmani, V. Barone, G. A. Petersson, X. Nakatsuji, H.; Li, M. Caricato, A. V. Marenich, J. Bloino, B. G. Janesko, R. Gomperts, B. Mennucci, H. P. Hratchian, J. V. Ortiz, A. F. Izmaylov, J. L. Sonnenberg, D. Williams-Young, F. Ding, F. Lipparini, F. Egidi, J. Goings, B. Peng, A. Petrone, T. Henderson, D. Ranasinghe, V. G. Zakrzewski, J. Gao, N. Rega, G. Zheng, W. Liang, M. Hada, M. Ehara, K. Toyota, R. Fukuda, J. Hasegawa, M. Ishida, T. Nakajima, Y. Honda, O. Kitao, H. Nakai, T. Vreven, K. Throssell, J. A. J. Montgomery, J. E. Peralta, F. Ogliaro, M. J. Bearpark, J. J. Heyd, E. N. Brothers, K. N. Kudin, V. N. Staroverov, T. A. Keith, R. Kobayashi, J. Normand, K. Raghavachari, A. P. Rendell, J. C. Burant, S. S. Iyengar, J. Tomasi, M. Cossi, J. M. Millam, M. Klene, C. Adamo, R. Cammi, J. W. Ochterski, R. L. Martin, K. Morokuma, O. Farkas, J. B. Foresman, D. J. Fox, *Gaussian 16, Revision B.01*, Gaussian, Inc., Wallingford CT, **2016**.
[30] O. V. Dolomanov, L. J. Bourhis, R. J. Gildea, J. A. K. Howard, H. Puschmann, *J. Appl. Crystallogr.* **2009**, *42*, 339.
[31] G. M. Sheldrick, *Acta Crystallogr. Sect. A Found. Adv.* **2015**, *71*, 3.
[32] G. M. Sheldrick, *Acta Crystallogr. Sect. C Struct. Chem.* **2015**, *71*, 3

Chapter 4

Incorporation of Cationic Nitrogen into Strained π-Conjugated Systems: Synthesis of Cationic AzaBis(tricyclic) Aromatic Enes

4-1. Introduction

Quaternary cationic nitrogen-doped polyaromatic hydrocarbons, the so-called azonia aromatic heterocycles (AZAHs),[1] have potentials to be applied for the development of optical materials such as absorption/fluorescent dyes.[2] However, previously reported AZAHs are almost limited to highly planar quinolizinium derivatives, which consist only of hexagonal rings because synthetic ways for AZAHs have mainly depended on photocyclization reactions or transition-metal-catalyzed reactions,[1] such as Ru-catalyzed ring-closing metathesis reactions and Rh-catalyzed and [4+2] annulation between phenylpyridines and acetylenes. On the other hand, the strained π-conjugated systems have much attention due to their intriguing optical properties, such as chiroptical properties[3] and stimuli-responsive photophysical properties, based on conformational changes. [4-12] Therefore, the synthetic methods of strained-AZAHs are desired for the further development of AZAH-based optical materials, but there are very few examples of succeeding in the preparation of strained-AZAHs, which have been limited to the incorporation of cationic nitrogen into carbohelicenes[13-16] via the photocyclizations or Rh-catalized reactions as mentioned above.

Bis(tricyclic) aromatic enes (BAEs) are classified as overcrowded ethylenes (OCEs), which are one of the most famous strained π-conjugated systems.[4-12] For OCEs, there are mainly two conformers, such as folded-form (**F**-form) and twisted-form (**T**-form), due to the steric repulsion around the central C=C double bond. Until now, so many BAEs have been reported, especially fluorenylidene-substituted BAEs including [5.6]fulvalene scaffolds have been under intense investigation for over a century[17] and applied for organic optical materials.[11,12,18,19] The **F**-form of BAEs generally exhibits UV-Vis absorption ($\lambda < 500$ nm) in solution and fluorescence in a solid state, while the **T**-form shows strong absorptions in the longer wavelength region, which sometimes extends to the NIR region in solution. Thus, BAE-based stimuli-responsive chromic materials have been developed utilizing the conformational changes accompanied by a large change in photophysical properties. The author envisaged that if cationic nitrogen is incorporated into BAEs, the absorption/fluorescence properties could be drastically changed by an electronic perturbation. Furthermore, by considering that these properties should be drastically affected by the electronic structure of molecules, the conformation of cationic nitrogen-doped BAEs could be controlled not only by conventional external stimuli such as heat but also by counterions. However, since all of the reported BAEs were constructed by a Barton-Kellogg reaction[11,12,18,19]

or dehydration of the corresponding alcohol,[20] there are no synthetic methods for incorporating cationic nitrogen into the BAE skeleton.

Herein, the author reports the synthetic method for the newly designed cationic nitrogen-doped BAEs based on an intramolecular cyclization triggered by two-electron oxidation of phenylpyridine derivatives and their structural and optical properties.

4-2. Results and Discussion

4-2-1. Molecular Design

When a quaternary sp^2-carbon in the central part of fluorenylidene-based BAEs is replaced with a cationic quaternary nitrogen, four types of conformers can be considered (Scheme 4-1). If the carbon atom on the central olefin moiety is changed to the cationic nitrogen (A-type), the decrease of stability in solution is concerned because a nucleophilic attack from a small molecule, such as water or MeOH, is likely to proceed due to a high electrophilicity of the central iminium moiety (Scheme 4-1a). In the case of B-type and C-type replacements, the contribution of an electron donation from an electron-rich moiety (E) of tricyclic skeletons to the cationic nitrogen is considered. Although the electron donation from the E part in the B-type compound causes a decrease in the stability due to a change in the number of Clar's sextet from four to three (Scheme 4-1b), that in the C-type compound is considered to be more stable due to the formation of a stable σ-bonded isomer with two 14π aromatic skeletons (Scheme 4-1c). Hence, the C-type replacement with the cationic quaternary nitrogen is most favorable from the viewpoint of stability for isolation and detailed investigation. Additionally, since the energy gap between two conformers, **F**-form and **T**-form, is expected to be controllable by the difference of electro-donating characters of the E part bridging two benzene rings, photophysical properties based on the change in conformation would be observed.

Scheme 4-1. The pattern for an incorporation of cationic nitrogen into tetrabenzo[5.6]fulvalene.

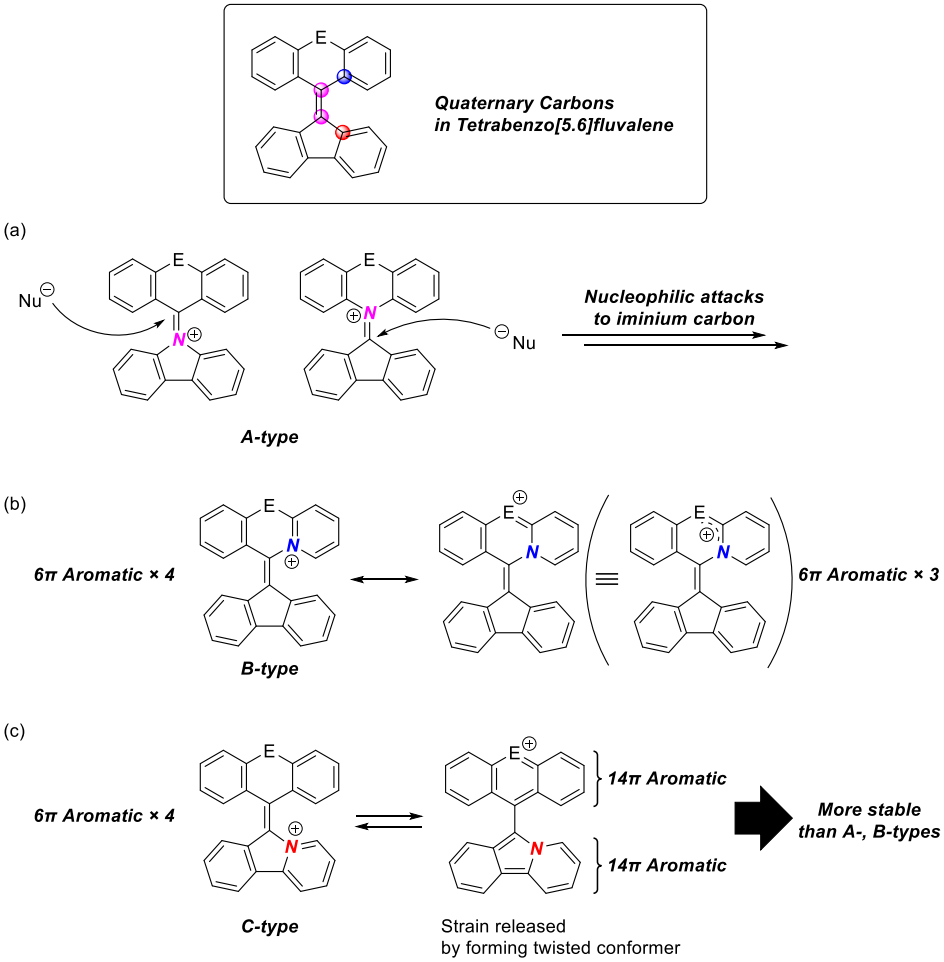

Based on the aforementioned design strategy for the C-type doping of cationic nitrogen into fluorenylidene-substituted BAE skeletons, the author designed the novel cationic aza-doped BAEs **18-N**$^+$, **18-S**$^+$ and **18-2C**$^+$ (Figure 4-1). These cations **18**$^+$ are distinguished by two criteria, i.e., the strength of the electron-donating ability and the size of the tether part in tricyclic skeletons on the opposite side of the fluorenylidene unit. Depending on these factors, a contribution of the conformation for **18**$^+$ could change, accompanied by a change in the electronic structure. To investigate the difference in energy between two conformers, the author conducted DFT calculations at CAM-B3LYP/6-31G(d,p) level. As a result, the **T**-form of **18-N**$^+$ was estimated to have a lower Gibbs energy (-6.38 kcal/mol), meaning that it is more stable than the **F**-form conformer, while that of **18-S**$^+$ and **18-2C**$^+$ were predicted to have a higher Gibbs energy (3.60 kcal/mol and 16.7 kcal/mol, respectively) than the **F**-form.

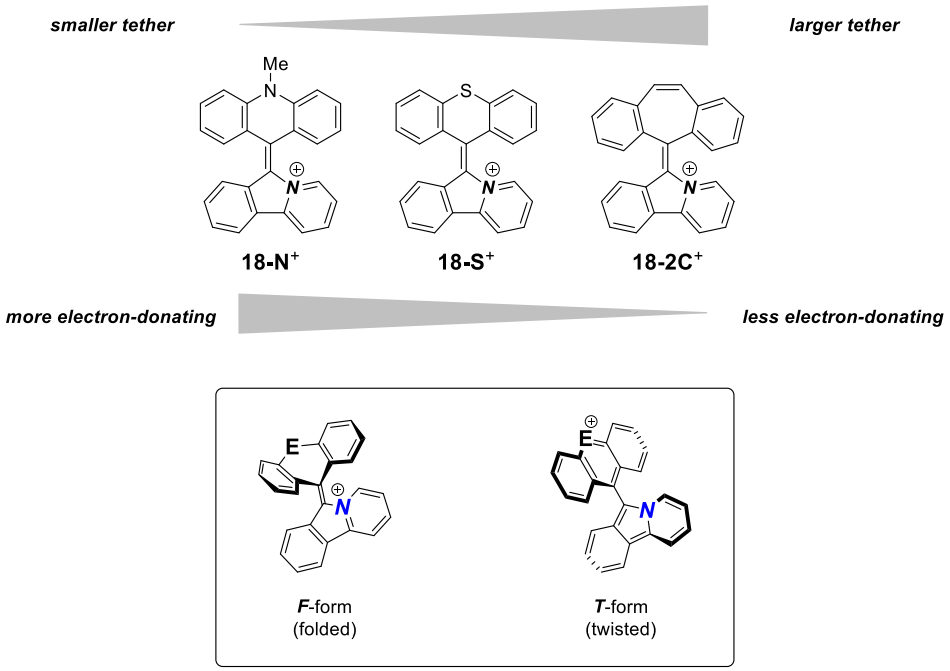

	18-N$^+$	18-S$^+$	18-2C$^+$
ΔE(***F*** - ***T***) [kcal/mol]	+6.38	-3.60	-16.7

CAM-B3LYP/6-31G(d,p) level

Figure 4-1. Newly designed cationic aza-BAEs and their relative energies calculated at CAM-B3LYP/6-31G(d,p) level.

4-2-2. Preparations and X-ray Analyses of Cationic Salts of 18$^+$

The newly designed cations **18**$^+$ were synthesized by an oxidative intramolecular cyclization of phenylpyridine-substituted triarylethenes **17**, which were prepared by a Stille-coupling reaction of bromides **16** with tributyl(2-pyridyl)tin.

Firstly, by Wittig-Horner reaction or Peterson olefination of **13**/*n*BuLi or **14**/*n*BuLi with 2-bromobenzaldehyde, ethenes **16-N** and **16-S** were obtained in 99% and 80% yields, respectively. On the other hand, **16-2C** was prepared by Wittig-Horner reaction of benzylphosphonate **15**/KO*t*Bu with dibenzosuberenone, according to the reported procedure.[21] Subsequently, triarylethenes **17** were obtained by the Stille-coupling reaction of **16** with tributyl(2-pyridyl)tin in toluene in 28-61% yields (Scheme 4-2).

Scheme 4-2. Preparation of the precursor of $\mathbf{18}^{+}$.

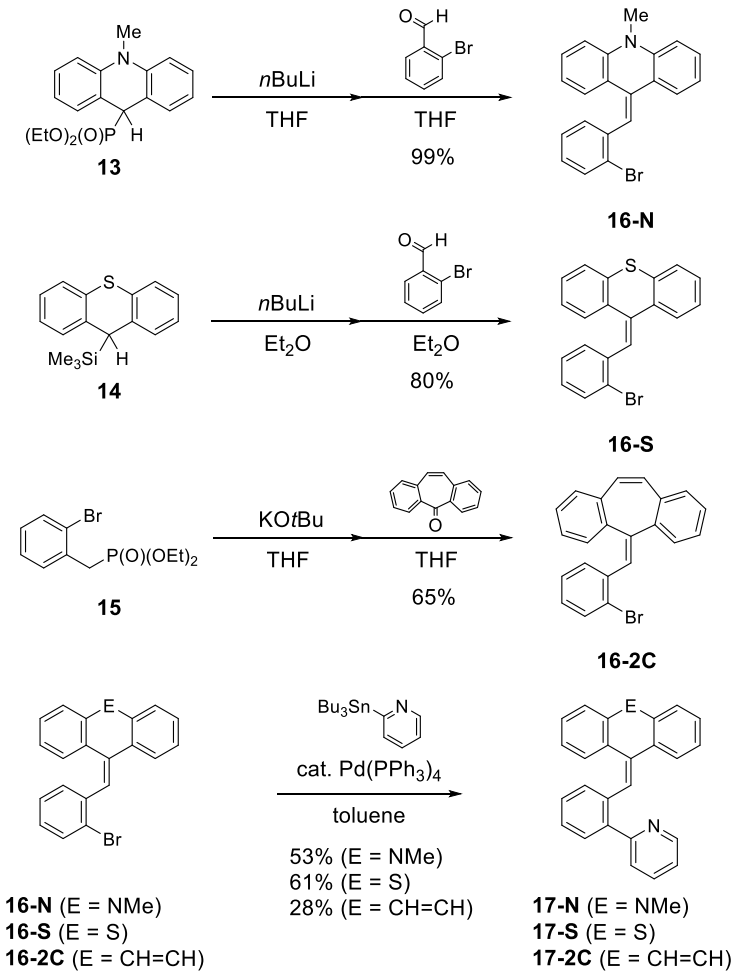

Two-electron oxidation of **17-N** with iodine followed by anion exchange with silver tetrafluoroborate yielded **18-N**$^{+}BF_4^{-}$ as dark green solids in 44%. In the cases of **17-S** and **17-2C**, tris(4-bromophenyl)aminium salt was utilized as an oxidant to produce **18-S**$^{+}BF_4^{-}$, **18-2C**$^{+}BF_4^{-}$ and **18-2C**$^{+}SbCl_6^{-}$ as yellow solids in moderate yields (Scheme 4-3).

Scheme 4-3. Preparation of cation **18**$^{+}$.

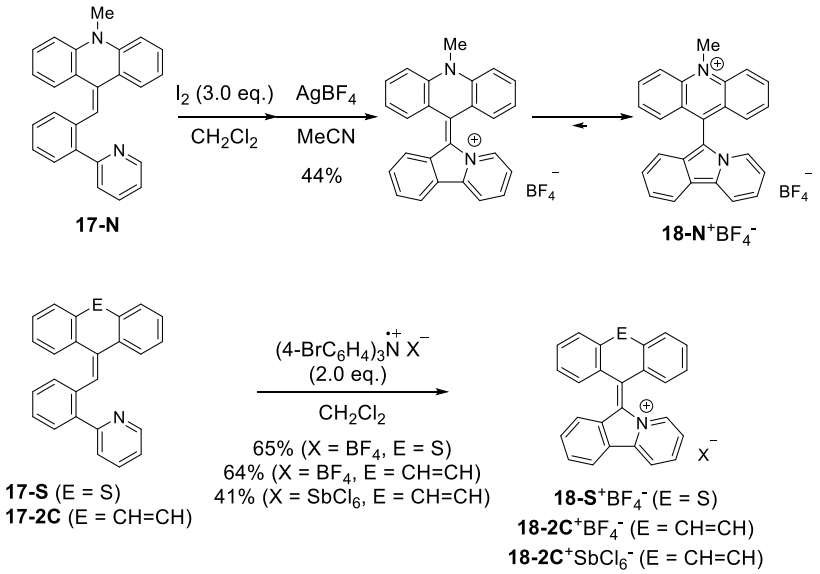

Single-crystal X-ray structure analyses revealed that **18-N**$^{+}$$BF_4^{-}$ adopts a twisted conformation with a large torsion angle (57.57 °) whereas both **18-S**$^{+}$$BF_4^{-}$ and **18-2C**$^{+}$$SbCl_6^{-}$ adopt a folded conformation (Figure 4-2). These results are in accord with the DFT calculated relative energy between the **F**-form and **T**-form (Figure 4-1). The lengths of the central C(9)=C(9') bond of **18-S**$^{+}$$BF_4^{-}$ and **18-2C**$^{+}$$SbCl_6^{-}$ are ca. 1.35 Å, which is almost the same as the standard C=C bond length (1.33 Å), while that of **18-N**$^{+}$$BF_4^{-}$ was extremely larger (1.451 Å). Considering that the standard bond length of conjugated C(sp^2)-C(sp^2) single bond (1.455 Å),[22] **18-N**$^{+}$$BF_4^{-}$ is estimated to be the structure of acridinium-connected benzo[*a*]indolizine in the crystalline state.

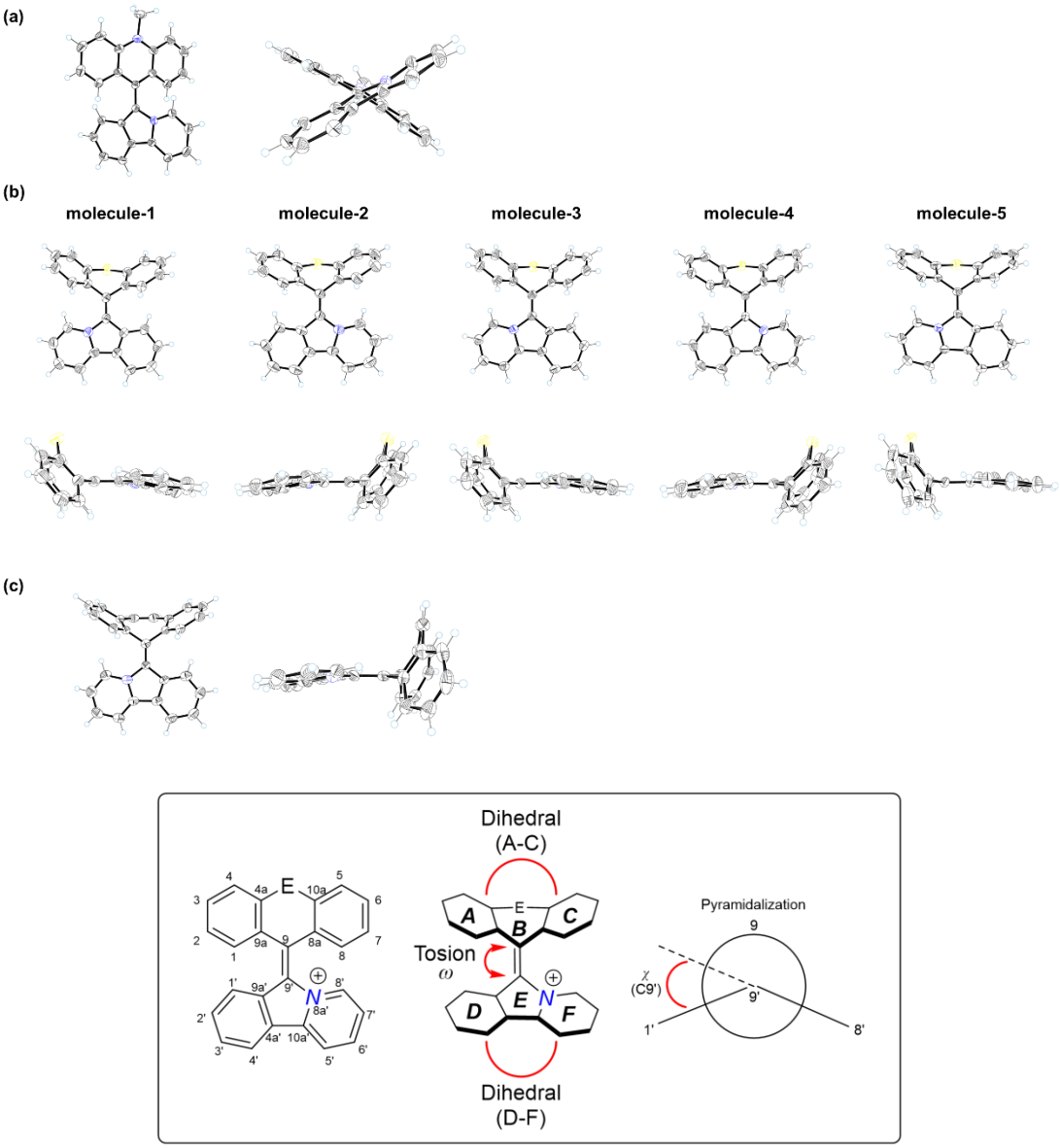

			ω/°	A-C/°	D-F/°	χ (C9)/°	χ (C9')/°	C9-C9'/ Å	C1-C1'/ Å	C8-C8'/ Å
18-$N^+BF_4^-$	twisted		57.57	9.91	5.24	2.14	13.65	1.451	3.350	3.195
		mol 1	3.10	52.36	9.47	7.50	1.79	1.355	3.137	3.072
		mol 2	0.65	57.36	14.66	3.65	2.97	1.349	3.088	3.059
18-$S^+BF_4^-$	folded	mol 3	1.66	58.47	12.95	3.06	5.18	1.352	3.067	3.107
		mol 4	3.72	54.02	15.39	3.81	4.13	1.353	3.045	3.053
		mol 5	3.26	48.53	13.06	5.40	4.10	1.347	3.023	3.009
18-$2C^+SbCl_6^-$	folded		4.12	62.15	8.69	1.38	5.19	1.341	3.131	3.280

Figure 4-2. ORTEP drawings of (a) **18-N**$^+$$BF_4^-$, (b) **18-S**$^+$$BF_4^-$ (five crystallographically independent molecules), and (c) **18-2C**$^+$$SbCl_6^-$ obtained by X-ray analyses at 150 K. Counterion are omitted for clarity.

4-2-3. UV-Vis-NIR Spectroscopy of Cationic Salts of 18^+

To gain insight into the conformation in solution, optical properties of **18-N**$^+BF_4^-$, **18-S**$^+BF_4^-$, and **18-2C**$^+BF_4^-$ were evaluated by UV-Vis-NIR spectroscopy (Figure 4-3). The UV-Vis-NIR spectrum of **18-N**$^+BF_4^-$ showed absorption maxima at 780 nm, 469 nm, and 360 nm in CH_2Cl_2 and at 751 nm, 459 nm, and 360 nm in MeCN, respectively. On the other hand, those of **18-S**$^+BF_4^-$ and **18-2C**$^+BF_4^-$ showed absorption maxima mainly in the UV-Vis region. For all azonia-type compounds $\mathbf{18}^+$, the spectra were red-shifted compared to those for the neutral counterparts without cationic nitrogen (Figure 4-4). While fluorenylidene-acridan (FA) shows absorption maximum at 680 nm in CH_2Cl_2 based on the **T**-form,[11] the corresponding absorption band of **18-N**$^+BF_4^-$ (λ_{max} = 780 nm, green color in CH_2Cl_2) is significantly red-shifted by ca. 100 nm thanks to the narrower HOMO-LUMO gap induced by cationic nitrogen doping. In addition, since the strong absorption band at 260 nm ($\varepsilon \geq 80000$ M^{-1} cm^{-1}) is assigned to the specific transition from acridinium, **18-N**$^+BF_4^-$ is considered to exist as the structure of acridinium-connected benzo[*a*]indolizine also in solution.

In contrast, a colorless solution of fluorenylidene-dibenzosuberene (FD) in THF showed absorption maximum at 317 nm,[20] while the yellow-colored solution of **18-2C**$^+BF_4^-$ showed absorption maximum at around 360 nm in both CH_2Cl_2 and MeCN. These results indicate that both dibenzosuberene-type compounds exist as the **F**-form in solution as well as the solid state. In addition, the observed red-shift in the spectrum for **18-2C**$^+BF_4^-$ can also be accounted for by the lowering LUMO level due to the incorporation of quaternary cationic nitrogen into FD scaffold.

In the case of thioxanthene-type BAE, which is expected to have intermediary properties between the above two derivatives regarding the donating-ability and the size of the tether part, a unique chromic behavior was reported for fluorenylidene-thioxanthene (FT).[19] A change in color from yellow to malachite green was observed by heating the solid-state samples to the melting point (245 °C) probably because of a change in conformations from the **F**-form to the **T**-form, though, the yellow-colored solution showed that FT adopts the **F**-form in solution. This is also the case in **18-S**$^+BF_4^-$ that shows a yellow color in solution, but the absorption band (marked with a * in Figure 4-3b) at around 800 nm was observed very weakly yet clearly even at room temperature. The longer-wavelength absorption in the NIR region was attributed to a contribution of the **T**-form of **18-S**$^+BF_4^-$ in a thermal equilibrium because the calculated energy difference between folded conformer and twisted conformer is relatively small (3.6 kcal/mol, Figure 4-1).

(a)

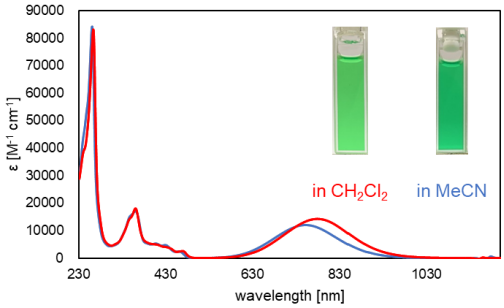

	λ_{max} [nm] (ε [M^{-1} cm^{-1}])
CH_2Cl_2	262 (83000), 360 (18100), 469 (2600), 780 (14300)
MeCN	260 (84000), 360 (17100), 459 (2400), 751 (12000)

(b)

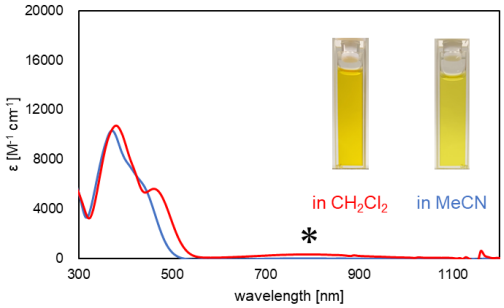

	λ_{max} [nm] (ε [M^{-1} cm^{-1}])
CH_2Cl_2	380 (10700), 461 (5600)
MeCN	371 (10300), 460 (4000)

(c)

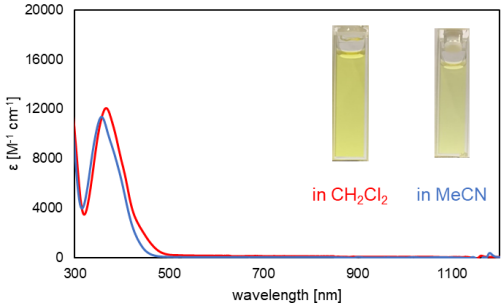

	λ_{max} [nm] (ε [M^{-1} cm^{-1}])
CH_2Cl_2	367 (12000)
MeCN	358 (11300)

Figure 4-3. UV-Vis-NIR spectra of (a) **18-N**$^{+}BF_4^{-}$, (b) **18-S**$^{+}BF_4^{-}$, and (c) **18**-2C$^{+}BF_4^{-}$ in CH_2Cl_2 and MeCN. (*Slightly observed light-absorption in the NIR region due to the contribution from the **T**-form.)

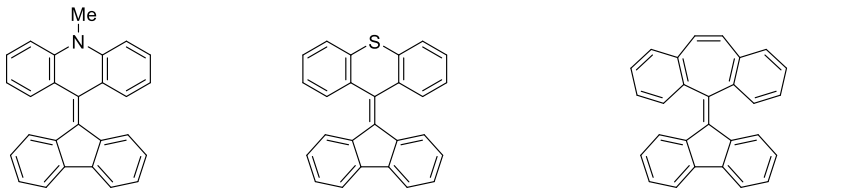

Fluorenylidene-Acridane **(FA)**[11] Matsuo, 2018

Fluorenylidene-Thioxanthene **(FT)**[19] Alexander Schönberg, 1959

Fluorenylidene-Dibenzosuberene **(FD)**[20] Nguyen, 2019

Figure 4-4. Reported neutral BAEs having the same skeleton as **18**$^{+}$.

4-2-4. Emission Properties of Cationic Salts of 18^+

Then, the author investigated photoluminescence behavior of **18-N**$^+$$BF_4^-$, **18-S**$^+$$BF_4^-$, and **18-2C**$^+$$BF_4^-$ in a solid state. For **18-S**$^+$$BF_4^-$ and **18-2C**$^+$$BF_4^-$, yellow fluorescence was observed with absolute quantum yields of 3-10% and emission maxima at 604 nm and 602 nm, respectively, while **18-N**$^+$$BF_4^-$ showed no emission (Figure 4-5). Considering that previously reported FD without cationic nitrogen showed fluorescence at 458 nm with an absolute quantum yield of 34.7% in the solid state, the fluorescence quantum yield of **18-2C**$^+$$BF_4^-$ was lower than that of FD, but an obvious red-shift in the emission wavelength was observed. These results suggested that the replacement of quaternary carbon atom with quaternary cationic nitrogen in FD can induce a large red-shift in the emission spectra from 458 nm to 602 nm, indicating the effectiveness of cationic nitrogen doping for tuning of emission properties as well as absorption properties. Furthermore, based on the small difference in energy between the **F**-form and **T**-form, since these properties could be switched by applying an external stimulus such as grinding, cationic nitrogen-doped BAEs would be promising candidates for the development of NIR (fluoro)chromic materials.

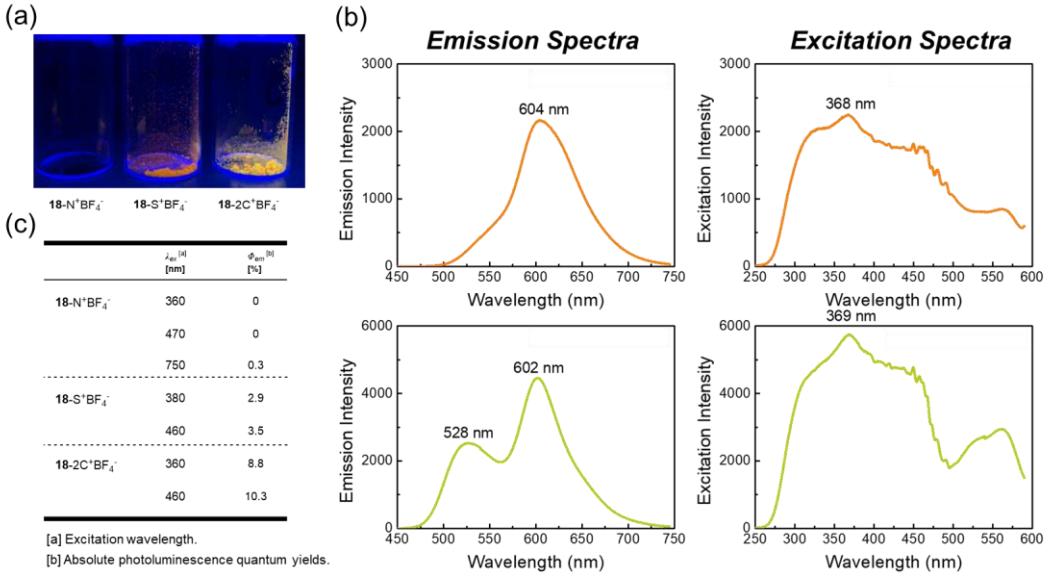

(c)

	λ_{ex} [a] [nm]	Φ_{em} [b] [%]
18-N$^+$$BF_4^-$	360	0
	470	0
	750	0.3
18-S$^+$$BF_4^-$	380	2.9
	460	3.5
18-2C$^+$$BF_4^-$	360	8.8
	460	10.3

[a] Excitation wavelength.
[b] Absolute photoluminescence quantum yields.

Figure 4-5. (a) Photographs of **18-N**$^+$$BF_4^-$ (left) **18-S**$^+$$BF_4^-$ (middle) **18-2C**$^+$$BF_4^-$ (right) under UV light (365 nm). (b) Emission spectra and Excitation spectra of **18-S**$^+$$BF_4^-$ (upper, orange) and **18-2C**$^+$$BF_4^-$ (lower, light green) in a solid state. (c) Excitation wavelength and absolute quantum yields of **18-N**$^+$$BF_4^-$ (left) **18-S**$^+$$BF_4^-$ (middle) **18-2C**$^+$$BF_4^-$ in a solid state.

4-3. Conclusion

In this work, the author designed and synthesized the quaternary cationic nitrogen-doped BAEs **18-N**$^+$, **18-S**$^+$, and **18-2C**$^+$, which are the first examples of strained-AZAHs with the exception of cationic aza-doped helicenes, and investigated their structural and optical properties. In the crystal, **18-N**$^+$$BF_4^-$ exists as the twisted conformer while **18-S**$^+$$BF_4^-$ and **18-2C**$^+$ adopt the folded conformer, as expected by DFT calculations. Especially, the central carbon-carbon bond of **18-N**$^+$$BF_4^-$ was extremely longer than those of neutral BAEs with the **T**-form synthesized thus far. Furthermore, **18-N**$^+$$BF_4^-$ showed strong absorption in the NIR region based on the dominantly populated **T**-form even in solution. For **18-S**$^+$$BF_4^-$ and **18-2C**$^+$$BF_4^-$, the solid-state fluorescence was observed at around 600 nm, which was assigned to the emission from the **F**-form. Since these absorption and fluorescence spectra are largely red-shifted from the neutral counterparts without cationic nitrogen, azonia-type BAEs can induce drastic changes in optical properties. In addition, **18-S**$^+$ has a relatively small energy difference between the folded and the twisted conformers, so further structural and electronic modifications of **18-S**$^+$ to attain stimuli-responsibility based on a conformational change would lead to the development of novel chromic materials accompanying the moving of the cation center between the nitrogen atom and the sulfur atom.

4-4. Experimental Section

4-4-1. General

All reactions were carried out under an argon atmosphere. All commercially available compounds were used without further purification unless otherwise indicated. Compounds **13**[23] , **14**[24] and **16**-2C[21] were synthesized according to the reported procedures. Dry MeCN was obtained by distillation from CaH_2 prior to use. Column chromatography was performed on silica gel 60N (KANTO KAGAKU, spherical neutral) of particle size 40–50 μm or Wakogel® 60N (neutral) of particle size 38-100 μm. ^{1}H and ^{13}C NMR spectra were recorded on a BRUKER Ascend™ 400 (^{1}H/400 MHz and ^{13}C/100 MHz) spectrometer. IR spectra were measured on a Shimadzu IRAffinity-1S spectrophotometer using the attenuated total reflection (ATR) mode. Mass spectra were recorded on a JEOL JMS-T100GCV spectrometer in FD mode (GC-MS&NMR Laboratory, Research Faculty of Agriculture, Hokkaido University). Melting points were measured on a Stanford Research Systems MPA100 Optimelt and are uncorrected. UV-Vis-NIR spectra were recorded on a JASCO V-770 spectrophotometer. DFT calculations were performed with the Gaussian 16 W program package.[25] The geometries of the compounds were optimized by using the CAM-B3LYP method in combination with the 6-31G(d,p) basis set. Single-crystal X-ray structure analyses were performed by a Rigaku XtaLAB Synergy (Cu-Kα radiation, λ = 1.54184 Å) with HyPix diffractometer. Using Olex2,[26] the structure was solved with the SHELXT[27] structure solution program using Intrinsic Phasing and refined with the SHELXL[28] refinement package using Least Squares minimization. All the hydrogen atoms were located at the calculated positions and refined with riding.

4-4-2. Preparations

Synthesis of 16-N

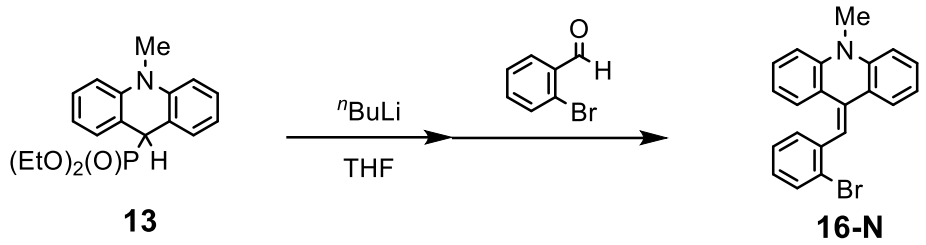

To a solution of phosphonate **13** (10.9 g, 33.0 mmol) in dry THF (120 mL) was added ^{n}BuLi (1.56 M in hexane, 21.1 mL, 33.0 mmol) dropwise over 3 min at -78 °C. After stirring at -78 °C for 1 h, 2-bromobenzaldehyde (5.55 g, 30.0 mmol) was added to the reaction mixture at -78 °C. The resulting solution was stirred for 30 min at -78 °C and for another 2.5 h at 23 °C, then the reaction was quenched with water (120 mL). The organic layer was collected and the aqueous layer was extracted with CH_2Cl_2 (150 mL × 2). The combined organic layers were washed with water and brine, and dried over anhydrous sodium sulfate. After filtration, the solution was evaporated under reduced pressure. The crude product was purified by a silica gel column (diameter, 5.0 cm, height, 20 cm) using EtOAc/hexane (1:9, v/v) as eluent (R_f = 0.41) to give compound **16-N** (10.8 g) as an orange solid in 99% yield.

Mp 164-165 °C; ^{1}H NMR (400 MHz, $CDCl_3$): δ/ppm = 7.81 (1H, dd, *J* = 1.5, 7.8 Hz), 7.61 (1H, dd, *J* = 1.5 , 7.4 Hz), 7.33 (1H, dt, *J* = 1.5, 7.6 Hz), 7.25-7.16 (2H, m), 7.11-7.01 (6H, m), 6.71-6.67 (2H, m), 3.51 (3H, s); ^{13}C NMR (100 MHz, $CDCl_3$): δ/ppm = 142.81, 141.15, 139.26, 132.79, 132.56, 130.40, 128.96, 128.67, 128.44, 128.00, 127.00, 126.17, 124.72, 124.10, 121.81, 121.61, 121.48, 120.10, 113.24, 112.55, 33.71; IR (ATR): ν/cm^{-1} = 3062, 3036, 2877, 2826, 1617, 1592, 1499, 1465, 1455, 1429, 1350, 1294, 1269, 1172, 1130, 1106, 1042, 1021, 951, 940, 930, 873, 857, 838, 821, 780, 746, 720, 668, 649, 635, 601, 550; LR-MS (FD) m/z (%): 364.06 (23), 363.06 (97), 362.06 (23), 361.06 (bp, M^+); HR-MS (FD) Calcd. for $C_{21}H_{16}BrN$: 361.04661; Found: 361.04812.

Synthesis of 17-N

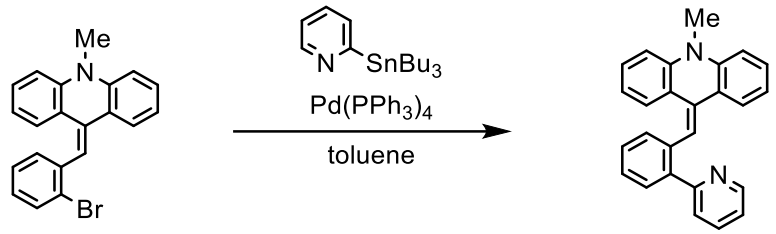

16-N **17-N**

A mixture of arylbromide **16-N** (2.54 g, 7.00 mmol), tributyl(2-pyridyl)tin (3.35 g, 9.10 mmol), and $Pd(PPh_3)_4$ (809 mg, 0.700 mmol) in toluene (55 mL) was refluxed for 14 h. After cooling to 23 °C, the mixture was diluted with water (100 mL) and extracted with CH_2Cl_2 (100 mL × 2). The combined organic layers were washed with water, and dried over anhydrous sodium sulfate. After filtration, the solution was evaporated under reduced pressure. The crude product was purified by a 10% w/w K_2CO_3 (anhydrous)-silica gel column (diameter, 4.0 cm, height, 20 cm) using EtOAc/hexane (3:7, v/v) as eluent (R_f = 0.35) to give compound **17-N** (1.33 g) as a yellow solid in 53% yield.

Mp 81-84 °C (decomp.); ^{1}H NMR (400 MHz, $CDCl_3$): δ/ppm = 8.69 (1H, dt, *J* = 1.2, 5.5 Hz), 7.72-7.67 (3H, m), 7.42 (1H, d, *J* = 7.7 Hz), 7.34-7.28 (3H, m), 7.24-7.18 (4H, m), 6.99-6.94 (3H, m), 6.72 (1H, dt, *J* = 1.0, 7.2 Hz), 6.64 (1H, s), 3.44 (3H, s); ^{13}C NMR (100 MHz, $CDCl_3$): δ/ppm = 158.91, 149.51, 142.79, 141.24, 139.62, 137.10, 135.55, 131.41, 130.04, 129.49, 128.60, 128.35, 128.32, 127.97, 127.02, 126.58, 124.50, 123.64, 122.29, 122.21, 121.62, 121.20, 120.10, 113.02, 112.39, 33.51; IR (ATR): ν/cm^{-1} = 3057, 3005, 2961, 2886, 2823, 1685, 1653, 1590, 1583, 1559, 1507, 1457, 1420, 1345, 1292, 1268, 1212, 1166, 1128, 1105, 1092, 1057, 1045, 1022, 989, 953, 936, 866, 796, 745, 691, 668, 657, 638, 603, 559, 550, 536; LR-MS (FD) m/z (%): 362.13 (5), 361.12 (30), 360.12 (bp, M^+); HR-MS (FD) Calcd. for $C_{26}H_{20}N_2$: 360.16265; Found: 360.16345.

Synthesis of 18-$N^+BF_4^-$

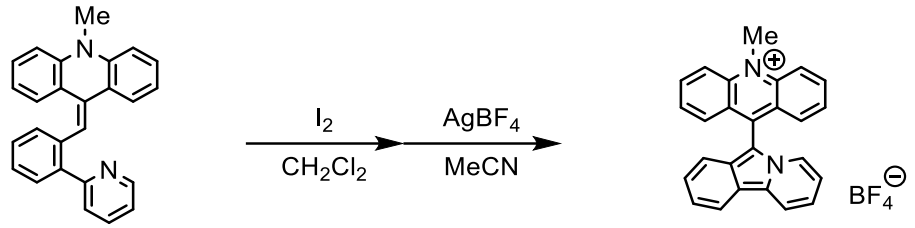

17-N **18-$N^+BF_4^-$**

To a solution of **17-N** (260 mg, 0.721 mmol) in degassed CH_2Cl_2 (20 mL) was added I_2 (548 mg, 2.16 mmol) at 25 °C. After stirring at 25 °C for 24 h, the addition of dry Et_2O (120 mL) and the supernatant was removed by decantation. The precipitates were washed with dry Et_2O (120 mL), and the supernatant was removed by decantation. The resulting solids were dissolved in MeCN (200 mL) and $AgBF_4$ (310 mg, 1.59 mmol) was added at 0 °C. After stirring for 68 h at 25 °C, insoluble solids were removed by filtration and the filtrate was evaporated under reduced pressure. The crude product was purified by a silica gel column (diameter, 4.0 cm, height, 24 cm) using MeOH/CH_2Cl_2 (1:9, v/v) as eluent (R_f = 0.37) to give cation salt **18-$N^+BF_4^-$** (141 mg) as a green solid in 44% yield.

Mp 215-217 °C (decomp.); ^{1}H NMR (400 MHz, CD_3CN): δ/ppm = 8.48 (2H, d, *J* = 9.2 Hz), 8.44 (1H, d, *J* = 8.8 Hz), 8.39 (1H, d, *J* = 8.3 Hz), 8.31 (1H, d, *J* = 7.0 Hz), 8.24 (1H, dd, *J* = 1.5, 6.7 Hz), 8.21 (1H, dd, *J* = 1.5, 6.8 Hz), 8.11 (2H, d, *J* = 8.6 Hz), 7.63 (2H, ddd, *J* = 0.90, 6.8, 8.4 Hz), 7.51-7.44 (3H, m), 7.40 (1H, ddd, *J* = 1.6, 6.4, 7.8 Hz), 7.12 (1H, dt, *J* = 1.4, 6.9 Hz), 4.69 (3H, s); ^{13}C NMR (100 MHz, CD_3CN): δ/ppm = 148.48, 142.71, 138.30, 135.30, 132.97, 131.37, 129.51, 127.85, 125.65, 125.17, 124.66, 123.06, 121.60, 121.49, 119.96, 119.80, 118.88, 117.88, 111.13, 38.90; IR (ATR): $\tilde{\nu}$/cm^{-1} = 3134, 3048, 1607, 1575, 1546, 1505, 1478, 1458, 1442, 1431, 1382, 1351, 1338, 1300, 1266, 1249, 1215, 1180, 1165, 1122, 1086, 1046, 1034, 962, 940, 880, 854, 783, 769, 751, 734, 719, 675, 641, 624, 603, 567, 554, 519; LR-MS (FD) m/z (%): 361.13 (4), 360.13 (29), 359.13 (bp, M^+); HR-MS (FD) Calcd. for $C_{26}H_{19}N_2$: 359.15482; Found: 359.15642.

Synthesis of 16-S

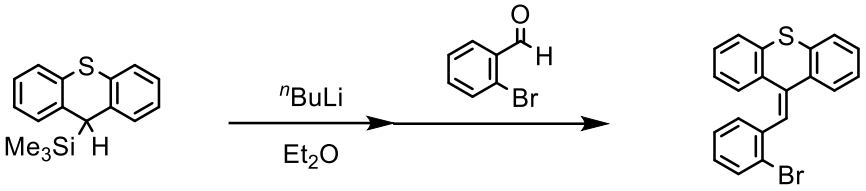

To a solution of trimethyl(9*H*-thioxanthen-9-yl)silane **14** (4.06 g, 15.0 mmol) in dry Et_2O (110 mL) was added ^{n}BuLi (1.56 M in hexane, 10.1 mL, 16.5 mmol) dropwise over 4 min at 0 °C and then the resulting mixture was refluxed for 1 h. To the resulting solution, a solution of 2-bromobenzaldehyde (2.92 g, 15.8 mmol) in dry Et_2O (5.0 mL) was added slowly at 0 °C. After stirring at 23 °C for 2 h, the mixture was diluted with sat. aqueous $NaHCO_3$ (150 mL) and extracted with EtOAc (100 mL × 2). The combined organic layers were washed with water and brine, and dried over anhydrous sodium sulfate. After filtration, the solution was evaporated under reduced pressure. The crude product was purified by a silica gel column (diameter, 5.0 cm, height, 26 cm) using hexane as eluent (R_f = 0.31) to give compound **16-S** (4.37 g) as a yellow sticky oil in 80% yield.

^{1}H NMR (400 MHz, $CDCl_3$): δ/ppm = 7.81 (1H, dd, *J* = 1.1, 7.7 Hz), 7.61 (1H, dd, *J* = 1.7, 7.7 Hz), 7.46-7.43 (2H, m), 7.35 (1H, dt, *J* = 1.3, 7.4 Hz), 7.27 (1H, dt, *J* = 1.4, 7.5 Hz), 7.16 (1H, dt, *J* = 1.4, 7.3 Hz), 7.09-7.01 (3H, m), 6.97-6.91 (3H, m); ^{13}C NMR (100 MHz, $CDCl_3$): δ/ppm = 137.89, 137.28, 137.05, 137.80, 132.72, 132.66, 132.17, 131.35, 129.86, 129.21, 128.72, 127.55, 127.44, 127.21, 127.04, 126.97, 126.09, 125.95, 125.84, 124.54; IR (ATR): ν/cm^{-1} = 3059, 3005, 2951, 2921, 2853, 1583, 1559, 1458, 1437, 1363, 1268, 1259, 1211, 1154, 1124, 1115, 1064, 1038, 1020, 979, 941, 873, 849, 835, 781, 762, 751, 735, 719, 701, 665, 645, 596, 576, 532, 510; LR-MS (FD) m/z (%): 367.91 (6), 366.91 (23), 365.91 (bp, M^+), 364.92 (22), 363.91 (96); HR-MS (FD) Calcd. for $C_{20}H_{13}BrS$: 363.99213; Found: 363.99087.

Synthesis of 17-S

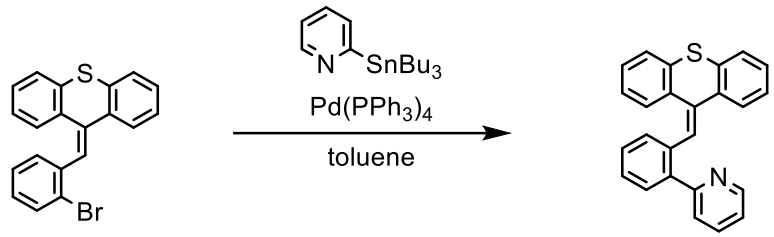

16-S **17-S**

A mixture of arylbromide **16-S** (3.37 g, 9.23 mmol), tributyl(2-pyridyl)tin (4.42 g, 12.0 mmol), and $Pd(PPh_3)_4$ (1.07 g, 0.923 mmol) in toluene (75 mL) was refluxed for 15 h. After cooling to 23 °C, the mixture was diluted with water (130 mL) and extracted with CH_2Cl_2 (150 mL × 2). The combined organic layers were washed with water, and dried over anhydrous sodium sulfate. After filtration, the solution was evaporated under reduced pressure. The crude product was purified by a 10% w/w K_2CO_3 (anhydrous)-silica gel column (diameter, 5.0 cm, height, 25 cm) using EtOAc/hexane (1:4, v/v) as eluent (R_f = 0.33). After evaporation, the resulting solid was washed with CH_2Cl_2/hexane (1:7, 40 mL) using an ultrasonic bath. The precipitates were collected and washed with hexane (25 mL), and dried *in vacuo* to give compound **17-S** (2.03 g) as a white solid in 61% yield.

Mp 121-123 °C; ^{1}H NMR (400 Hz, 1,1,2,2-tetrachloroethane-d_2): δ/ppm = 8.75 (1H, d, J = 4.8 Hz), 7.81 (1H, dt, J = 1.8, 7.7 Hz), 7.69 (1H, d, J = 7.1 Hz), 7.64 (1H, d, J = 7.9 Hz), 7.52-7.18 (11H, m), 7.03 (1H, dt, J = 1.1, 7.6 Hz), 6.96 (1H, s); ^{13}C NMR (100 MHz, $CDCl_3$): δ/ppm = 158.82, 149.62, 140.04, 137.73, 135.92, 135.86, 135.36, 133.69, 133.22, 132.17, 130.48, 130.00, 129.82, 129.69, 128.29, 127.65, 127.27, 127.03, 126.94, 126.85, 126.05, 125.94, 125.45, 124.21, 121.96; IR (ATR): ν/cm^{-1} = 3060, 3005, 1584, 1555, 1476, 1460, 1439, 1423, 1303, 1270, 1254, 1155, 1125, 1115, 1089, 1066, 1050, 1035, 1023, 988, 978, 956, 945, 883, 875, 865, 803, 782, 766, 756, 750, 739, 704, 650, 632, 620, 600, 577, 520, 506; LR-MS (FD) m/z (%): 365.10 (9), 364.10 (31), 363.10 (bp, M^+); HR-MS (FD) Calcd. for $C_{25}H_{17}NS$: 363.10817; Found: 363.10656.

Synthesis of 18-S$^+$BF$_4^-$

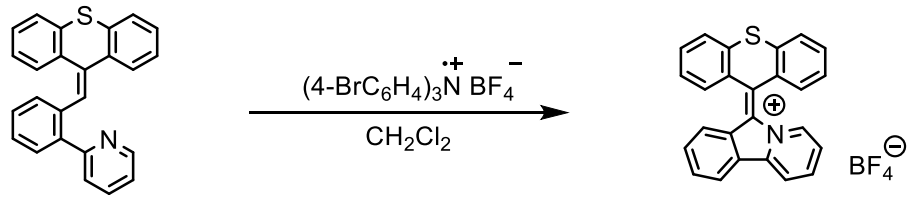

17-S **18-S$^+$BF$_4^-$**

To a solution of **17-S** (300 mg, 0.830 mmol) in degassed CH_2Cl_2 (45 mL) was added tris(4-bromophenyl)aminium tetrafluoroborate (939 mg, 1.65 mmol) at 23 °C. After stirring at 23 °C for 1 h, the addition of dry Et_2O (180 mL) led to precipitation of the cation salt and the supernatant was removed by decantation. The resulting solid was washed with Et_2O (180 mL × 2) using an ultrasonic bath. The precipitate was collected and rinsed with Et_2O (50 mL) and dried *in vacuo.* The precipitates were purified by a silica gel column (diameter, 4.0 cm, height, 22 cm) using MeOH/CH_2Cl_2 (1:9, v/v) as eluent (R_f = 0.31) to give cation salt **18-S**$^+$BF$_4^-$ (241 mg) as a yellow solid in 65% yield.

Mp 152-153 °C (decomp.); ^{1}H NMR (400 MHz, CD_3CN): δ/ppm = 8.77 (1H, d, *J* = 6.7 Hz), 8.44-8.38 (2H, m), 8.22 (1H, d, *J* = 7.8 Hz), 7.95 (2H, d, *J* = 7.3 Hz), 7.84 (2H, d, *J* = 7.2 Hz), 7.70 (1H, ddd, *J* = 1.7, 7.2, 7.4 Hz), 7.57-7.46 (7H, m); ^{13}C NMR (100 MHz, CD_3CN): δ/ppm = 152.14, 147.13, 139.81, 137.51, 137.37, 134.07, 133.73, 133.34, 133.04, 132.18, 131.55, 130.81, 130.64, 129.02, 127.95, 126.17, 124.20, 124.06, 121.41; IR (ATR): ν/cm^{-1} = 3151, 3065, 2365, 1636, 1577, 1559, 1499, 1461, 1436, 1350, 1323, 1303, 1288, 1223, 1188, 1164, 1048, 1026, 961, 887, 783, 767, 748, 730, 701, 633, 592, 521; LR-MS (FD) m/z (%): 364.07 (8), 363.07 (29), 362.07 (bp, M$^+$); HR-MS (FD) Calcd. for $C_{25}H_{16}NS$: 362.10034; Found: 362.10041.

Synthesis of 16-2C

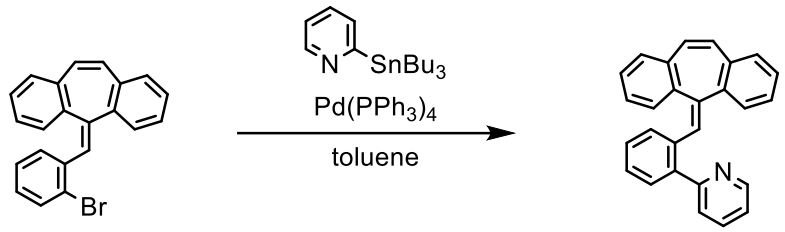

16-2C **17-2C**

A mixture of arylbromide **16-2C** (2.00 g, 5.57 mmol), tributyl(2-pyridyl)tin (2.67 g, 7.24 mmol), and $Pd(PPh_3)_4$ (647 mg, 0.560 mmol) in toluene (45 mL) was refluxed for 20 h. After cooling to 22 °C, the mixture was diluted with water (80 mL) and extracted with CH_2Cl_2 (100 mL × 2). The combined organic layers were washed with water, and dried over anhydrous sodium sulfate. After filtration, the solution was evaporated under reduced pressure. The crude product was purified by a 10% w/w K_2CO_3 (anhydrous)-silica gel column (diameter, 4.0 cm, height, 22 cm) using EtOAc/hexane (1:4, v/v) as eluent (R_f = 0.39). After evaporation, the resulting solid was washed with hexane (60 mL × 2) using an ultrasonic bath. The precipitates were collected and washed with hexane (40 mL), and dried *in vacuo* to give compound **17-2C** (550 mg) as a white solid in 28% yield.

Mp 154-155 °C; ^{1}H NMR (400 Hz, 1,1,2,2-tetrachloroethane-d_2): δ/ppm = 8.79 (1H, d, J = 4.0 Hz), 7.88 (1H, dt, J = 1.8, 7.7 Hz), 7.70 (1H, d, J = 7.9 Hz), 7.57 (1H, d, J = 6.6 Hz), 7.42-7.26 (8H, m), 7.18 (2H, d, J = 3.8 Hz), 7.11 (1H, t, J = 6.6 Hz), 6.92 (2H, s), 6.80 (1H, d, J = 7.7 Hz), 6.56 (1H, s); ^{13}C NMR (100 MHz, $CDCl_3$): δ/ppm = 159.16, 149.64, 142.42, 141.56, 140.34, 137.62, 135.92, 135.71, 135.28, 134.62, 133.09, 131.42, 131.30, 130.51, 129.65, 129.61, 128.87, 128.85, 128.55, 128.48, 127.81, 127.14 (2C), 127.07, 127.03, 124.56, 121.94; IR (ATR): ν/cm^{-1} = 3057, 3009, 1583, 1570, 1559, 1486, 1476, 1457, 1439, 1423, 1359, 1299, 1261, 1239, 1205, 1150, 1113, 1088, 1058, 1039, 1022, 988, 957, 947, 894, 885, 870, 837, 803, 793, 773, 761, 744, 728, 715, 691, 662, 649, 633, 614, 600, 588, 527; LR-MS (FD) m/z (%): 359.08 (4), 358.07 (30), 357.07 (bp, M^+); HR-MS (FD) Calcd. for $C_{27}H_{19}N$: 357.15175; Found: 357.15083.

Synthesis of 18-2C^{+}BF$_4^{-}$

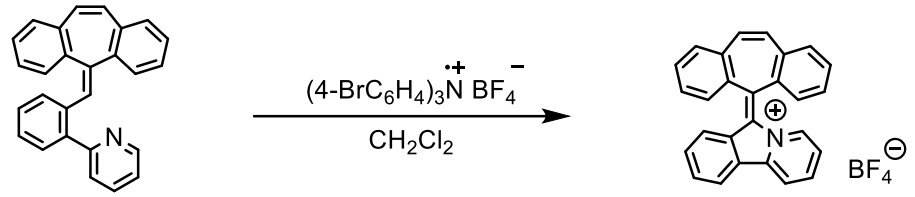

17-2C **18-2C^{+}BF$_4^{-}$**

To a solution of **17-2C** (200 mg, 0.560 mmol) in degassed CH_2Cl_2 (30 mL) was added tris(4-bromophenyl)aminium tetrafluoroborate (637 mg, 1.12 mmol) at 25 °C. After stirring at 25 °C for 1 h, the addition of dry Et_2O (120 mL) led to precipitation of the cation salt and the supernatant was removed by decantation. The resulting solid was washed with Et_2O (120 mL × 2) using an ultrasonic bath. The precipitate was collected and rinsed with Et_2O (20 mL) and dried *in vacuo*. The precipitates were purified by a silica gel column (diameter, 4.0 cm, height, 21 cm) using MeOH/CH_2Cl_2 (1:9, v/v) as eluent (R_f = 0.30) to give cation salt **18-2C**$^{+}$BF$_4^{-}$ (159 mg) as a yellow solid in 64% yield.

Mp 279-284 °C (decomp.); ^{1}H NMR (400 MHz, CD_3CN): δ/ppm = 8.43-8.36 (2H, m), 8.19 (1H, d, *J* = 7.8 Hz), 8.08 (1H, d, *J* = 6.8 Hz), 7.80-7.73 (2H, m), 7.67-7.59 (7H, m), 7.48-7.42 (2H, m), 7.25 (2H, s), 6.47 (1H, d, *J* = 8.1 Hz); ^{13}C NMR (100 MHz, CD_3CN): δ/ppm = 151.98, 146.74, 142.66, 139.04, 134.23, 134.19, 134.07, 133.98, 133.80, 133.61, 132.96, 131.89, 131.84, 131.50, 131.43, 131.14, 131.08, 130.91, 130.80, 130.47, 130.00, 126.47, 125.87, 124.75, 124.43, 124.04, 121.39; IR (ATR): $\tilde{\nu}$/cm^{-1} = 3150, 3062, 2894, 2365, 1637, 1617, 1594, 1559, 1533, 1499, 1464, 1442, 1351, 1324, 1307, 1285, 1214, 1191, 1158, 1050, 1032, 960, 880, 808, 781, 768, 747, 734, 632, 597, 522; LR-MS (FD) m/z (%): 358.11 (4), 357.11 (31), 356.10 (bp, M^{+}); HR-MS (FD) Calcd. for $C_{27}H_{18}N$: 356.14392; Found: 356.14558.

Synthesis of 18-2C^{+}SbCl$_6^{-}$

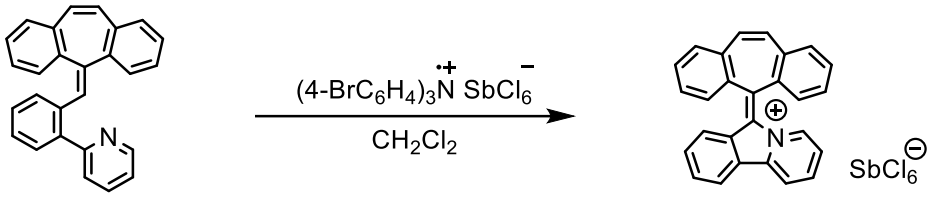

17-2C **18-2C^{+}SbCl$_6^{-}$**

To a solution of **17-2C** (143 mg, 0.400 mmol) in degassed CH_2Cl_2 (20 mL) was added tris(4-bromophenyl)aminium hexachloroantimonate (653 mg, 0.800 mmol) at 22 °C. After stirring at 22 °C for 1 h, the addition of dry Et_2O (100 mL) led to precipitation of the cation salt and the supernatant was removed by decantation. The resulting solid was washed with Et_2O (100 mL × 2) using an ultrasonic bath. The precipitate was collected and rinsed with Et_2O (20 mL) and dried *in vacuo*. The precipitates were purified by a silica gel column (diameter, 4.0 cm, height, 22 cm) using MeOH/CH_2Cl_2 (1:9, v/v) as eluent (R_f = 0.39) to give cation salt **18-2C**$^{+}$SbCl$_6^{-}$ (113 mg) as a yellow solid in 41% yield.

Mp 213-217 °C (decomp.); ^{1}H NMR and ^{13}C NMR spectra are identical to those of **18-2C**$^{+}$$BF_4^{-}$; IR (ATR): ν/cm^{-1} = 2886, 2366, 1685, 1653, 1636, 1559, 1460, 1437, 1349, 1319, 1305, 1244, 1212, 1188, 1162, 1140, 1112, 1082, 1036, 956, 890, 801, 767, 746, 728, 668, 632, 595; LR-MS (FD) m/z (%): 358.11 (4), 357.10 (30), 356.10 (bp, M^{+}); HR-MS (FD) Calcd. for $C_{27}H_{18}N$: 356.14392; Found: 356.14440.

4-4-3. X-ray Analysis

Table 4-1. Crystal data of **18-N**$^{+}$$BF_4^{-}$, **18-S**$^{+}$$BF_4^{-}$, and **18-2C**$^{+}$$SbCl_6^{-}$.

Compounds	**18-N^{+} BF_4^{-}**	**18-S^{+} BF_4^{-}**	**18-2C^{+} $SbCl_6^{-}$**
Solvent system	CH_2Cl_2/Et_2O	$EtNO_2$/toluene	$CHCl_3$/hexane
Empirical formula	$C_{26.5}H_{20}BClF_4N_2$	$C_{25.4}H_{17}$ $BF_4N_{1.2}O_{0.4}S$	$C_{27}H_{18}Cl_6NSb$
Formula weight	488.70	464.27	690.87
Temperature/K	150	150	150
Crystal system	monoclinic	triclinic	orthorhombic
Space group	$P2_1/n$	P-1	$P2_12_12_1$
a/Å	12.30918(13)	8.13915(9)	10.05380(7)
b/Å	8.36329(9)	24.3490(3)	17.70468(12)
c/Å	21.5440(2)	29.7110(3)	15.31307(12)
α/°	90	69.9429(10)	90
β/°	92.1444(10)	89.2855(8)	90
γ/°	90	82.8496(9)	90
Volume/Å^3	2216.30(4)	5485.12(11)	2725.72(3)
Z	4	10	4
ρ_{calc} g/cm^3	1.465	1.406	1.684
μ/mm^{-1}	1.988	1.755	13.582
Color and shape	dark green plate	orange plate	yellow plate
Crystal size/mm^3	0.211 × 0.077 × 0.032	0.331 × 0.065 × 0.031	0.3 × 0.046 × 0.033
Reflections	17499	98608	26432
R_{int}	0.0290	0.0337	0.0374
Data/restraints/para	4503/0/300	22381/75/1556	5588/5/362
GOF	1.062	1.059	1.135
R_1 [I>=2σ(I)]	0.0386	0.0650	0.0336
wR_2 [I>=2σ(I)]	0.1053	0.1794	0.0733
R_1 [all data]	0.0426	0.0739	0.0342
wR_2 [all data]	0.1083	0.1863	0.0735
Largest diff.peak/hole/e Å^{-3}	0.26/-0.23	0.91/-0.52	0.45/-0.55
Solvent mask	Used for the analysis	Used for the analysis	None

4-5. References

[1] D. Sucunza, A. A. Cuadro, J. Alvarez-Builla, J. J. Vaquero, *J. Org. Chem.* **2016**, *81*, 10126.

[2] (a) Bortolozzi. R, Ihmels. H, Thomas. L, Tian. M, Viola. G, *Chem. Eur. J.* **2013**, *19*, 8736. (b) T. Cañeque, A. M. Cuadro, J. Alvarez-Builla, J. Pérez-Moreno, K. Clays, O. Castaño, J. L. Andrés, J. J. Vaquero, *Dyes Pigm.* **2014**, *101*, 116. (c) Bortolozzi. R, von Gradowski. S, Ihmels. H, Schafer. K, Viola. G, *Chem. Commun.* **2014**, *50*, 8242. (d) Yue. X, Armijo. Z, King. K, Bondar. M. V, Morales. A. R, Frazer. A, Mikhailov. I. A, Przhonska. O. V, Belfield. K. D, *ACS Appl. Mater. Interfaces.* **2015**, *7*, 2833. I Marcelo. G, Pinto. S, Cañeque. T, Mariz. I. F. A, Cuadro. A. M, Vaquero. J. J, Martinho. J. M. G, Maçoas. E. M. S, *J. Phys. Chem. A.* **2015**, *119*, 2351.

[3] (a) Prince Ravat, *Chem. Eur. J.* 2021, 27, 3957. (b) P. Ravat, T. Šolomek, M. Juríček, *ChemPhotoChem.* **2019**, *3*, 180.

[4] D. Sahoo, R. Benny, N. Kumar KS, S. De, *ChemPlusChem.* **2022**, *87*, e202100322.

[5] W. T. Grubb, G. B. Kistiakowsky, *J. Am. Chem. Soc.* **1950**, *72*, 419.

[6] Y. Tapuhi, O. Kalisky, I. Agranat, *J. Org. Chem.* **1979**, *44*, 1949.

[7] M. Joergensen, K. Lerstrup, P. Frederiksen, T. Bjoernholm, P. Sommer-Larsen, K. Schaumburg, K. Brunfeldt, K. Bechgaard, *J. Org. Chem.* **1993**, *58*, 2785.

[8] P. U. Biedermann, J. J. Stezowski, I. Agranat, *Chem. Eur. J.* **2006**, *12*, 3345.

[9] W. R. Browne, M. M. Pollard, B. de Lange, A. Meetsma, B. L. Feringa, *J. Am. Chem. Soc.* **2006**, *128*, 12412.

[10] Y. Hirao, N. Nagamachi, K. Hosoi, T. Kubo, *Chem. Asian J.* **2018**, *13*, 510.

[11] T. Suzuki, H. Okada, T. Nakagawa, K. Komatsu, C. Fujimoto, H. Kagi, Y. Matsuo, *Chem. Sci.* **2018**, *9*, 475.

[12] Y. Wang, Y. Ma, K. Ogumi, B. Wang, T. Nakagawa, Y. Fu, Y. Matsuo, *Commun. Chem.* **2020**, *3*, 93.

[13] S. Arai, M. Ishikura, K. Sato, T. Yamagishi, *J. Heterocyclic. Chem.* **1995**, *32*, 1081.

[14] S. Arai, M. Ishikura, T. Yamagishi, *J. Chem. Soc., Perkin Trans. 1*, **1998**, 1561.

[15] K. Sato, S. Okazaki, T. Yamagishi, S. Arai, *J. Heterocyclic. Chem.* **2004**, *41*, 443.

[16] K. Xu, Y. Fu, Y. Zhou, F. Hennersdorf, P. Machata, I. Vincon, J. J. Weigand, A. A. Popov, R. Berger, X. Feng, *Angew. Chem. Int. Ed.* **2017**, *56*, 15876.

[17] de la Harpe. C, van Dorp. W. A. *Ber. Dtsch. Chem. Ges.* **1875**, *8*, 1048.

[18] Y. Matsuo, Y. Wang, H. Ueno, T. Nakagawa, H. Okada, *Angew. Chem. Int. Ed.* **2019**, *58*, 8762.

[19] S. Alexander, S. M. Mohame, *J. Am. Chem. Soc.* **1959**, *81*, 2259.

[20] R. D. Crocker, B. Zhang, D. P. Pace, W. W. H. Wong, T. V. Nguyen, *Chem. Commun.* **2019**, *55*, 11591.

[21] L. Yang, H. Matsuyama, S. Zhang, M. Terada, T. Jin, *Org. Lett.* **2020**, *22*, 5121.
[22] F. H. Allen, O. Kennard, D. G. Watson, L. Brammer, A. G. Orpen, R. Taylor, *J. Chem. Soc., Perkin Trans. 2,* **1987**, S1 —S19.
[23] (a) D. Redmore, *J. Org. Chem.* **1969**, *34*, 1420. (b) K.Ishikawa, K.-y. Akiba, N. Inamoto, *Bull. Chem. Soc. Jpn.* **1978**, *51*, 2684.
[24] S. Zhang, H. Matsuyama, I. Nakamura, M. Terada, T. Jin, *Org. Lett.* **2023**, *25*, 5027.
[25] M. J. Frisch, G. W. Trucks, H. B. Schlegel, G. E. Scuseria, M. A. Robb, J. R. Cheeseman, G. Scalmani, V. Barone, G. A. Petersson, X. Nakatsuji, H.; Li, M. Caricato, A. V. Marenich, J. Bloino, B. G. Janesko, R. Gomperts, B. Mennucci, H. P. Hratchian, J. V. Ortiz, A. F. Izmaylov, J. L. Sonnenberg, D. Williams-Young, F. Ding, F. Lipparini, F. Egidi, J. Goings, B. Peng, A. Petrone, T. Henderson, D. Ranasinghe, V. G. Zakrzewski, J. Gao, N. Rega, G. Zheng, W. Liang, M. Hada, M. Ehara, K. Toyota, R. Fukuda, J. Hasegawa, M. Ishida, T. Nakajima, Y. Honda, O. Kitao, H. Nakai, T. Vreven, K. Throssell, J. A. J. Montgomery, J. E. Peralta, F. Ogliaro, M. J. Bearpark, J. J. Heyd, E. N. Brothers, K. N. Kudin, V. N. Staroverov, T. A. Keith, R. Kobayashi, J. Normand, K. Raghavachari, A. P. Rendell, J. C. Burant, S. S. Iyengar, J. Tomasi, M. Cossi, J. M. Millam, M. Klene, C. Adamo, R. Cammi, J. W. Ochterski, R. L. Martin, K. Morokuma, O. Farkas, J. B. Foresman, D. J. Fox, *Gaussian 16, Revision B.01*, Gaussian, Inc., Wallingford CT, **2016**.
[26] O. V. Dolomanov, L. J. Bourhis, R. J. Gildea, J. A. K. Howard, H. Puschmann, *J. Appl. Crystallogr.* **2009**, *42*, 339.
[27] G. M. Sheldrick, *Acta Crystallogr. Sect. A Found. Adv.* **2015**, *71*, 3.
[28] G. M. Sheldrick, *Acta Crystallogr. Sect. C Struct. Chem.* **2015**, *71*, 3

Acknowledgements

This study has been carried out under the direction of Professor Dr. Takanori Suzuki, Department of Chemistry, Faculty of Science, Hokkaido University. The author would like to express his sincere gratitude to Professor Suzuki for his consistent guidance, suggestion, valuable discussions, encouragement, and so much help throughout the course of this work.

The author deeply grateful to Associate Professor Dr. Yusuke Ishigaki (Department of Chemistry, Faculty of Science, Hokkaido University), Assistant Professor Dr. Ryo Katoono (Department of Chemistry, Faculty of Science, Hokkaido University) and Assistant Professor Dr. Takuya Shimajiri (Department of Chemistry, Faculty of Science, Hokkaido University) for their kind guidance, suggestion, valuable discussion, encouragement, and so much help throughout the course of this work.

The author would like to thank Professor Dr. Keiji Tanino, Professor Dr. Masaya Sawamura and Professor Dr. Takeshi Ohkuma for their valuable suggestions and discussions.

The author expresses sincere thanks to Associate Professor Dr. Toshikazu Ono (Department of Chemistry and Biochemistry, Graduate School of Engineering, Kyushu University) for giving him the opportunity to make experiments for the contents of Chapter 4.

The author is really thankful to Dr. Eri Fukushi and Mr. Yusuke Takada (GC-MS & NMR Laboratory, Graduate School of Agriculture, Hokkaido University) for the measurements of mass.

The author gives thanks to the members in Suzuki Laboratory for their valuable discussion and giving his invaluable time.

The author is in acknowledgement of the Hokkaido University Ambitious Doctoral Fellowship (Information Science and AI).

Finally, the author would like to express his deep and sincere gratitude to his parents, Yong-Bo Chong and Yoko Lee, for their continuous financial help and encouragement.

Su-Gi Chong